

# **Politechnika Wrocławска**

Faculty of Electronics, Photonics and Microsystems

---

FIELD OF STUDY: Advanced Applied Electronics

## **MASTER THESIS**

TITLE OF THESIS:  
Development and Optimisation of a High  
Efficiency RF Power Amplifier

AUTHOR:  
Grzegorz Krupa

SUPERVISOR:  
dr inż. Grzegorz Budzyń

# Contents

<b>1 Theoretical Background</b>	<b>3</b>
1.1 Project Specification . . . . .	3
1.1.1 Constraints . . . . .	4
1.1.2 Available Technologies . . . . .	4
1.1.3 Market Solutions . . . . .	7
<b>2 Electrical design</b>	<b>8</b>
2.1 Designed Amplifier - Forte 600 . . . . .	8
2.1.1 Block Diagram . . . . .	8
2.2 Theory of Operation . . . . .	9
2.2.1 RX/TX Board . . . . .	9
2.2.2 Controller Board . . . . .	12
2.2.3 Low Pass Filters . . . . .	17
2.3 Impedance Matching . . . . .	22
2.3.1 Input Section . . . . .	24
2.3.2 Output Matching - TLT . . . . .	25
2.3.3 Tested TLTs . . . . .	27
2.3.4 1:4 vs 1:9 Ratios . . . . .	31
2.3.5 Output Capacitors . . . . .	31
2.4 BALUN Measurement . . . . .	32
2.5 Bias Supply . . . . .	33
2.6 Feedback, Stability . . . . .	36
2.7 PA Board . . . . .	37
2.8 Power Supply . . . . .	38
<b>3 Mechanical construction</b>	<b>39</b>
3.1 Enclosure . . . . .	39
3.2 Cooling System . . . . .	41
<b>4 Amplifier Tests</b>	<b>42</b>
4.1 Measurement Setup . . . . .	42
4.2 Bias Setup . . . . .	45
4.3 Initial Test . . . . .	45
4.4 Power, Gain, PAE . . . . .	47
4.4.1 1:9 TLT, 3 Turns $17\ \Omega$ , Ferrite Material 61 . . . . .	48
4.4.2 1:9 TLT, 4 Turns $50  25\ \Omega$ , Ferrite Material 43 . . . . .	50
4.4.3 1:4 TLT, 5 Turns $25\ \Omega$ , Ferrite Material 43 . . . . .	51
4.4.4 TLT and Efficiency . . . . .	52
4.4.5 TLT and Output Power . . . . .	53
4.5 Linearity . . . . .	54

4.6	Impact of TLT on Harmonics . . . . .	55
4.7	Harmonics with LPFs . . . . .	58
4.7.1	LPF Measurement . . . . .	58
4.8	SFDR Measurement . . . . .	61
4.9	IMD . . . . .	64
4.9.1	IP3 . . . . .	66
<b>5</b>	<b>Software</b>	<b>67</b>
<b>6</b>	<b>Conclusions</b>	<b>70</b>
<b>7</b>	<b><i>forte 600 Operation Manual</i></b>	<b>71</b>
7.1	Introduction . . . . .	71
7.2	Specification . . . . .	71
7.3	Front Panel . . . . .	72
7.4	Rear Panel . . . . .	72
7.5	Installation and First Start . . . . .	73
7.6	Operation . . . . .	73
7.6.1	Band Switching Modes . . . . .	74
7.6.2	Stand By Mode . . . . .	75
7.6.3	Antenna Recommendation and ATUs . . . . .	76
7.7	Protection . . . . .	76
7.7.1	Error Codes . . . . .	76
7.8	In Case of Difficulty . . . . .	79
7.9	Warnings . . . . .	80
7.10	Service and Repair . . . . .	80
7.11	Schematics . . . . .	80
7.11.1	PA Board Main Schematic . . . . .	81
7.11.2	LPF Schematic . . . . .	84
7.11.3	TX/RX Schematic . . . . .	85
7.11.4	Controller Schematic . . . . .	86
7.12	PCB Silkscreens . . . . .	90
7.12.1	LPF Board Front Silkscreen . . . . .	91
7.12.2	LPF Board Back Silkscreen . . . . .	92
7.12.3	Controller Board Front Silkscreen . . . . .	93
7.12.4	Controller Board Back Silkscreen . . . . .	94
7.13	PCB Copper Layers . . . . .	95
7.13.1	LPF Board Front CU . . . . .	97
7.13.2	LPF Board Back CU . . . . .	98
7.13.3	Controller Board Front CU . . . . .	99
7.13.4	Controller Board Back CU . . . . .	100
7.14	BOM . . . . .	101
7.14.1	PA Deck . . . . .	101
7.14.2	Controll Board . . . . .	102
7.14.3	TX/RX Relay Board . . . . .	103
7.14.4	LPF Board . . . . .	103
<b>Bibliography</b>		<b>104</b>

## Abstract

This work focuses on the development and characterization of a high power RF amplifier designed for operation in the shortwave spectrum, spanning from 1.8 to 30 MHz. Despite contemporary telecommunication trends favoring high bandwidth and microwave frequencies, the propagation limitations of such high frequencies often necessitate use of relay stations for long distance communication. The short wave spectrum facilitates a long distance point to point communication thanks to ionosphere bounces of EM waves. In order to establish a reliable communication on distance of hundreds or even thousands of kilometers a system with sufficient link budget has to be deployed. Beside high gain antennas, the RF power amplifier is important part of such a system. While the market offers various amplifiers with power higher than 400 W, including both silicon transistor and vacuum tube based options, this work addresses the increasing demand for power-efficient electronics.

This work presents efficient and broadband matching technique for laterally-diffused metal-oxide semiconductor (LDMOS) transistors within a push pull amplifier in the shortwave spectrum. Peak output power of 600 W was obtained for continuous wave operation with power added efficiency of 71.8% at 14.15 MHz. The study has also involved a measurement of six different transformers for return loss across a bandwidth of 1-60 MHz, with three selected transformers further tested in circuit. A comprehensive comparison of output power and power-added efficiency was conducted. Notably, the investigation highlighted the significance of transformer construction in second harmonic cancellation, with the best observed free spectral range of 28 dB for the second harmonic. The finalized version of the amplifier operates in AB class and is able to output more than 500 W from 3.6 to 30 MHz with power added efficiency from 56.7% to 69.96% and 400 W at 1.9 MHz with power added efficiency of 48.4%. Peak power of 600 W is maintained from 5.4 to 18 MHz with gain larger than 18 dB. Points of 1 dB compression were also determined for three transformers and three bands. For a final configuration of the amplifier a simple dual tone test was performed to observe the third and fifth products of intermodulation where it was proven that linearity of the amplifier decreases significantly in the compression region. This part of the research concluded that the recommended input power is only 4 W while maximum safe input power is 7 W.

Designed amplifier is a single-box solution, integrating a switching mode power supply, RF amplifier board, controller, low-pass filters, transmit/receive switching, and a cooling system. The complete system underwent testing for spurious harmonics, with the worst-case scenario exhibiting a spurious harmonic at -53.89 dB below the fundamental signal.

## Keywords:

LDMOS, RF power amplifier, broadband, efficiency, HF, transmission line transformer, TLT, transmitter, amateur radio, short wave, high frequency trading

# Chapter 1

## Theoretical Background

### 1.1 Project Specification

The goal of this work was to design and build a DC to RF efficient high-power amplifier intended to operate in the HF spectrum. Although this spectrum includes ISM bands (Industrial, Scientific, Medical), the primary focus was put on the amateur radio bands. In these bands, Single Sideband (SSB) and continuous wave (CW) are the predominant modulation types. As most amateur base station transceivers come with a 100 W Peak Envelope Power (PEP) output, the power of the amplifier should exceed 400 W, which is 6 dB above the typical station. This 6 dB budget link improvement is often considered a minimum and worthwhile investment when upgrading RF power amplifiers, as it corresponds to an increase in received signal strength by one S unit. The S unit is a commonly used scale in amateur radio receivers and is standardized by the International Amateur Radio Union [1].

The amplifier should possess a high enough gain so that it can be driven to a full power with a low power transmitter. In amateur radio a common power for portable transceivers is 10 W. Therefore the amplifier should have the gain of at least 16 dB in order to reach the power of 400 W with 10 W of input power.

In the context of rising electricity costs and increasing environmental awareness, prioritizing power efficiency becomes a cru-

cial consideration. Given the need for good linearity in single sideband modulation and recognizing that the efficiency curve is dependent on the output power, it is assumed that the peak efficiency should exceed 70%. This aspect warrants thorough investigation, particularly concerning Power Added Efficiency (PAE), a parameter often overlooked in marketing materials.

In order to conform to local regulations, the amplifier should not produce excessive harmonics. The acceptable level of spurious emissions from a radio transmitter is determined by the ITU (International Telecommunication Union), and for amateur radio service, it is specified as 50 dB below the power supplied to the antenna [2]. This criterion is also outlined by the FCC (Federal Communication Commission) in the US. However, the required level of spurious suppression in the US is less stringent, with only 43 dB below the fundamental average power [3].

The designed amplifier must exhibit stability under typical operating conditions and maintain a proper input impedance of  $50 \Omega$  for the transmitter. Additionally, it should incorporate an intuitive and responsive user interface, along with internal monitoring and fail-safe mechanisms. Finally, the device should be fully integrated within a single enclosure, including a power supply, essential control electronics, the amplifier board itself, low-pass filters, etc.

Below is the summary of the goal specification for the project:

- Peak CW output: 600 W PEP (57.8 dBm)
- Bandwidth: 1.8 to 30 MHz (wavelengths from 160 m to 10 m)
- Best case PAE: > 70%
- Gain: > 16 dB
- Harmonics level: < 50 dBc
- Power supply: AC mains single phase (230V)

### 1.1.1 Constraints

Among the numerous constraints that need to be considered when designing a high-power RF amplifier, the power supply section often poses a limiting factor. For a solid-state amplifier, high currents are necessary, while for a vacuum tube amplifier, high voltages are required. Each presents different challenges. However, both solutions demand significant DC power. In this design, special attention must be paid not only to the efficiency of the power supply section but also to whether the mains installation in a building can supply the necessary voltage and current for the power supply unit. Another factor concerning the power supply is its size and mass. These aspects will be further investigated in Sec. 2.8.

Size and mass of the whole amplifier constitute another important aspect. While the goal is not to design a portable device, it is an objective to create a device that is contained in a single enclosure. Components that can contribute significantly to the mass of such a device typically include the power supply and cooling system. While no specific constraint will be imposed on the mass of the amplifier, the size should be kept under 50x50x50 cm. Additionally, the construction should facilitate easy repair and access to the most crucial parts.

Final constraint is the cost of components and their availability. While high power RF amplifiers are expensive devices this project should investigate affordable solutions for RF applications such that they can be presented as affordable alternatives to used surplus or vacuum tube equipment to an average amateur radio operator.

### 1.1.2 Available Technologies

#### Vacuum Tube Amplifier

Vacuum tubes have been used in amateur radio since the 1920s [4]. Even though tubes in low-power applications have been replaced with transistors, they can still be found in RF power systems. An example of a still used and developed vacuum tube in microwave engineering is the traveling wave amplifier, which can provide high gain and output power even at a frequency of 0.34 THz [5].

A vacuum tube is a device in which free electrons flow through a vacuum from the emitting surface (cathode) to the anode, which collects electrons. The flow is controlled by one or more grids. In order to move the electrons from the cathode to the surrounding surface, a sufficiently high temperature needs to be reached, this phenomenon is known as thermionic emission [6]. From these, two characteristics of vacuum tubes follow: they require heating of the cathode and a high voltage between the cathode and anode.

For example, let's consider an 813 tube, which is a general-purpose transmitting beam power tube [7]. The datasheet claims that under Intermittent Commercial or Amateur Service (ICAS), a single tube can output 375 W with an input of only 4 W. The power supply for an amplifier with an 813 would require about 2.5 kV anode voltage with more than 300 mA anode current. The next consideration would be the driving scheme. The designer can either ground the

grids and drive the cathode for higher output power or use a more typical grid modulation for higher gain. The grid configuration also requires an additional second grid voltage, which is 750 V. For both cases, the bias voltage needs to be considered. For the 813, a value of 50 mA is specified for the AB class, resulting in 125 W of plate dissipation. Additionally, one has to account for the heater filament, which needs to be constantly powered to keep the cathode heated. In the 813, the heating filament is powered by 10 V at 5 A, resulting in 50 W of additional power draw at all times.

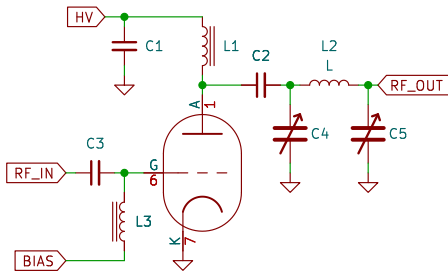


Figure 1.1: Schematic of a simplified tube RF amplifier

Tube amplifiers operated in class A or AB have low harmonic content, and they exhibit low nonlinear distortion when used in plate amplitude modulation circuits [8].

Advantages of tube amplifiers:

- + Good linearity
- + Cheap tubes are available
- + Robust to high SWR

Disadvantages of tube amplifiers:

- Tunable output matching network
- Lethal anode voltages
- Low efficiency
- Loss of emission over time

Overall, while tubes themselves are relatively inexpensive and can provide high power with good linearity, building a suitable power supply is neither easy nor cheap. This is because it requires a high-voltage transformer or a multiplier circuit with a transformer that has a high current capability.

## Solid State

For a long time, tube amplifiers dominated the domain of high-power RF amplifiers. Early solid-state amplifiers could only provide relatively small power therefore, power combiners had to be used to couple multiple smaller amplifiers in order to achieve higher power. However, combining power decreases efficiency, as each combiner adds loss to the system, along with potential phase errors [9].

To this day, high-power BJTs provide a limited output power of 300 to 600 Watts due to factors such as intrinsic limitations of the BJT or the ability to evacuate the heat dissipated in the die [8]. For example, one can examine the datasheet of the MRF448 produced by MACOM, a manufacturer with a rich portfolio of power RF BJT devices. This transistor is specified for an output power of 250 W up to 30 MHz when the collector is supplied by 50 V at a continuous current of 16 A [10]. These types of transistors use special flange packages for improved heat conductivity (see Fig. 1.2). The manufacturer claims IMD of up to -30 dB, which is a good reference value from a dual-tone test and will be discussed later. Unfortunately, the MRF448 has a typical gain of 14 dB, which is not sufficient for our application requirements. Therefore, an additional amplifier stage would have to be added in a cascade configuration. Furthermore, this BJT transistor achieves a collector efficiency of 65% for CW, which falls below our desired 70%. It is also noteworthy that the BJT is less rugged, it can withstand a 3:1 SWR at all phase angles, which is much less than what a tube amplifier can withstand.

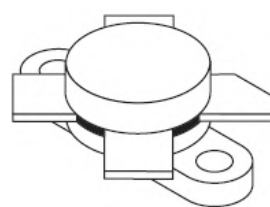


Figure 1.2: Flange case of MRF448

Advantages of RF BJT devices:

- + Small package
- + Easier manufacturing
- + Less power consumption in idle
- + Good mechanical robustness
- + Output matching can have a wide bandwidth

Disadvantages of RF BJT devices:

- Cannot withstand high VSWR or temperature
- Relatively small power per unit, requires coupling

## LDMOS

Another category of solid-state devices is the MOSFET. While it is possible to create an RF power amplifier using traditional power MOSFETs [11], the gate capacitance and internal parasitics do not make them suitable for high-power RF devices. Instead, lateral diffused metal oxide semiconductor (LDMOS) technology is used. In LDMOS, the structure can withstand large drain voltages without significant changes to the electrical channel length [8].

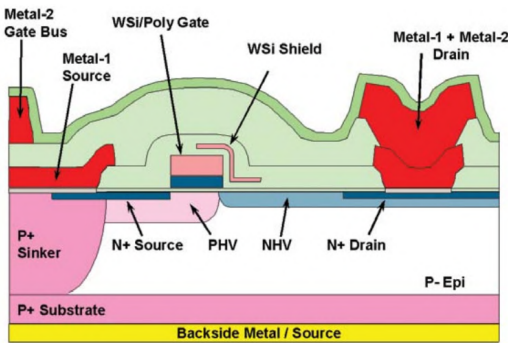


Figure 1.3: LDMOS structure, source metal connects N+ to P+ sinker which connects through P+ substrate to back metal this lowers inductance[12]. Ground shield between gate and drift region lowers transfer capacitance[13] allowing for operation at higher frequencies.

Catastrophic failure in MOSFET devices occurs due to internal power dissipation, which is related to high VSWR resulting from improper matching and drain efficiency. Freescale (now NXP) has developed an enhanced ruggedness 50 V LD-MOS structure that can withstand a VSWR higher than 65:1 at all phase angles while still maintaining rated power [12]. Transistors developed in this EVHV6 50V LD-MOS process are aimed at the ISM market, for example, CO<sub>2</sub> lasers or plasma generators where load impedance changes. NXP offers such LDMOS transistors in a range of powers from 100 W to 1800 W, where the larger devices are actually adapted to work in a push-pull configuration containing two transistors in one package. For example, the MRFX1K80H can be used to create an amplifier with an output of 1800 W with narrow-band matching circuits [14].

A similar transistor was described in an application report prepared by NXP, demonstrating a 1300 W amplifier working in the range of 2-30 MHz using the BLF188XR transistor with a peak efficiency of 81.4% [15]. The evaluation board created by NXP for the BLF188XR uses a transmission line transformer (TLT) as a means of output impedance matching, a method that will be further described in Sec. 2.3.2.

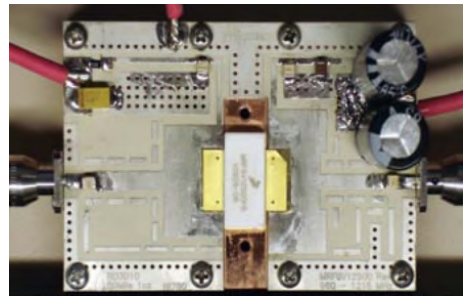


Figure 1.4: MRF6V12500HS broadband test fixture by NXP, output power of pulsed 500 W for 960 to 1215 MHz was obtained[12]. It can be seen that microstrip stepped impedance matching is being used.

Switching mode power amplifiers operating in spectrum 3-26 MHz can achieve efficiency of 74 %[16].

Advantages of LDMOS:

- + Very robust to impedance mismatch
- + Simple biasing
- + High drain efficiency
- + Wide bandwidth
- + Lots of devices on the market
- + Ready for easy push-pull operation

Disadvantage of LDMOS:

- High power packages require special mounting

The chosen transistor for this project is the MRF300, a 50 V LDMOS transistor produced by NXP that provides 300 W of CW power output [17]. This LDMOS device is specified for a frequency range from 1.8 MHz to 250 MHz and can withstand a VSWR of 65:1 at all phase angles. With efficiency claims of up to 80% and a gain of 26 dB, this device is a good candidate as a power transistor for this project. Additionally, the MRF300 comes in a TO-247-3 package, which is common in power electronics but not in RF devices. This significantly lowers the cost of the transistor but is most likely also a reason for the relatively low cutoff frequency. The MRF300 comes in two versions of the same package, A and B. While in both cases the source pin is in the middle, the gate and source are swapped between the A and B variants (Fig. 1.5). This allows for a simplified push-pull layout of a PCB, which will be demonstrated in Sec. 2.7.

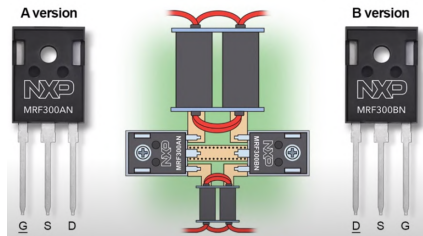


Figure 1.5: Push-pull configuration of MRF300A and MRF300B

### 1.1.3 Market Solutions

In order to estimate the acceptable cost of an amplifier with the desired specifications stated in Sec. 1.1, it is worth checking off-the-shelf market products.

The amateur radio market still offers tube amplifiers, which tend to be the cheapest option. For example, the Ameritron AL-811 is a 600 W CW amplifier based on the 811A tube and costs approximately \$1500 at the time of writing. The manufacturer does not specify efficiency, but the amplifier draws 1200 W from the mains and requires typically 65 W of input power [18]. This amplifier is a bare minimum and requires manual tuning. On the other hand, Ameritron also offers a solid-state solution, the ALS-600s, which costs \$2400 and uses four MRF150 RF power FETs from MACOM [19]. The ALS-600, uses an external power supply and covers the 10 m band only in the more expensive version ALS-600x, which costs \$2500. If one wants a digital display of power, as was the desired specification in Sec. 1.1, the price only goes up. RM Italy offers a BLA600 amplifier for a price of \$2800, this amplifier also includes coverage of the 6 m band.

There are also amplifiers sold in the form of kits or modules. Noteworthy in this category is the RF amplifier board developed by Razvan Fatu, which won second place in an NXP design contest. Razvan has designed a deck for an RF amplifier that provides about 600 W CW power with more than 60% efficiency and operates from 1.8 to 54 MHz [20]. This project was originally the inspiration for the work presented here. Razvan's board, together with MRF300 transistors, can be purchased in kit form for \$400. Buyers also need to add a power supply, control circuits, low-pass filters, and housing. Continuing the research and design initiated by Razvan Fatu, this work will present the benefits of LDMOS technology and attempt to demonstrate that due to its low cost and high efficiency, LDMOS provides better value per dollar in comparison to quite obsolete tubes.

# Chapter 2

## Electrical design

### 2.1 Designed Amplifier - Forte 600

#### 2.1.1 Block Diagram

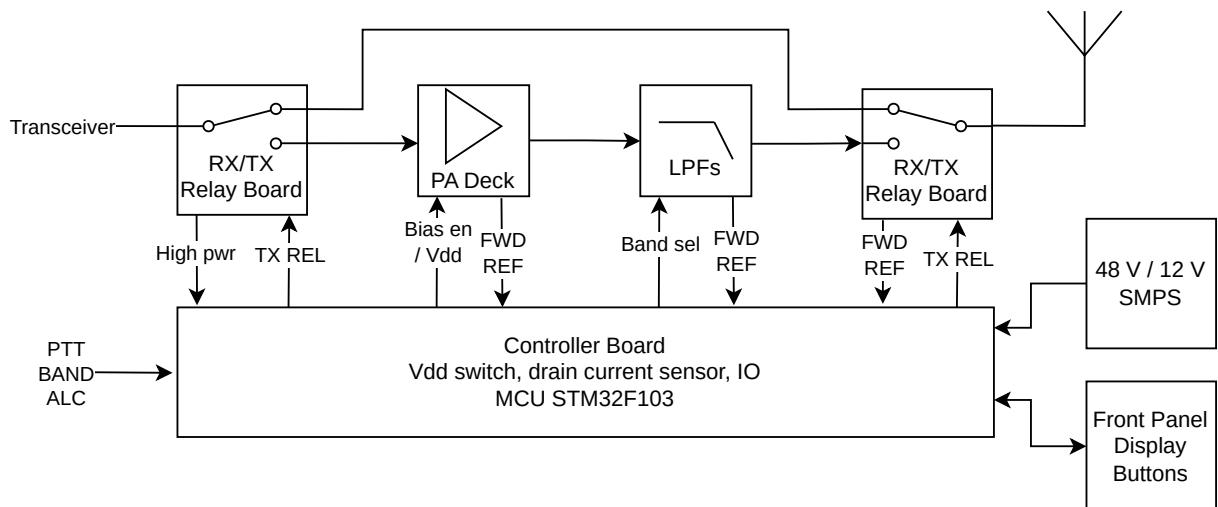


Figure 2.1: Block diagram of the amplifier

The amplifier designed during this project was named Forte 600. This section describes the theory of operation of each element of the amplifier. A modular design approach was used during the development, so the amplifier as a whole device is split into distinctive modules and PCBs.

The front panel and display interface was constructed using point to point wiring so that no large PCB had to be ordered, minimizing prototyping cost. Due to the relatively low frequencies, all designed boards can be manufactured on a FR-4 substrate.

Because of the  $50 \Omega$  impedance or lower, there is no risk of breakdown voltage for this type of substrate at 600 W of power.

Several PCBs were designed to accommodate the modular approach. These include:

- TX/RX Relay board
- Controller board
- PA Deck board
- LPFs bank board

## 2.2 Theory of Operation

### 2.2.1 RX/TX Board

The main role of the receive/transmit board is to switch the signal path inside the amplifier during transmit mode. When the transceiver is receiving, the amplifier serves as the pass-through connection between the transceiver (TRX) and antenna. On transmit, the RX/TX board switches the antenna to the output of the low-pass filter board (LPF in Fig. 2.1) and the output of the TRX to the PA deck board, which contains the MRF300 transistors. Additionally, the RX/TX board contains a directional coupler that can measure input power to the amplifier. This coupler is an example of a lumped element coupler known as a tandem match.

### Tandem Match Circuit

Measurement of VSWR is an important aspect in every RF system, and it becomes particularly crucial when high powers are a concern. When a source and impedance load are not ideally matched, a reflection wave can be observed in a transmission line that connects the source and load. This reflected wave travels across the transmission line and together with the forward-propagating wave, creates a standing wave pattern [21]. This pattern will have minima and maxima separated by:

$$l = \frac{\pi}{2\beta} = \frac{\lambda}{4} \quad (2.1)$$

Where  $\lambda$  is a wavelength and  $\beta = \omega\sqrt{LC}$  is a propagation constant. Measuring the voltage maxima and minima in the pattern knowing that they are spaced by a quarter wavelength it is possible to determine the VSWR since its definition is given as a voltage ratio:

$$VSWR = \frac{V_{MAX}}{V_{MIN}} = \frac{1 + |\Gamma|}{1 - |\Gamma|} \quad (2.2)$$

Where  $\Gamma$  is the reflection coefficient, such that  $\Gamma \in [-1, 1]$ . From Equations 2.1 and

2.2, it can be seen that in order to measure VSWR, a coupler would need to sample a voltage at two points separated by  $\lambda/4$ . Such a solution is possible for higher frequencies using microstrip structures or slotted line. However, for a wavelength of 10 m and higher, lumped element circuits are used instead, which can measure the voltages only at one point. The Tandem match is a circuit that uses two transformers to sample the voltage and current. Measurements made with such a coupler can be interpreted as an actual representation of forward and reflected waves only when the circuit is matched to the characteristic impedance of a transmission line [22].

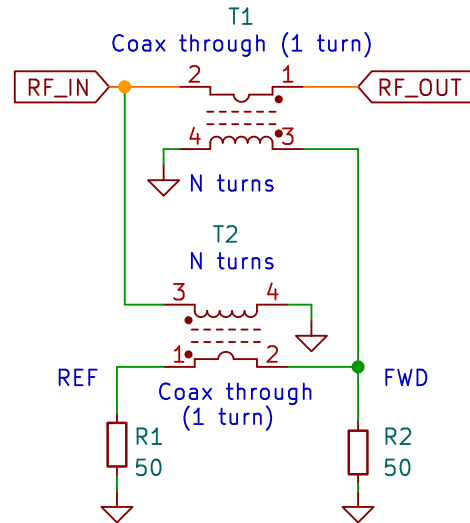


Figure 2.2: Schematic of a Tandem match

Derivation of the coupler's equation for voltages across  $R_1$  and  $R_2$  using current and voltage sensing independent transformer models and superposition theorem is presented by Jeffrey Anderson (K6JCA) in [22].

$$V_{R2} = -V_{R1} \cdot \frac{Z_{Load} - 50}{Z_{Load} + 50} \quad (2.3)$$

With the negative voltage denoting  $180^\circ$  phase difference. From here the relationship with VSWR formula in 2.2 can be seen, so the reflection coefficient can be calculated.

$$\Gamma = \frac{Z_{Load} - Z_0}{Z_{Load} + Z_0} \quad (2.4)$$

This property will be used especially at the output of the amplifier to protect the

final transistors from being damaged due to high SWR. However, the transistors cannot also handle excessive input power to their gates. Here, the forward voltage across R2 (see Fig. 2.2) can be rectified using a diode, and the obtained DC voltage will be proportional to the power going from the input port of the coupler to the pass through port. However, the diode is a nonlinear device with some offset of about 0.6 V. Several analog compensation methods are available, such as using the precision rectifier with a diode in the feedback of an op-amp [23]. Ultimately, a Schottky diode was used to lower the offset voltage, and the nonlinearity for the lower power will be compensated in software using a numerical regression method. To test the input coupler forward output voltage vs. the input RF power, a 20 W amateur radio transceiver, Xiegu G90, was used in CW mode. Power was stepped, and the DC voltage was noted.

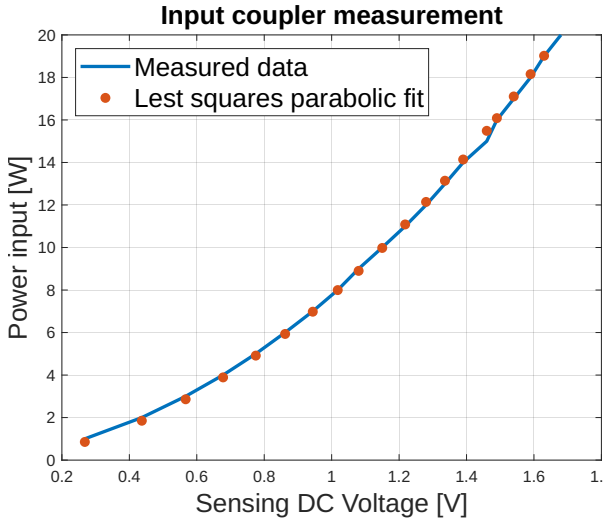


Figure 2.3: Characteristics of coupler

As seen in Fig. 2.3, the characteristic of the sensing forward voltage is nonlinear. However, a simple polynomial can be used to accurately approximate it. This can be calculated in software so that when the input power is larger than a given amount, the relays are switched back to receive mode, preventing the amplifier from damage. In Matlab, a least squares nonlinear regression was implemented [24], a quadratic equation

was obtained for the curve describing:

$$P_{IN}(U[V]) = 6.23 \cdot U^2 + 1.24 \cdot U + 0.273 \text{ [W]} \quad (2.5)$$

T1 was made using a FT50-61 toroid, with the primary winding formed by the core of the RG142 coax, and the secondary was wound using 30 turns of copper enameled wire. T2 was wound on a FT82-61 core, with RG213 coax serving as the secondary and 30 turns as the primary winding.

## Over Power Protection

An analog protection circuit was designed that uses a comparator (U2 in Fig. 2.4) to switch the input, using PIN diodes, to a dummy load. This method is expected to be faster than a mechanical relay and serves as a secondary measure in case of a software glitch in the microcontroller.

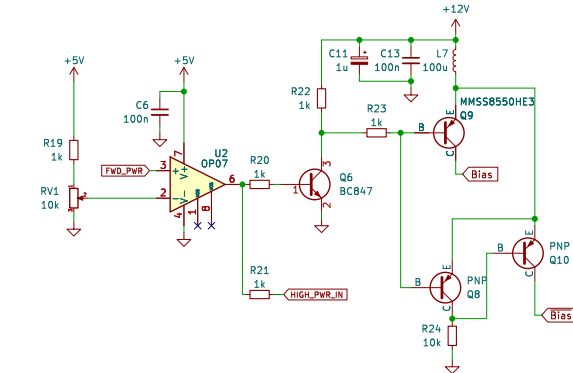


Figure 2.4: Schematic of analog protection

During normal operation, the transistor Q6 (see Fig. 2.4) is open, and the transistor Q10 is fully open, providing approximately 100 mA to the PIN diode, making it conduct with low loss. When the voltage from the forward power detector crosses the threshold set by potentiometer RV1, the comparator turns on the base of Q6. This acts like a negation of bias, lowering the voltage on the bases of Q9 and Q8 by about 0.7 V, which shuts down Q10 and opens Q9, providing about 58 mA of bias for the PIN diode. This redirects excessive RF power into a dummy load using SPDT PIN diode switch (see Fig. 2.5).

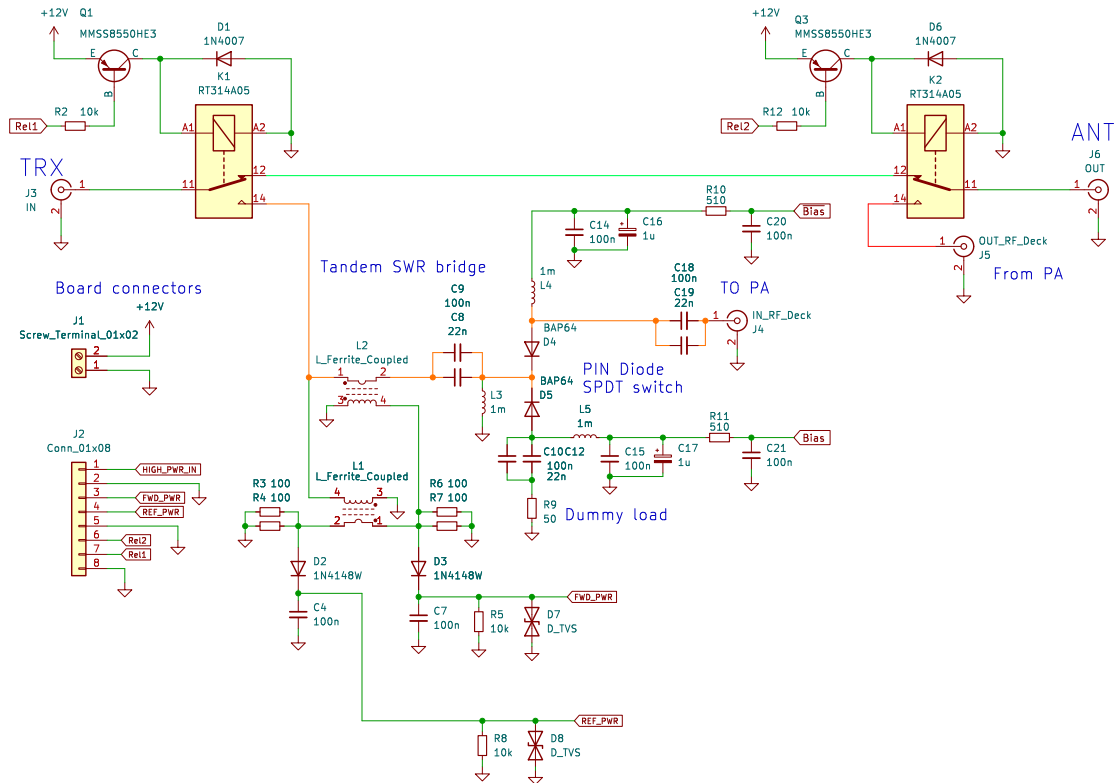


Figure 2.5: Schematic of transmit/receive PCB

During testing, some problems were encountered with the circuit that switches the PIN diodes. Firstly, for a frequency of 1.8 MHz, a very high inductance is necessary to provide sufficient choking of RF from passing to the DC section. The equivalent resistance of an inductor for frequency  $f$  is given as  $2\pi fL$ . It was discovered that even with  $470 \mu H$  inductors the choking was not sufficient and so the inductor was overheating when more than 5 W was applied to the input board. In addition, the circuit shown in Fig. 2.4 would benefit from a latch circuit that blocks the operation of the amplifier until it is reset, instead of temporarily disconnecting the input. During testing, it was found that the software overpower protection is sufficient, as the coupler measurement was precise, and the real-time operating system allowed for fast interrupts when necessary. This analog protection circuit might be beneficial for customers expecting harsh environments. The amplifier board also features a diode clamping circuit that adds another layer of overpower protection for the LDMOS gates.



Figure 2.6: Assembled TX/RX PCB

The first iteration of the board included op-amps for amplifying the signal from the detector diodes, this was found to be unnecessary, so the op-amps were bypassed. The relays used are non-latching RM85 12 V SPDT relays, rated for 250 V at 16 A AC. An important aspect of the designed PCB was the separation between the input and output. For this purpose, a location for soldering the electromagnetic (EM) shield was added between the relays.

### 2.2.2 Controller Board

The controller board has two main functions: first, it switches the 48 V drain power supply, and second, it collects and sends signals from and to various other modules of the amplifier. The LDMOS transistors in this project require both bias voltage across the source and gate to put them in the correct class of operation, as well as a source to drain voltage. In this project, both of these can be turned on and off by the control board, allowing for multiple ways of emergency shutdown in case of a failure. The 48 V supply rail directly connects to the control board, which contains a MOSFET (Q2) acting as a switch (see Fig. 2.7).

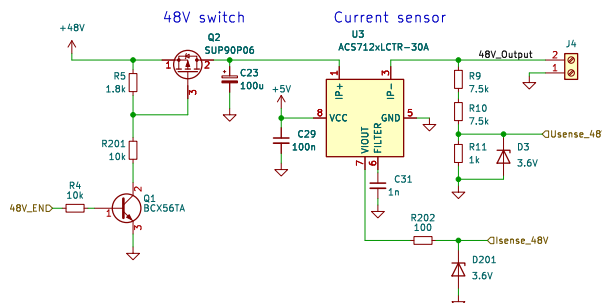


Figure 2.7: 48 V rail schematic

#### 48 V Rail Switch

For a switching transistor, a SUP90P06 P-channel MOSFET was chosen. It can withstand 60 V across the drain and source, providing  $R_{DS}$  smaller than  $15 \text{ m}\Omega$  for  $V_{GS} = -10 \text{ V}$ , at which the datasheet specifies a maximum current of -67 A[25]. The maximal gate to source voltage for this MOSFET is  $\pm 20 \text{ V}$ . Resistors R5 and R201 were chosen to set the gate-to-source voltage close to 14 V when transistor Q1 is closed. Transistor Q1 is a general-purpose switching transistor that can withstand more than 50 V between collector and emitter. The base of Q1 is driven by a microcontroller pin through the R4 current limiting resistor. When Q1 is open (logic pin is low), the difference between the gate and source on Q2 is small, and the MOSFET is closed, shut-

ting down the 48 V rail for the amplifier. According to the performed LTspice simulation, the Q2 MOSFET does not dissipate more than 3 W of power at a 20 A load. While this is not a large amount, an increase in temperature causes an increase in resistance. Therefore, the MOSFET was placed in a cutout of the PCB with a heatsink beneath it.

#### Drain Current Sensor

Monitoring the drain current is a vital aspect of ensuring reliable operation. The control board measures the sum of currents that go to both transistor drains using a Hall-effect based linear current sensor IC. The sensor used is the ACS712, produced by Allegro Microsystems. It outputs a DC voltage that is proportional to the DC or AC current flowing through a conductive path that is galvanically isolated from other signal pins[26].

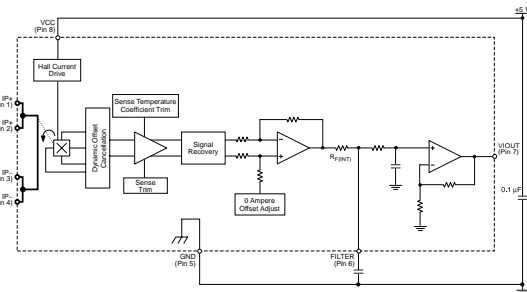


Figure 2.8: Diagram of ACS712[26].

This is a ratiometric output sensor supplied by the 5 V rail, meaning that the output is scaled to the supply rail. For zero current flow through the sensor, the output voltage is half of the supply rail. Knowing that the sensitivity of the sensor is 66 mV/A, the drain current can be calculated in software using Equation 2.6.

$$I_D(U_{Sensor}) = \frac{U_{Sensor} - \frac{V_{DD}}{2}}{0.066} \quad (2.6)$$

The output of the 48 V rail also features a voltage divider built with resistors R9, R10, and R11. It divides the drain voltage

rail by a factor of 15, which for 48 V gives 3.2 V, well suited for a 3.3 V microcontroller's ADC. For every analog signal that goes to a microcontroller, a small value resistor ( $100 \Omega$ ) and a 3.6 V Zener diode was added as a simple clamp circuit.

Additionally, 100 nF capacitors provide a low impedance path for any stray RF in the circuit, which could normally build up due to the high ADC impedance. It was found that additional decoupling was especially necessary on the divider output. Otherwise, the microcontroller would often detect too high voltage on the drains. After many SMD capacitors in parallel were added ( $10 \mu\text{F} \parallel 1 \mu\text{F} \parallel 100 \text{ nF} \parallel 10 \text{ nF}$ ), the problem was solved. Notice that in the voltage divider, two resistors were used in the upper part to increase the creepage voltage from the high side of the rail. This is because 0805 resistors were used to reduce the overall footprint.

## Relay Driving

The controller board features two outputs for controlling 12 V relays. The output consists of a 12 V rail and the collector of an NPN transistor (Q5 in fig 2.9) with a flywheel diode across it for back EMF protection. Note that this is a universal output to control an external relay. However, for use with the system presented in Fig. 2.5, a  $10 \text{ k}\Omega$  resistor has to be placed across terminal J5.

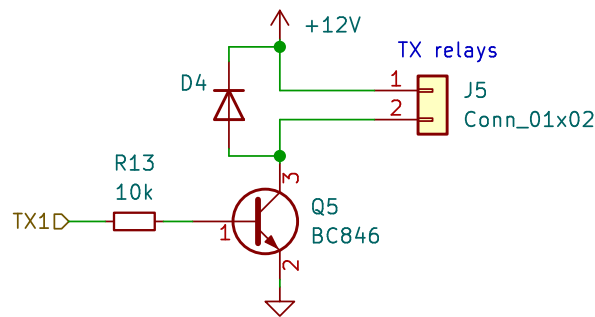


Figure 2.9: Relay driver schematic

## Temperature Sensors

The control board facilitates the option to connect multiple temperature sensors on a single-wire interface bus. By default, the software scans for available devices and expects to find two, corresponding to each output transistor. Extra sensors can be added for PSU monitoring or when two PA decks are coupled to create higher power. This flexibility allows the control board to be used not only in Forte 600 but also in other modern RF amplifiers or in modernized amplifiers that previously did not feature digital monitoring. The temperature sensor to be used is the DS18B20, which is a digital thermometer with programmable resolution from 9 to 12 bits in the range from  $-55^{\circ}\text{C}$  to  $+125^{\circ}\text{C}$ [27]. The sensor allows for a precise 12-bit measurement however, it will require more time for data transmission, especially when more devices on the same one-wire bus are present. This, was found not to be a limitation in the project. In fact, the temperature is measured every 100 ms and is controlled by the real-time operating system in the microcontroller.

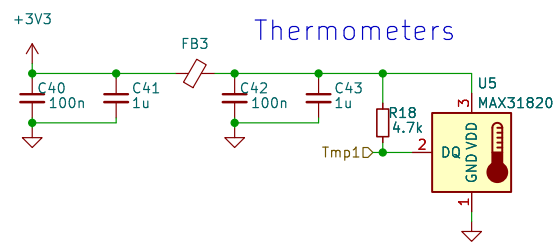


Figure 2.10: Temperature sensors schematic

## Fan Speed Control

To enhance user comfort and minimize fan usage, a PWM signal is generated by the microcontroller to regulate the speed of both fans. The appropriate duty cycle of the PWM signal is chosen based on the fan curve. The fan will start with a default speed of 20% when the temperature of any sensor is below  $T_0 = 28^{\circ}\text{C}$ . Then, the fan linearly increases its speed up to 100% for  $T_{\text{max}} = 55^{\circ}\text{C}$ .

## 2. Electrical design

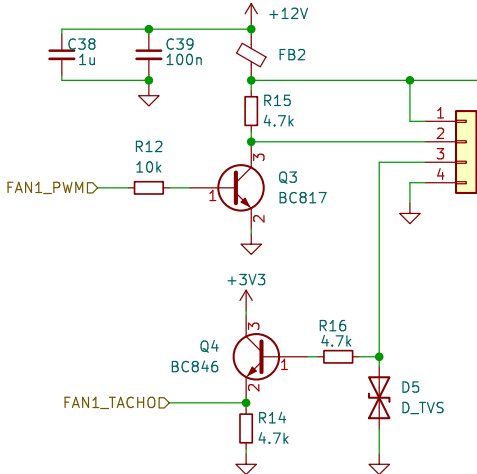


Figure 2.11: Fan controller schematic

The PWM signal is a square wave that opens and closes Q3. According to this modulation, the resistor between the 12 V rail and collector of Q3 generates the same waveform but with a larger peak to peak value. This signal can be used to control a PWM DC fan. More advanced fans can also feature a tachometer that allows the master device to read the rotational speed of the blades. This is useful in control loops where precise rotation is desired, but it can also be used to detect the failure of a fan to spin. The control board features a common collector transistor Q4 connected to 3.3 V and a  $4.7\text{ k}\Omega$  shunt resistor connected to the emitter, serving as an output connected to the I/O of the microcontroller. The base of Q4 is connected through the current-limiting resistor R16 to the output of the fan with tachometer capability. A Transil diode D5 is added to protect Q4 from unexpected spikes and it also helps to shape the square waveform.

### PTT

Push To Talk, or PTT, is a circuit that receives an external signal from the transceiver and switches the amplifier into transmit mode. The circuit is adapted to accept a wide range of input voltages, and it also includes an optical isolator (U401, see Fig. 2.12) because different transceivers might use various signal levels. The output

is taken from the collector of Q402. This signal can then be used by the microcontroller to detect an incoming PTT signal.

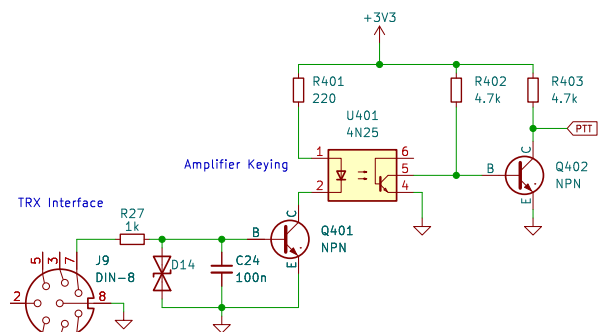


Figure 2.12: PTT schematic

### Band Switching

Similarly to PTT, different transceivers use different signaling methods to communicate the currently selected band to external peripheral devices. The amplifier needs to know which band the transceiver is going to transmit on because, before transmission, a proper low pass filter needs to be switched. Two of the most popular methods were implemented in the control board. The first is the 3-bit binary code. Although many transceivers use 4-bit binary coding, the used MCU has a limited number of pins, and the amplifier has 6 filters, so 3 bits are the minimum. The truth table used for band decoding is shown in table 2.1. If the need arises for communication with a 4-bit output, a simple translation device can be implemented on any microcontroller with a sufficient number of pins. External input and output signals are treated as potential sources of EMI and ESD. Therefore, a  $\pi$  network of capacitors and TVS diodes alongside series resistors is used to eliminate voltage spikes and high frequency content. The signals switching on those lines are in the order of Hz, so the low pass filters used here don't attenuate the desired content.

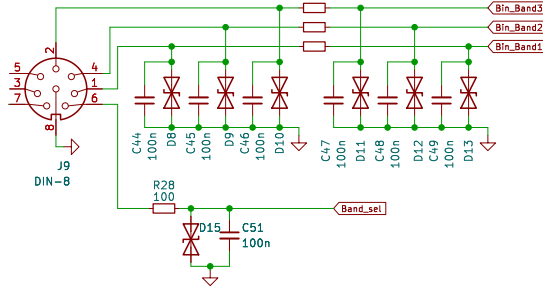


Figure 2.13: Band information input

Decimal	Band [m]	B1	B2	B3
1	160	0	0	1
2	80	0	1	0
3	40-30	0	1	1
4	20-17	1	0	0
5	15-10	1	0	1
6	6	1	1	0

Table 2.1: Truth table for band decoding

The second option for band switching is the analog voltage method, where the ranges of DC voltage dictate the current band selection. This method was used by the test transceiver during the development of the amplifier. The table of bands and corresponding ranges of voltages is shown below.

Decimal	Band [m]	Range [mV]
1	160	$\leq 250$
2	80	(250, 500>
3	40-30	(750, 1250>
4	20-17	(1250, 1650>
5	15-10	(1650, 2500>
6	6	>2500

Table 2.2: The voltage ranges for analog band switching. The discontinuity between the second and third range arises from the fact that on the 60 m band, the legal power limit is very small. The amplifier will refuse to operate for any undefined band.

Using the front panel, the user can switch between manual (M), analog voltage (V), and binary mode (B). The manual mode utilizes the front panel microcontroller to override the binary inputs. While

this is a simple solution, it presents a disadvantage in the exclusivity of manual and binary mode. Specifically, the binary mode cable should not be connected when the manual mode is selected.

## Microcontroller

The microcontroller gathers signals from the board and generates appropriate control signals based on prepared software algorithms. For this project, the STM32F103C8T6 was chosen. This is an inexpensive 32-bit microcontroller with an ARM Cortex-M3 core, a 72 MHz master clock, and 64 KiB of flash memory, as well as 20 KiB of RAM[28]. Because the control board's first revision was seen as a prototype, the BluePill development board from WeAct was used. This board originates from China, but in comparison to many other clones, it contains the original STM32 microcontroller, which allows for easy SWD connection.

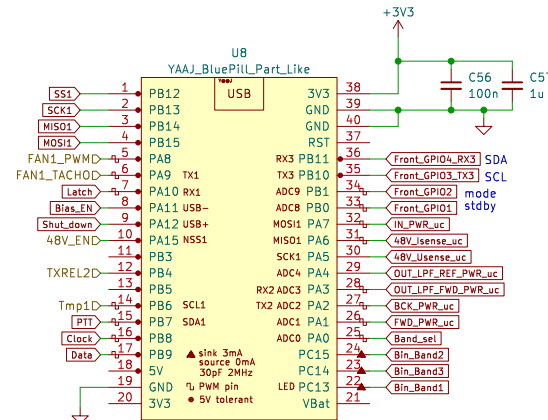


Figure 2.14: Microcontroller schematic

The control board is one of the elements of Forte 600 that sets this amplifier apart from cheaper entry level amplifiers. Featuring digital control over all aspects of the amplifier, a liquid crystal display, flexibility for future expansion, and multiple layers of protection are key aspects of a modern RF amplifier.

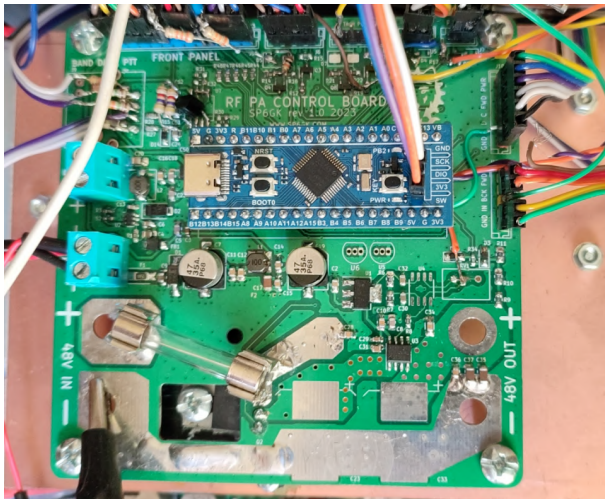


Figure 2.15: Control board during hardware in the loop testing

### Front Panel

In order to enhance user convenience, all important buttons and indicators of the amplifier operation are present on the front panel. To minimize the cost of the prototype, instead of using a PCB, a point to point wiring technique was employed to connect the modules that make up the panel. These modules themselves are placed in a 3D printed piece. At the top left of the panel, a 16x2 liquid crystal display module with the HD44780 controller IC[29] was mounted. It communicates with the control board using the PCF8574 8-bit I/O I<sub>2</sub>C expander IC[30].

On the right side of the display, a bar graph LED display was placed. The top bar graph has a row of 30 diodes, which, for a maximum scale of 600 W, gives 20 W per diode as resolution. The two bottom bar graphs each have 10 diodes. The one on the left displays SWR with a maximum scale of 3:1, and the one on the right displays total drain current with a maximal scale of 20 A. Each row of LEDs changes color from green to yellow and then red as the indicated value increases. The LEDs used for the bar graph display are multiplexed using the MAX7219, which is a serially interfaced 8-digit LED display driver[31] connected to the control board using SPI.

Below the LCD, three LEDs are placed to indicate the supply power (PWR), transmit mode (TX), and failure detected warning (WARN). When controller detects fault or abnormality it flashes the orange WARN LED and displays error code with short description on the LCD screen. Refer to Sec. 7.7.1 for description of error codes and troubleshooting steps.



Figure 2.16: Back of the panel assembly

Finally at the bottom of the panel a row of semi transparent push buttons with illuminated background is situated. These buttons are used for changing the mode of band selection, standby mode (amplifier acts as a pass through at all time) and 6 buttons for manual selection of the bands. Selection of the bands is translated to a 3 bit binary number using Arduino Nano, this microcontroller also uses its EEPROM memory to remember last used mode and selected band so that even after shutdown the amplifier will startup with last remembered settings.



Figure 2.17: Front panel during operation

### 2.2.3 Low Pass Filters

As mentioned previously in Sec. 1.1, for SSB operation the amplifier should ideally be linear. A linear system is a special class of system for which the output is the sum or superposition of the inputs [32]. In other words, a linear system has to satisfy the following properties at all times for all inputs:

- Additivity:  $\forall x_1, \forall x_2$   
 $f(x_1) + f(x_2) = f(x_1 + x_2)$
- Homogeneity (scaling):  $\forall x, \forall a$   
 $f(x) = y \wedge a \cdot f(x) = a \cdot y$

This means that a linear amplifier should ideally only output the signal that was provided at the input but with a higher magnitude. However, active components are used in the amplifier, and each active component exhibits inherent nonlinearities. Because of these nonlinearities, the output from the amplifier is not fully linear, meaning that some new signals will be produced even if the input signal is a pure continuous wave signal. These new signals include both intermodulation products, which are close to the fundamental signals and cannot be filtered (see Sec. 4.9 for characterization of IMD3), and harmonics, which occur at multiples of frequencies of the fundamental signal. The latter can be attenuated using appropriate low pass filters.

Initially, the filter was designed using a method presented in the book "Experimental Methods in RF Design" [33]. This method starts with normalized values  $g(n)$  for a filter that has a cutoff frequency of  $\frac{1}{2\pi}$  and a termination impedance of  $1 \Omega$ . The book provides a table with values of  $g$  for the desired polynomial type and pass band ripple so that the normalized values can be scaled to obtain the desired L and C component values.

$$L(n) = \frac{g(n) \cdot R_0}{2\pi f} \quad (2.7)$$

$$C(n) = \frac{g(n)}{R_0 \cdot 2\pi f} \quad (2.8)$$

Where  $R_0$  is the termination impedance of the filter. Here, we take the characteristic impedance of the system, which is  $50 \Omega$ . A Chebyshev type filter of 7th order with 0.1 dB ripple in the passband was chosen as a design prototype, using the coefficients from Equation 2.9.

$$g = (1.18, 1.423, 2.097, 1.573, 2.097, 1.423, 1.18) \quad (2.9)$$

Using Equation 2.7 and coefficients from 2.9, a Matlab script was written to compute the necessary components L and C for a desired frequency. Note that this method does not treat the desired frequency as the -3 dB cutoff but rather as the point where the filter starts the transition into the cutoff region. For a test of the script, a 50 MHz LPF was calculated, and the following components were obtained:

- Capacitors 75.21, 133.49, 133.49, 75.21 [pF]
- Inductors 0.22  $\mu H$ , 0.25  $\mu H$ , 0.22  $\mu H$

The used topology consists of multiple  $\pi$  networks with series inductors and shunt capacitors. Notice that for  $n=7$ , there are more capacitors than inductors if the capacitors are shunts. This is beneficial since inductors for low frequencies tend to be more problematic, they require special cores and have large footprints, while capacitors come in small SMD packages and are cheaper.

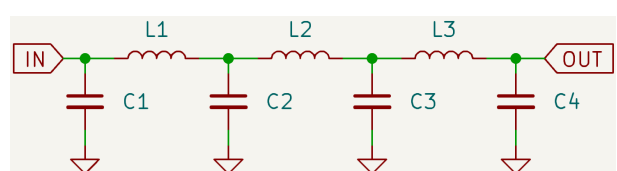


Figure 2.18: Schematic of used LPFs

Filter was then tested in AWR Designer using closed form simulation.

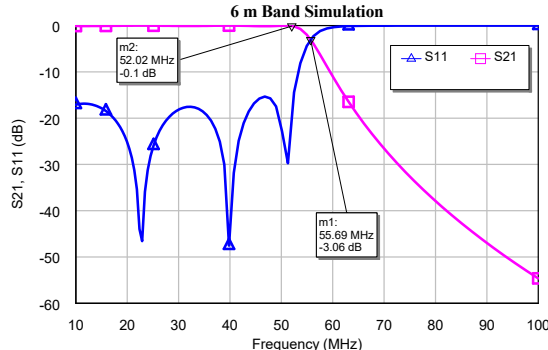


Figure 2.19: Simulation of designed LPF

In Fig. 2.19, it can be seen that the designed filter transitions very close to the desired frequency of 50 MHz. It can be seen that the passband region is very flat and return loss is better than 10 dB in the entire pass band. For a cross validation of the design method a low pass filter for 6 m band was also simulated in LT-Spice. In Spice simulation end of the passband experienced 0.12 dB ripple with a minimum at 47.6 MHz, followed by a peak at 51.2 MHz, which then starts the transition into the stop band. The designed LPF board features 6 filters, some of which combine bands that are relatively close in frequency. Fig. 2.20 shows a plot with all simulated filter S21 traces.

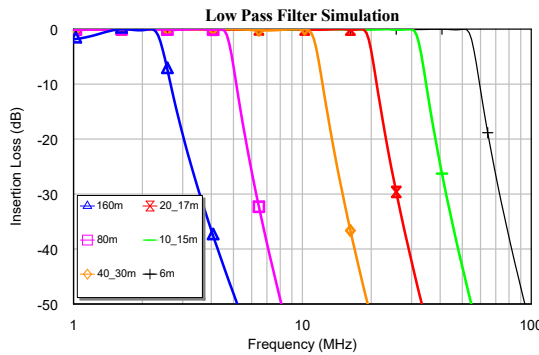


Figure 2.20: Simulation of designed LPFs

The Matlab script produces correct values of capacitors and inductors in pF and  $\mu H$ , however, those values are impractical for lumped elements. In practice, the values had to be rounded to the closest E24

series values. For capacitors, the difference between calculated values and the real value was minimized by connecting four capacitors in parallel for each band, except for the 160 m band, where a large value of capacitance was needed, and six parallel capacitors were used for each filter section. The parallel connection of capacitors also has the advantage of lowering their equivalent series resistance (ESR). Since parasitic inductance and resistance of capacitors are now minimized, their handling of high RF currents should be improved. Additionally, only capacitors with NPO/C0G dielectric with a 1 kV or more rating are used in the filter. In order to provide sufficient creepage distance, the 1206 SMD package was chosen.

### Choice of Inductor Cores

Inductors used in the designed filters should have low resistance to achieve a high quality factor and minimize the insertion loss. The quality factor of an inductor at frequency  $f$  can be calculated using Equation 2.10.

$$Q_L = \frac{2\pi f}{R_L} \quad (2.10)$$

Since the frequencies in this project are relatively low, the calculated inductance is quite high. Some topologies can reduce this inductance. The previously presented Chebyshev filter would require  $5.44 \mu H$  for the 160 m band. Therefore, for 160 m an ultra-spherical filter of the 5th order was used. This prototype of a filter is characterized by a larger ripple but also a steeper transition region[33]. With this change, instead of two  $4.9 \mu H$  and one  $5.44 \mu H$  inductors, only two  $3 \mu H$  inductors are necessary. Furthermore, inductors can be wound on a ferromagnetic material with high permeability to increase inductance:

$$L = \mu_r \frac{N^2 A}{2\pi r} \quad (2.11)$$

Where  $\mu_r$  is the relative permeability (a measure of how easily the material is mag-

netized),  $A$  is the cross-sectional area of the toroid, and  $r$  is the radius of the toroid. This formula is similar to the formula for a single layer cylindrical core where  $2\pi r$  is replaced by the length of the coil.

For a proper design, a material specified for the used frequency has to be chosen, the core should also be of sufficient size. The used cores come from Micrometals, and the manufacturer specifies that the initial permeability ( $\mu_0$ ) is given as a reference value, and cores are produced with regard to  $A_L$ , which is the inductance rating of a core in nH per turn[34]. Since in Equation 2.11, we use  $N^2$  to represent the number of turns around the core, the unit used for  $A_L$  is  $\frac{nH}{N^2}$ .

The choice of size and type of material for a core is also important when it comes to power handling. When subjected to an alternating magnetic field, the ferromagnetic material will generate heat, and this heat is a core loss expressed in W or mW. This effect leads to an increase in temperature ( $\Delta T$ ), which can be expressed by Equation 2.12, in which  $P_{loss}$  is the total of core and copper wires losses, and  $A_{surface}$  is the surface area[34]. It can be seen that from Equation 2.12, it follows that one way of managing temperature rise is the usage of larger core so that a larger area can dissipate heat.

$$\Delta T(C^\circ) = \frac{P_{loss}[mW]}{A_{surface}[cm^2]} \quad (2.12)$$

Iron powder cores also experience thermal aging, when the core is exposed to elevated temperatures, a permanent decrease in inductance and quality factor (Q) will gradually occur[35]. The decrease in Q contributes to an increase in eddy current, which, in turn, leads to the generation of more heat.

In a high power design, flux density (B) is another important factor when designing

an inductor. In a too small core, magnetic saturation can be reached, meaning that further increase in magnetization force will not result in a further increase in flux density, leading to a loss of permeability and a decrease in inductance[36]. This might lead to a change in the impedance of the filter and a loss of its properties.

Lower flux density can be achieved by using a larger core with smaller permeability or using a material with lower permeability but more turns. The maximal flux density in a toroidal core was calculated using Equation 2.13<sup>1</sup>, where  $V_{rms}$  is the applied RMS voltage, N is the number of turns, f is the operating frequency in MHz, and A is the cross-sectional area in  $cm^2$ [37]. For 600 W in 50 Ω system, the peak to peak voltage is 489.9 V or 173.2 V RMS. The inductor designed for the 80 m band has 21 turns, and the cutoff is designed for 4.5 MHz, but the lowest frequency of the band is 3.5 MHz. The effective magnetic cross-sectional area for T94-2 core is 0.362  $cm^2$ . We can then calculate the maximal flux density in gauss:

$$B_{MAX} = \frac{V_{RMS} \cdot 10^2}{4.44 \cdot N \cdot f \cdot A} = 146.44[\text{gauss}] \quad (2.13)$$

Next, the plot of permeability vs magnetic flux density was found in the datasheet of core T94-2, and a point of approximately 146 Gauss was read, see Fig. 2.21.

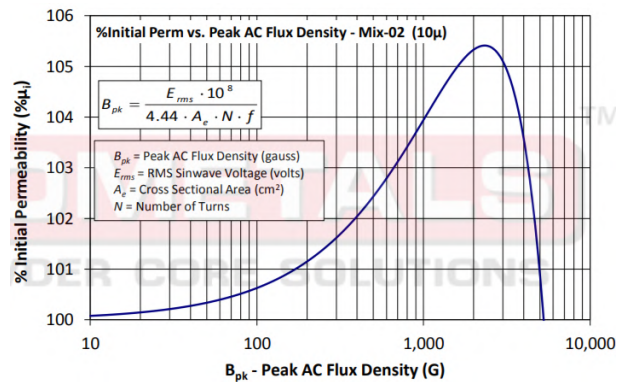


Figure 2.21:  $\mu[\%]$  vs  $B_{peak}$ [37]

<sup>1</sup>This formula does not account for DC bias, which in the used example was not present. Some designers also use peak to peak voltage for additional margin.

It can be seen that this core operates close to the end of approximately linear part of the curve, with less than 1% change in  $\mu$ .

Another source of loss comes from the resistance of the winding and can be calculated as  $I^2R$ . This is especially important when dealing with continuous wave (CW) signals. In our case, to minimize it, a thick 1 mm diameter copper wire will be used to wind the coils. It is important to note that for higher frequencies, the skin effect plays an important role in estimating the effectiveness of a conductor. Micrometals recommends wire size smaller than 35 AWG ( $\phi 0.15$  mm) at 1 MHz in order for the skin depth to be less than the wire radius[36]. Therefore, our 1 mm diameter wire is used mainly to increase the surface for the RF current. The center of the wire experiences a much smaller current distribution.

Ultimately, for the lower bands (160, 80, 40-30 m), type 2 material toroids by Micrometals were used. This material presents low permeability of 10, allowing for low flux density. A larger core T130 was used to accommodate more turns for the 160 m band, and T94 was used for 80 m. Other bands used smaller but still relatively big T80 cores, ensuring adequate flux density at higher frequencies. Type 2 material is recommended to be used between 250 KHz and 10 MHz for the largest Q and lowest core losses[35]. For the upper bands (20-17, 15-10 m), the T80-10 cores were used. Type 10 material is specified for a frequency range from 15 to 100 MHz with  $\mu_i = 6.0$ [35]. Here, a material with mix nr. 6 could be a good alternative, offering slightly lower losses on the 20 and 17 m bands. Because of the low inductance required for the 6 m band, the coils were created as single-layer air core coils. Dimensions were calculated in Coil64, a program by Valery Kustarev. 3D printed form was used to wind the coils with a precise pitch and diameter.

## LPF Switching

To switch each low pass filter in line, two SPDT RM85 12 V relays are used. These relays are rated at 250 V, 16 A AC. When a filter is in use, it is switched in line, and all the other filters are grounded. Relays are driven by U4 ULN2003 (see Fig. 2.23), which is an IC that contains 7 Darlington transistor pairs. This IC was designed for applications such as relay switching[38]. ULN2003 contains flywheel diodes however, external ones were added next to each relay alongside 100 nF decoupling capacitors (see Fig. 2.23).

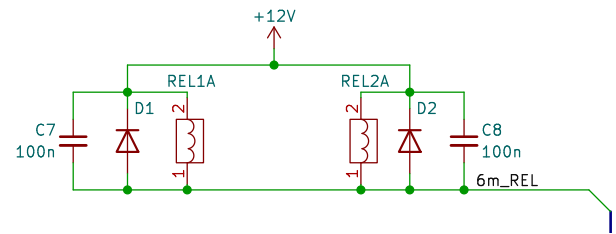


Figure 2.22: Relay bank connected to a bus

The ULN2003 relay driver is controlled by U5 HC595, which is an 8-bit shift register used to reduce the number of connections necessary to the control board. The serial input to HC595 is protected by a  $\pi$  network of series resistors and transil diodes. In addition, the shift register can be bypassed by driving the pins at connector J5 directly.

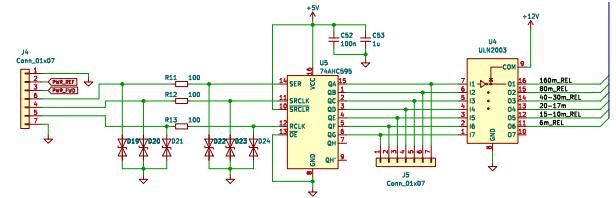


Figure 2.23: Schematic of LPF relay driver

The final element of the LPF PCB is the tandem match coupler, which was described in Sec. 2.2.1. The only difference is that this coupler uses 24 turns on T1 and T2 instead of 30 in order to lower the induced voltage.

## Photos of the Designed LPF PCB



Figure 2.24: Designed LPF PCB, capacitors are mounted on the bottom layer

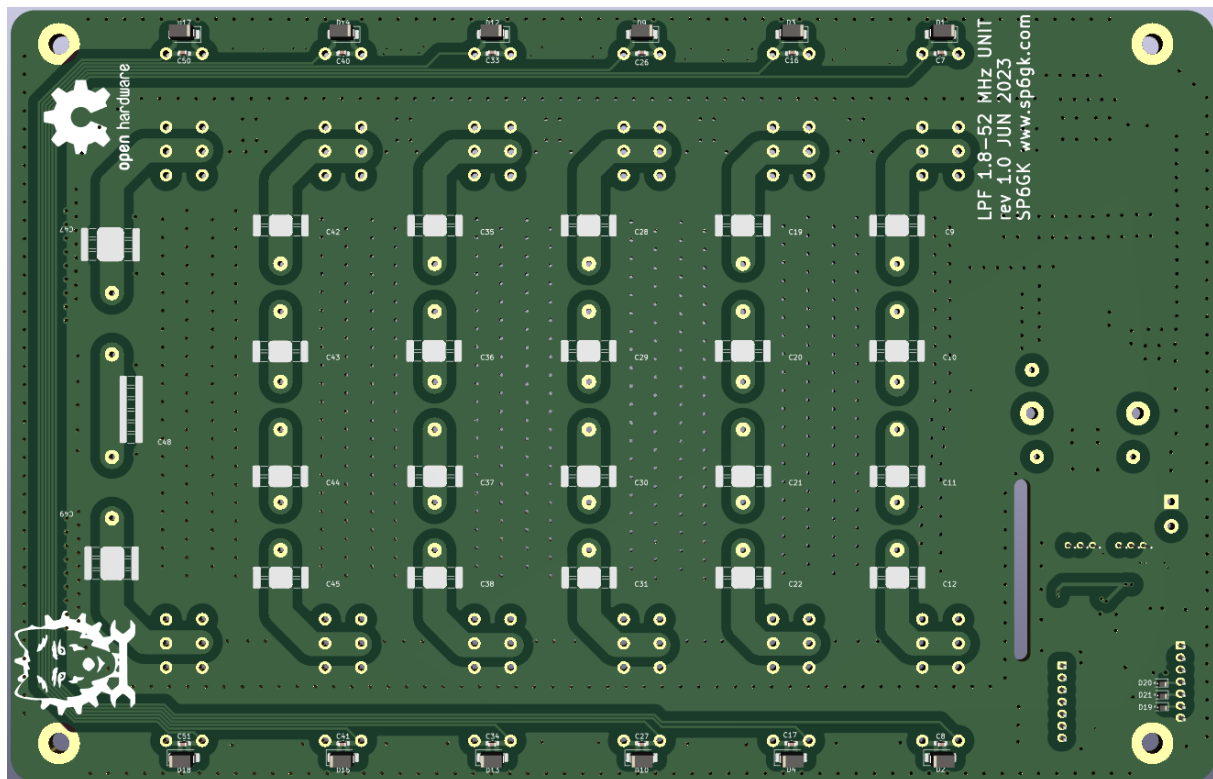


Figure 2.25: Back side of the LPF PCB

## 2.3 Impedance Matching

Impedance matching is a crucial aspect of building an efficient power amplifier. According to the maximum power transfer theorem, maximum power is delivered to the load when both the transmission line and generator have matched impedance to the load. The impedance matching of the amplifier has to transform the input and output impedance of the transistors to the characteristic impedance of  $50 \Omega$ . For an impedance with a real part, there always exists a possible matching network[21]. However, factors such as complexity, bandwidth, and implementation feasibility might vary. Discussed in Sec. 1.1.2 structure of the LD-MOS transistor presents relatively low input and output impedance. Furthermore, our design goals of high bandwidth (1.8–30 MHz), defined in Sec. 1.1, will further parameterize our matching network. A general diagram showing the matching of a device under test (DUT) is shown in Fig. 2.26

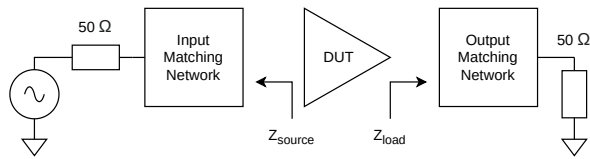


Figure 2.26: Impedance matching diagram

NXP provides a source impedance ( $Z_{\text{source}}$  in Fig. 2.26) measured from gate to ground and load impedance measured from drain to ground for a few design reference circuits. For example, for a 13.56 MHz reference circuit (ISM band), we get[17]:

- $Z_{\text{source}} = 12.0 + j5.2 \Omega$
- $Z_{\text{load}} = 5.1 - 1.0 \Omega$

NXP provides reference designs for given frequencies with a relatively narrow bandwidth of operation. These evaluation boards use LC-type matching circuits with lumped elements. The choice of lumped elements is natural because the use of distributed technology, like a transmission line

on a microstrip shown in Fig. 1.4, is infeasible for low frequencies. Another popular solution is to use an impedance transformer, where the impedance transformation ratio is the square of the turns ratio, as shown in equation 2.14.

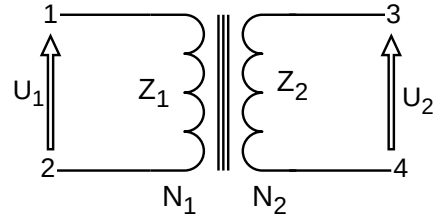


Figure 2.27: DC isolated transformer

$$Z_2 = \left( \frac{N_1}{N_2} \right)^2 \cdot Z_1 \quad (2.14)$$

Alternating current passes through the first winding (primary) and generates a magnetic field, which induces alternating voltage in the secondary winding[39]. Since impedance is defined as the ratio of voltage to current, then in Fig. 2.27,  $Z_1 = U_1/I_1$ , where  $I_1$  is the current flowing from port 1 to port 2. The number of windings  $N_2$  changes voltage  $U_2$  and current from port 3 to 4, so that the impedance  $Z_2 = U_2/I_2$  can be controlled.

Besides the DC isolation transformer shown in Fig. 2.27, an auto-transformer can be used. By calculating the absolute value of the complex input impedance, we obtain the input impedance of the amplifier.

$$|Z_{IN}| = \sqrt{12^2 + 5.2^2} = 13.08 \ [\Omega] \quad (2.15)$$

Next, the nearest integer ratio to  $50 \Omega$  was determined.

$$\text{Ratio} = \frac{50}{13.8} = 3.82 \approx 4 \quad (2.16)$$

This information is valuable because the impedance transformation ratio is the square of the winding ratio, making it easy to achieve a 1:4 transformer.

Ideal transformation is not necessary, as demonstrated by the calculation of the reflection coefficient ( $\Gamma$ ), mismatch loss ( $ML$ ), and return loss ( $RL$ ) below.

$$\Gamma = \frac{50 - (4 \cdot 13.08)}{50 + 4 \cdot 13.08} = 0.022 \quad (2.17)$$

$$ML = -10 \log(1 - |\Gamma|^2) = -0.21 \text{ [dB]} \quad (2.18)$$

$$RL = -20 \log(|\Gamma|) - 33.15 \text{ [dB]} \quad (2.19)$$

Input transformer is designed to handle relatively low power, and to maximize its bandwidth, a small core will be used. The bandwidth of a transformer is determined by the loss of signal at 1 or 3 dB referenced to the midband insertion loss. The insertion loss is influenced by parallel inductance at low frequencies, while at high frequencies, the attenuation is limited by interwinding capacitance[39]. To mitigate the reduction of insertion loss due to parasitic capacitance, a smaller transformer with tight coupling is employed, which helps minimize flux leakage[40]. The transformer was constructed using a BN43-302 core, a binocular core made of 43 NiZn material typically used for EMI suppression but suitable for BALUNs, common-mode chokes, and RF transformers in the 0.5 to 30 MHz range. The transformer was wound using RG142 coaxial cable, with the cable passed through the core in a way that the shield formed a one-turn secondary winding, while the core itself contributed two turns, for the higher primary impedance.

In order to measure the transformer in circuit the rest of the PA deck board was assembled excluding final transistors. Between gates of MRF300s a parallel combination of two  $25 \Omega$  resistors was connected to approximate the gate impedance. Of course the impedance changes with frequency for a real transistor however this test is to check whether the transformer works as expected. Further experiments can be carried out if the S parameters are known. NanoVNA

was used for S11 measurement, Smith chart is shown in Fig. 2.29a. In order to cancel out series inductance of the transformer and improve a bandwidth a shunt capacitor of 22 pF was added to the primary side.

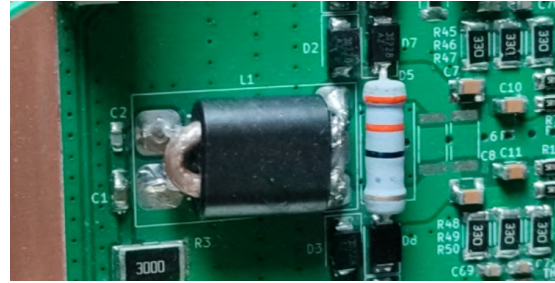
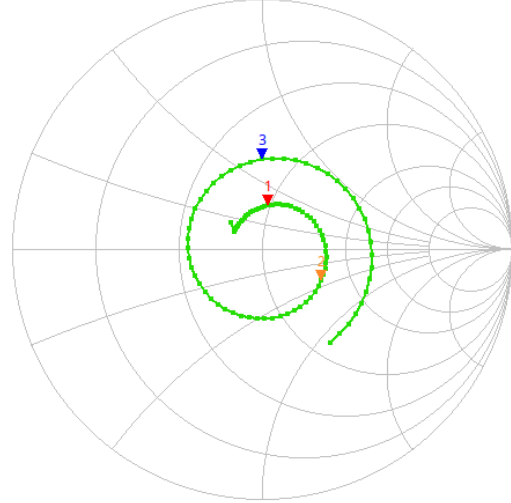
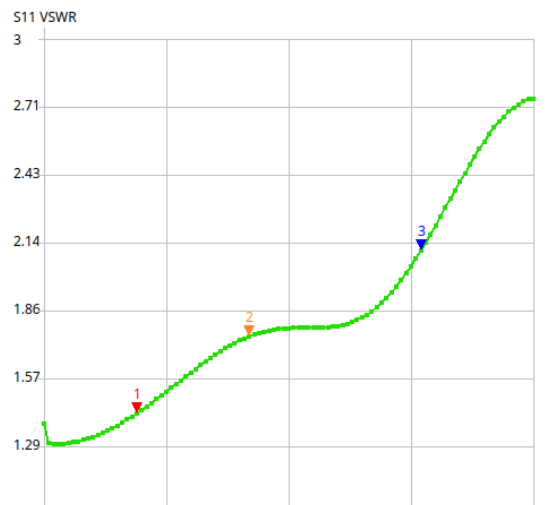


Figure 2.28: 1:4 input transformer

S11 Smith Chart



(a) Smith chart



(b) VSWR

Figure 2.29: VNA measurement of input

In Fig. 2.29, marker 1 (red) indicates 14.1 MHz, which is the midband of the amplifier. Marker 2 (orange) is positioned at 30 MHz, representing the end of the desired spectrum, and marker 3 (blue) is set at 54 MHz, marking the end of the 6 m band, the first UHF amateur radio band after HF. All these points are close to the center of the Smith chart, indicating a good match. Some improvement at 54 MHz was observed with the addition of a shunt capacitor. It's also evident that as the frequency increases, the dominant component changes from inductive to capacitive beyond 60 MHz. The VSWR rectangular plot in Fig. 2.29b is presented because it is a more common format when dealing with amateur radio transceivers when compared to return loss in dB. Most transceivers will accept a VSWR of 2.0, which is close to a return loss of -10 dB. Tested input matching circuit fulfills this requirement with a VSWR better than 1.76 (-11 dB RL) up to 30 MHz and a VSWR of 1.93 for 54 MHz.

### 2.3.1 Input Section

To fully understand how the wide bandwidth operation of this transformer was achieved a schematic in Fig. 2.30 is shown.

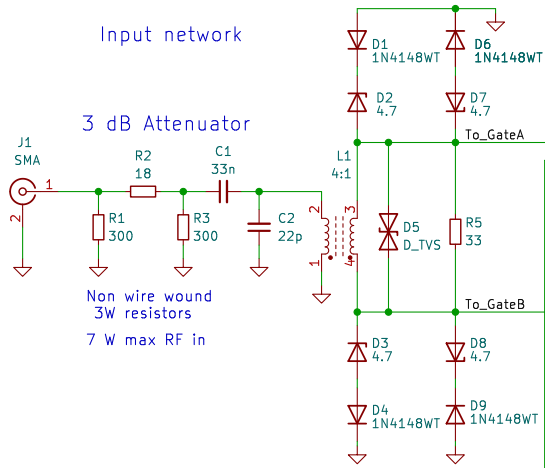


Figure 2.30: PA deck input schematic

It should be noted that the reflection observed in Fig. 2.29 was improved by a 3 dB input attenuator, which is constructed as a

$\pi$  network of R1, R2, and R3 in Fig. 2.30. This attenuator was added so that more precise control of power output can be achieved with transmitters that allow a change of output power in 1 W steps. Additionally, every passive attenuation device acts as an improvement to the return loss, enhancing matching since the reflected wave also gets attenuated.

Defined in Equation 2.10, the Q factor of an inductor also applies to the winding of a transformer. A high-Q circuit exhibits a narrow bandwidth but low insertion loss. Since bandwidth is a priority for this transformer, a parallel resistor R5 with low resistance was added to the secondary winding to lower the Q. This increases the bandwidth at the cost of higher losses.

A network of clamp diodes was added but, the D5 footprint was left empty. Instead, a combination of Zener diodes and standard signal diodes was employed to clamp excessive RF levels. Excess power should be dissipated in these diodes, protecting the gates of more expensive transistors. This might cause clipping distortion at higher drive levels, but the amplifier is expected to lose its linearity despite the presence of diodes for high drive levels.



Figure 2.31: Bias and input section

### 2.3.2 Output Matching - TLT

The next critical aspect in designing an efficient amplifier is output matching. The concept of impedance matching networks and fundamental theory was presented in Sec. 2.3. Output matching presents additional challenges. The transformer used in the input section had a relatively small winding size, but its performance has diminished at high frequencies due to leakage capacitance. Higher power passing through this transformer would require a considerably larger core size to prevent magnetic field saturation.

First of all, it is important to specify the output type of the amplifier configuration. Since the desired output power is 600 W, two transistors in a push-pull construction will be used, making the output balanced. The benefits of a push-pull configuration are not limited to an increase in power. For a long time, balanced amplifiers have been developed in CATV systems to increase bandwidth and limit second-order harmonics [41]. The push-pull configuration was shown in Fig. 1.5 of Sec. 1.1. The push-pull configuration of output matching with ideal power splitters (those that maintain proper phase) presents a short circuit at the second harmonic [42]. This approach was used in the development of efficient HF amplifiers. For example, a paper by V. N. Gromorushkin describes simulating a 1.5 kW MRFX1K80H LDMOS amplifier with 64% efficiency and improved linearity [43]. The winding of the transformer can be made using coaxial cable or copper tubes to reduce the inductance of the transformer however, parasitic components are still present. In addition, they also limit the effectiveness of short circuits for the second harmonic, so ideal cancellation is not possible. Nevertheless, this approach is still advantageous because low-loss coax with high power handling capability can be used. This idea is further expanded in transmission line transformer theory.

### Transmission Line Transformer

In 1944, G. Guanella published a concept of an impedance transformer consisting of a pair of transmission lines. The main motivation for this work was achieving wide bandwidth with a small-size transformer, which was successfully accomplished [44]. The simplest form of Transmission Line Transformer (TLT) used to this day is the 1:1 transformer, where a transmission line is wound (often around a ferrite) to form a choke that attenuates unwanted modes [45]. Such circuit creates a Balun, or a system with a balanced input and unbalanced output. Guanella transformers are made using parallel-series configurations of transmission lines and can be implemented using twisted wire pairs with the correct twisting pitch [46]. The schematic of the Guanella 1:4 transformer is shown in Fig. 2.32. This circuit transforms voltage with a ratio of 1:2 (impedance ratio 1:4) by suppressing common mode through chokes, effectively providing conversion of voltage and current [47, 48].

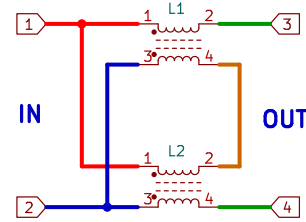


Figure 2.32: Schematic of Guanella 1:4 TLT

Work on broadband transmission line transformers was continued, and in 1959, C. L. Ruthroff published a paper describing some TLTs with a bandwidth of 20,000:1 in the frequency range from a few tens of kHz to a thousand MHz [49]. The 1:4 configuration of the Ruthroff transformer is shown in Fig. 2.33. It can be observed that the Ruthroff transformer sums a voltage that is delayed to a direct voltage, while the Guanella transformer sums up voltages of equal delay. Therefore, Ruthroff has an inherent frequency cut-off [45].

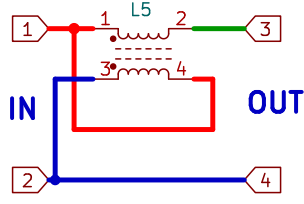


Figure 2.33: Schematic of Ruthroff 1:4 TLT

Guanella transformers can provide a wider bandwidth due to the use of (ideally) frequency independent transmission lines of the same length. While Ruthroff transformers are easier to implement and still allow for wide operation. Broad bandwidth is achieved because parasitic inductance and leakage capacitance are absorbed into the characteristic impedance of the transmission line. Due to the canceling out of flux in the core, an efficiency of more than 95% (or 0.02 to 0.04 dB of insertion loss) is possible [45] (higher for lower permeability). Therefore, a limiting factor is not the size of the core but its permeability (to provide choking across the frequency range) and the conductor's power handling capability.

A disadvantage of Transmission Line Transformers is lower efficiency for low frequencies, which require more inductance from the winding [47], making them less practical for low frequencies. TLTs are also unilateral devices, a TLT can transform only one set of impedances. Therefore, a 1:4 transformer designed to transform 12.5 to 50  $\Omega$  will not work as a 50 to 200  $\Omega$  transformer even though both ratios are 1:4. Moreover, TLT's efficiency is higher for lower impedances [45]. Low impedance operation is not a problem because the balanced output of the MRF300s transistor is of low impedance. Since all transformers are limited by possible ratios, the options have to be analyzed.

Module impedance of output can be calculated as:

$$|Z_{OUT}| = \sqrt{5.1^2 + 1^2} = 5.197 \approx 5.2 \quad (2.20)$$

Values in Equation 2.20 were taken from the data sheet of the MRF300 for the output impedance at the reference frequency

of 13.56 MHz (see Fig. 2.26). In order to match it to 50  $\Omega$ , we need to calculate the ratio.

$$\text{Ratio} = \frac{50}{5.2} = 9.6 \quad (2.21)$$

The closest integer that is also a square to 9.6 is 9. For a conventional 1:9 transformer, this would imply a 1:3 turns ratio. Such a third-order TLT was presented in an article by Chris Trask [48], where lower-order transformers were connected a special way. See Fig. 2.34 for a schematic.

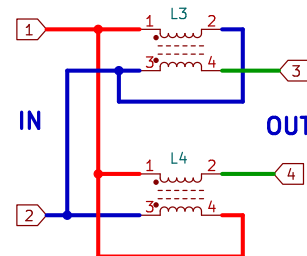


Figure 2.34: Schematic of 1:9 TLT

Notice that coax implementation is easy because both for L1 and L2 the primary winding can be a core of a coaxial cable while secondary winding becomes coax shield. For each TLT a characteristic impedance of used transmission line depends on termination impedances[47].

$$Z_{tr} = \sqrt{Z_{IN} \cdot Z_{OUT}} \quad (2.22)$$

Since the input impedance seen by the TLT is 5.55  $\Omega$ , and the output impedance is 50  $\Omega$ , the characteristic impedance of the transmission line used for the 1:9 transformer is 16.66  $\Omega$ . The characteristic impedance of a transmission line depends on its geometry [21]. In the case of coaxial cable, the characteristic impedance depends on the diameters of the core and shield, as well as the  $\epsilon_r$  of the insulating dielectric. The closest characteristic impedance of a coaxial cable that can be found on the market is 17  $\Omega$ . However, applications for such cables are rather sparse, so the offer is limited. One option is the TC-18, which was tested by Razvan Fatu [20].

During the early stages of amplifier development, no  $17 \Omega$  cables were found in stock at any online electronics or RF parts suppliers. This prompted an idea, inspired by the original 1944 Guanella paper [44], to test a TLT made with multiple parallel transmission lines. The hypothesis is that a  $5.55$  to  $50 \Omega$  TLT can be obtained using two parallel coaxial cables of  $50$  and  $25 \Omega$ , resulting in the equivalent of  $17 \Omega$ . Razvan Fatu proposed a similar solution with three  $50 \Omega$  coaxial cables however, such a solution

would be very difficult to wind on a ferrite core.

### 2.3.3 Tested TLTs

Although TLTs are well understood and described in the literature at this point, the characteristics of specific built transformers are more challenging to obtain. Four transformers in six configurations were constructed and compared using a VNA, and three of them were tested in a physical amplifier.

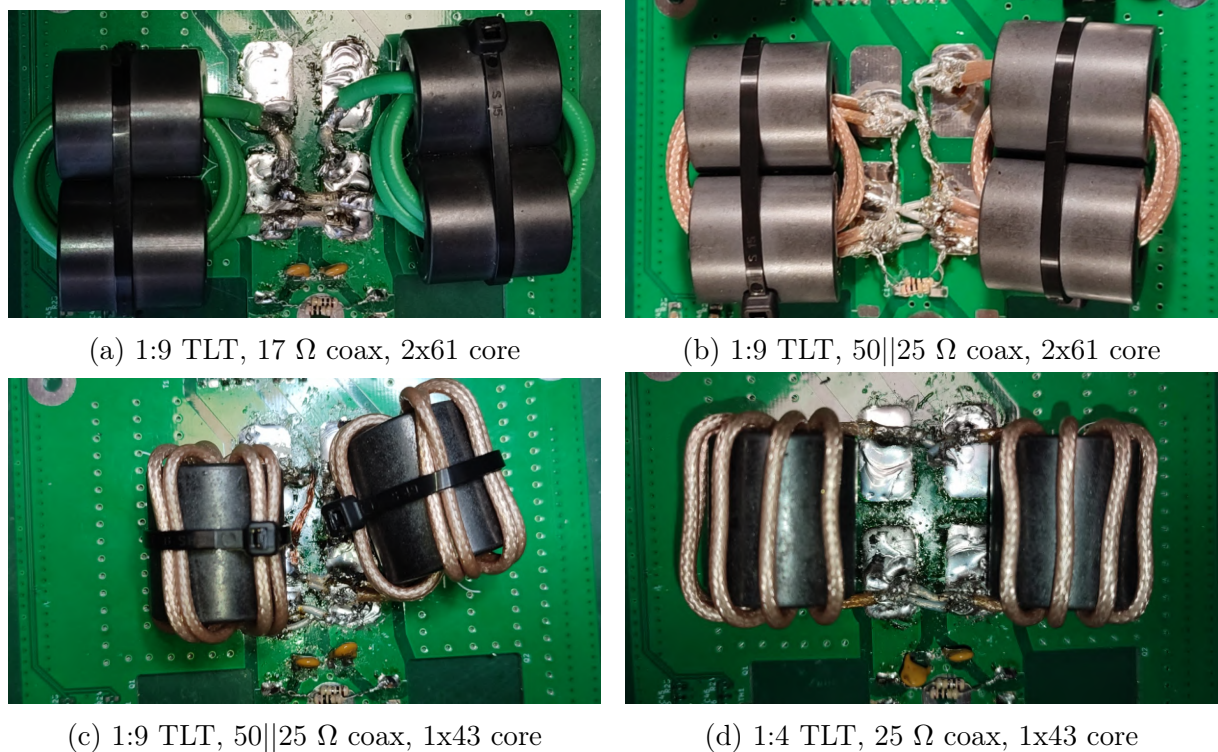


Figure 2.35: Photos of tested TLTs

TLT figure	Ratio	$Z_{tr0} [\Omega]$	Coax	Turns	Core (material / mfr. nr)
2.35a	1:9	17	HF141-17-FEP	3, 2	61 /Fair-Rite 2661102002
2.35b	1:9	17*	RG316-25-Flex    RG316-50	3	61 / Fair-Rite 2661102002
2.35c	1:9	17*	RG316-25-Flex    RG316-50	4	43 / Fair-Rite 2643102002
2.35d	1:4, 1:9	25	RG316-25-Flex	5	43 / Fair-Rite 2643102002

Table 2.3: Built comparison of four tested TLTs. '\*' denotes the theoretical impedance of parallel coaxes. Comma denotes variations on the same TLT.

Two different round ferrite cores were used for the tested TLTs. The first was 2661102002, made out of 61 type material, which is specified for higher frequencies [50]. At 100 MHz, the manufacturer specifies a typical impedance of  $216 \Omega$ . The second core was the 2643102002, which used material 43, designed for lower frequencies. Its impedance at 100 MHz is specified as  $204 \Omega$ , but the manufacturer also provides data for 10 MHz, which is  $87 \Omega$ . Both cores were manufactured by Fair-Rite and are designed as EMI suppression elements.

These specific cores were chosen not only because the material used is commonly applied for the construction of HF transformers (especially in the case of 43 material) but also because they are the same size and can accommodate many combinations of windings. Both cores have an outer diameter of 25.9 mm and an inner diameter of 12.8 mm with a length of 28.6 mm. A smaller core could most likely have a positive effect on bandwidth by decreasing the length of the used transmission line. However, a thinner and easier to wind  $17 \Omega$  coax was not possible to obtain at the time of building the amplifier.

Used  $17 \Omega$  coax is a special-purpose coaxial cable manufactured by QAxial. It utilizes non-magnetic conductors and is designed to operate up to 24 GHz, capable of handling 1200 W of average power at 100 MHz, making it a very suitable option for this application [51]. Disadvantage of this cable is its high price, relatively lower availability, and more difficult winding due to the dense shield used.

TLTs using  $17 \Omega$  characteristic impedance transmission lines were wound with three turns in the case of TLTs shown in Fig. 2.35a and 2.35b. However, more cores were used to increase the inductance, aiming to improve performance at lower frequencies since these TLTs used 61 material with lower permeability. TLTs using 43 type material were wound on a single core per side of the transformer, but additional turns were used.

In addition to the closest 1:9 transformation ratio, a 1:4 TLT was also tested (Fig. 2.35d). According to the theory presented in Sec. 2.3.2, its input should see a  $12.5 \Omega$  load, and as dictated by Equation 2.22, a transmission line with  $25 \Omega$  transmission line should be used. This 1:4 transformer was tested to evaluate the performance of much cheaper and more available coax, such as RG316-25 (the  $25 \Omega$  version of typical RG-316). Even though sub optimal, a similar transformer was used by NXP in a 1 kW amplifier with BLF188XR [52].

The 1:9 transformer with a parallel connection of 50 and  $25 \Omega$  cables using only two 43 cores (Fig. 2.35c) represents the second cheapest option after the 1:4 transformer. This is because RG-316 in its  $50 \Omega$  version is very easy to find and quite affordable. The Fair-Rite 43 type material core used in this project was also half the price of the 61 type material core.

The balanced low impedance side of the transformer was terminated with a parallel connection of two  $10 \Omega$  resistors, simulating a  $5 \Omega$  load, which is close to the expected  $5.2 \Omega$  of the MRF300s at 13.56 MHz. As the output on the  $50 \Omega$  side is balanced, a 1:1 balun was used to connect a coaxial cable, which is an unbalanced transmission line. Subsequently, a VNA was used to measure the return loss of the system.

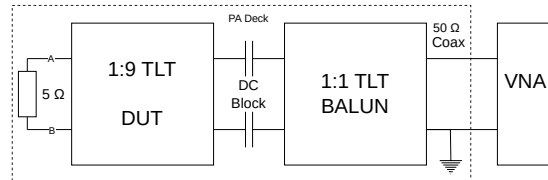


Figure 2.36: Test setup for TLT

Additionally, a variation of TLT from Fig. 2.35a (1:9 with  $17 \Omega$ ) was wound with one turn less. The second variation involved a change in the connection of the 1:4  $25 \Omega$  TLT (Fig. 2.35d) to serve as a 1:9 transformer, despite the incorrect characteristic impedance of the used transmission line.

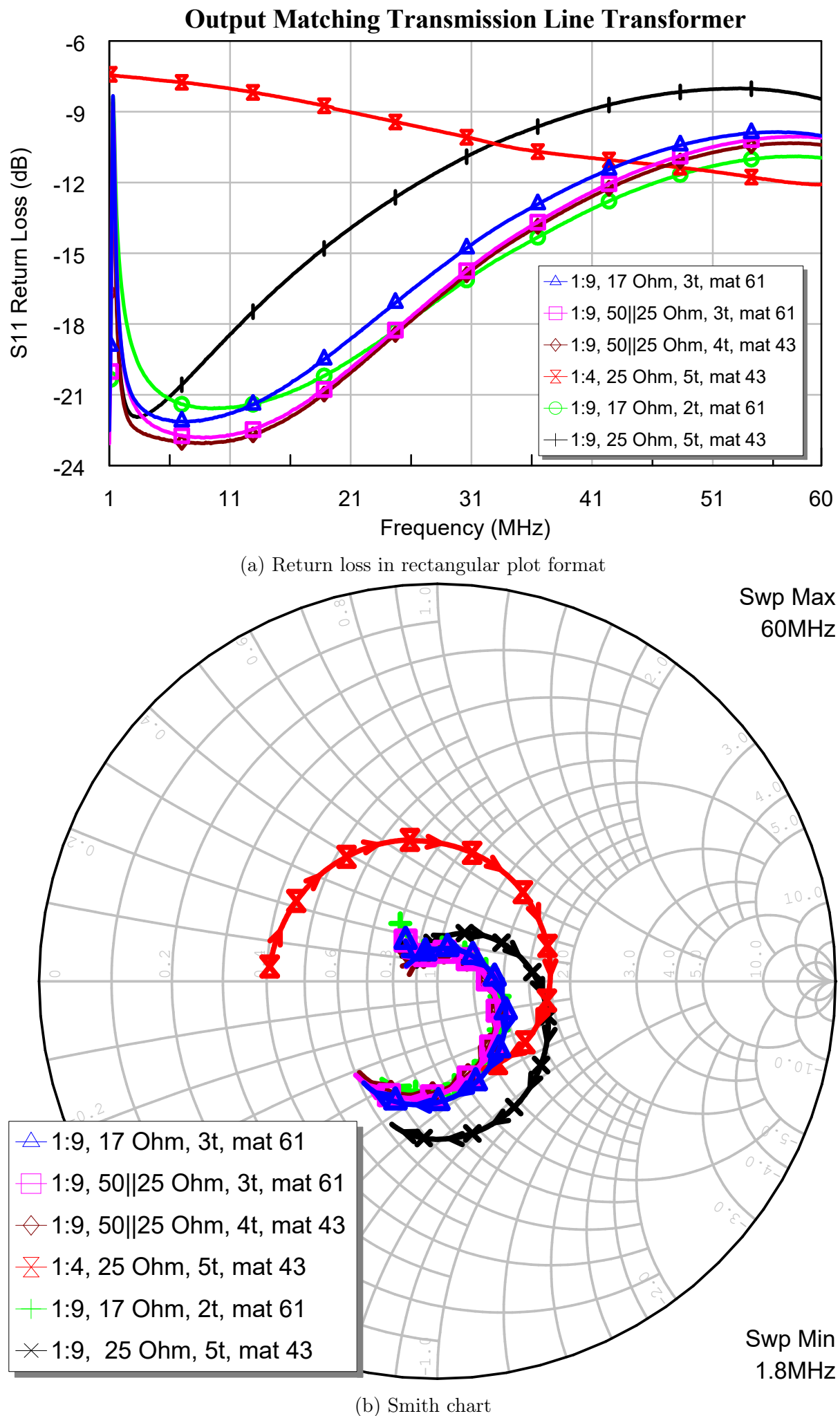


Figure 2.37: Measurement of S11 for various transmission line transformers

Measurements for each transformer were performed using LiteVNA 64 with a span from 1 to 60 MHz. The instrument was calibrated, and NanoVNA Saver software was used to capture 808 points for each series of measurements.

In Fig. 2.37a, it can be observed that the 1:4 transformer presents the worst match, as is also depicted in the Smith chart in Fig. 2.37b. The 1:4 trace is the furthest away from a match across entire HF frequency spectrum, showing worse than a 2:1 match (worse than -10 dB return loss) across most of the HF spectrum. This results in low efficiency of impedance matching but is still deemed safe for the MRF300.

Using a single 25  $\Omega$  coaxial cable and employing the same winding as in the 1:4 transformer but connecting it in a 1:9 configuration results in much better behavior for lower frequencies. Return loss of -14 dB, which we will further assume as a minimum goal for the entire spectrum (1.5 VSWR, 4% mismatch loss), is achieved between 1.6 to 20.8 MHz. This transformer violates Equation 2.22 for characteristic impedance. The consequence of this can be seen with rapidly decreasing return loss for higher frequencies, with the worst observed return loss above 30 MHz from all tested configurations.

We hypothesize that this configuration works very well below 8 MHz because the length of the used coaxial cable is very short at this wavelength and does not exhibit significant transmission line effects. Thus, the characteristic impedance does not have as much of an effect. The length of used coax for this 1:4 transformer was 46 cm, which at the minimum return loss of -22 dB at 3.26 MHz equates to  $0.005\lambda$ .

All other 1:9 transformers performed well in the test, confirming the theoretical background. The transformer wound on more 61 cores with 3 turns and 17  $\Omega$  special-purpose cable actually did not perform as well as the improvised transformer with a parallel combination of 50 and 25  $\Omega$

general purpose cables, at least according to return loss measurements. The test has also confirmed that the transformer made with a single 43 type core but more turns performs better at lower frequencies, but the difference is not significant. Ultimately, both transformers with a parallel connection of transmission lines resulted in a bandwidth of -14 dB return loss from 1.6 MHz to 36 MHz.

The last variation is the original 1:9 TLT with 17  $\Omega$  coaxial cable but with 2 turns instead of 3. As expected, this has moved the minimum Return Loss up in frequency from about 6.8 MHz to 10.3 MHz. This shift of the S11 trace has allowed for better RL for higher frequencies. This is most likely due to a smaller ratio of coax length to  $\lambda$  and also smaller leakage. Such a configuration offers -14 dB RL from 1.65 MHz to 37.4 MHz and results in a more flattened RL throughout the entire HF spectrum. Furthermore, this last variation also offers the lowest RL at 52 MHz of -11.2 dB, which is still an acceptable match resulting in a VSWR of 1.76.

Insertion loss or the S21 parameter of the transformers was not tested because such a measurement would require a second transformer. Connecting transformers back to back would bring the impedance back to 50  $\Omega$ , allowing for a S21 measurement setup of transmission line transformers [39]. However, this would introduce uncertainties since a professionally characterized 1:9 wideband transformer was not available in the laboratory. In the future, such a test with two transformers and de-embedding could be employed to measure the insertion loss of an unknown transformer.

Ultimately, the amplifier was tested with a 1:9 special purpose 17  $\Omega$  TLT on four 61 type cores in total, the 1:9 TLT made using a two 43 cores and parallel combination of coaxial cables, and lastly, the 1:4 transformer on two 43 cores using 25  $\Omega$  coax.

### 2.3.4 1:4 vs 1:9 Ratios

In the previous section, it was shown that even if the 1:4 transformer does not provide very good impedance matching between the balanced output of the amplifier and an unbalanced  $50\ \Omega$  load, the resulting SWR will not damage the amplifier under the controlled conditions. Because the transformer determines what load is "seen" by the amplifier output, it is worth considering the impact of 1:9 and 1:4 transformation on the theoretical output power.

In a balanced system of push-pull MOSFETs, the power on a load  $R$  with drain voltage  $U$  is given as:

$$P_{max} = \frac{U^2 \cdot 2}{R} \quad (2.23)$$

For a 1:4 transformer, the load seen between the drains in a  $50\ \Omega$  system is  $12.5\ \Omega$ . For a 1:9 transformer, the impedance on the lower side is  $5.5\ \Omega$ .

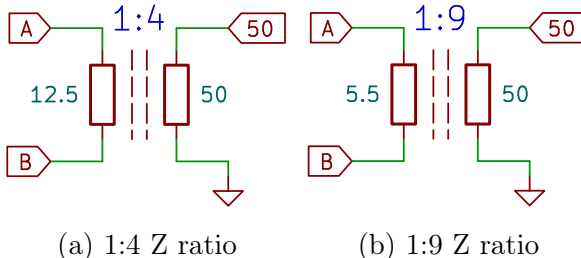


Figure 2.38: Diagrams of impedance transformation

From equation 2.23, it can be noticed that for high power, either  $R$  has to be low (low impedance of MOSFET) or  $U$  has to be high (high drain voltage).

$$P_{1:4} = \frac{48^2 \cdot 2}{12.5} = 368\ [W] \quad (2.24)$$

$$P_{1:9} = \frac{48^2 \cdot 2}{5.5} = 837\ [W] \quad (2.25)$$

For a 1:4 transformation, the power is close to the minimum desired of 400 W. Because of the higher presented load resistance, the current will be lower in comparison to the 1:9 transformation.

In the case of the 1:9 transformer, a low impedance will cause a very high current. In fact, two MRF300s are not able to deliver 837 W, so the drain current will have to be closely monitored.

### 2.3.5 Output Capacitors

Similarly to the input network described in Sec. 2.3, the output transformer has both inductive and capacitive components. For a conventional transformer at the input of the amplifier, a capacitor placed in parallel to the primary winding was used to cancel out the interwinding capacitance that limits bandwidth at higher frequencies. In order to tune the output transmission line transformer for maximum bandwidth, two capacitors were used, each connecting one balanced output to the ground. A vector network analyzer was used to choose the best value. In this test, a 1:9 transformer with 3 turns of  $17\ \Omega$  coax was used.

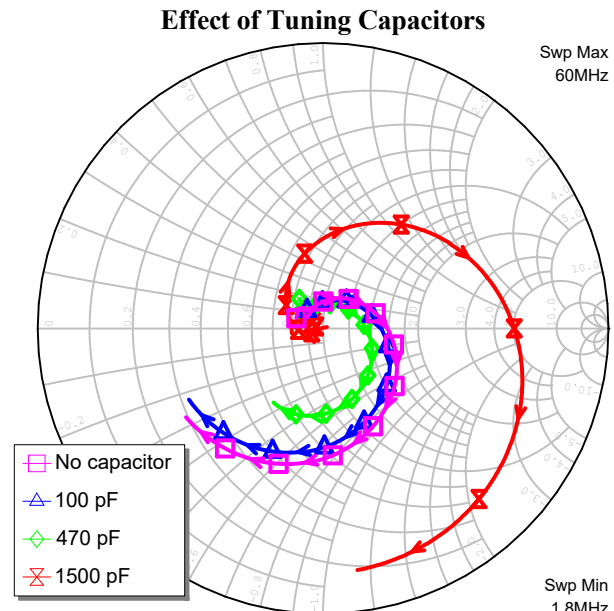


Figure 2.39: Output capacitors

Using the Smith chart, a value of 470 pF was chosen because it significantly improves the match across a wide range of frequencies. This value was also used in all the other tests.

## 2.4 BALUN Measurement

A balun is a circuit used to convert the output from balanced to unbalanced[21]. The amplifier utilizes a balanced output configuration of transistors, while the output from the PCB is an unbalanced coaxial cable. In the case of a push-pull amplifier, a simple transformer can be used with one side of the secondary winding grounded (see Fig. 1.5). For wideband operation, a transmission line 1:1 transformer can be used. Such a circuit attenuates common mode current that would occur on the shield of a coaxial cable if it were connected to a balanced output[44]. To test the  $50\ \Omega$  balun, a spectrum analyzer with a tracking generator was used.

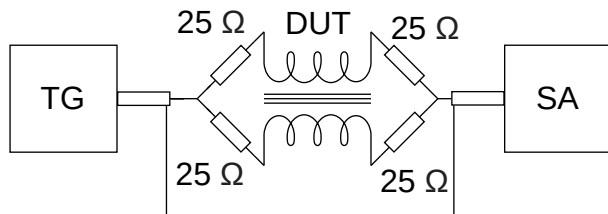


Figure 2.40: Test setup for balun common mode attenuation

The signal from the tracking generator is connected through two  $25\ \Omega$  resistors to the core and shield of the coax of a balun. The input to the spectrum analyzer was connected in the same way, through  $25\ \Omega$  resistors to the core and shield of the balun's output. The ground of the tracking generator was connected to the ground of the input port. Since the signal is split with a 50% ratio, the observed insertion loss should show the attenuation of common mode.

Two baluns were tested during the design of the amplifier. The main goal of this experiment was to observe the capacitive parasitic effects of multiple wound coaxial cables. For that, both baluns used two 43 material ferrite cores (Fair-Rite 2643102002), the same as those used for

some of the tested transmission line transformers. The first balun was wound with two turns of RG303/U, which is a thick, low-loss coaxial cable with a Teflon dielectric. Second balun used much thinner RG316 with 5 turns.

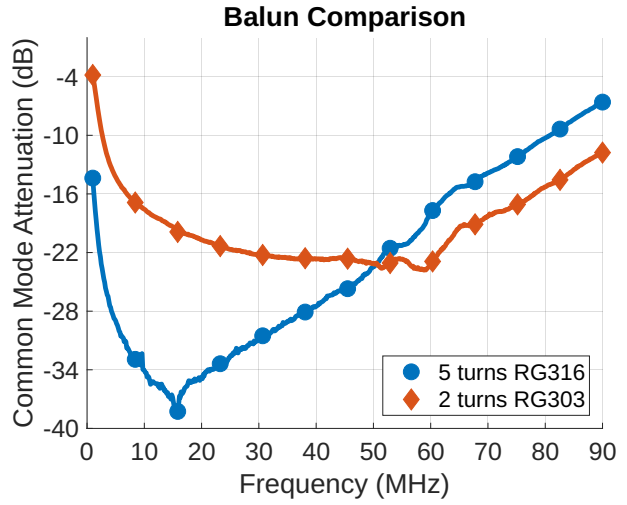


Figure 2.41: Comparison of two baluns

In Fig. 2.41, it can be seen that the balun with more turns presents excellent common mode choking capabilities from 1.9 MHz to 57 MHz. Its interwinding capacitance is most likely higher, and the visible minima around 15 MHz might be due to some resonance effect. The balun wound with a thicker 2 turns presents a much flatter response with still acceptable common mode attenuation. However, for lower bands such as 160 and 80 meters, this balun is non-ideal, providing only 7 and 12 dB of attenuation, respectively.

In the next test, a previous measurement setup for testing transmission line transformers was used (see Fig. 2.36). The tested transformer, made with two turns of  $17\ \Omega$  special-purpose coax on a 61 cores TLT, was connected through DC blocking capacitors and different baluns to a VNA in order to observe the impact of balun on a RL measurement.

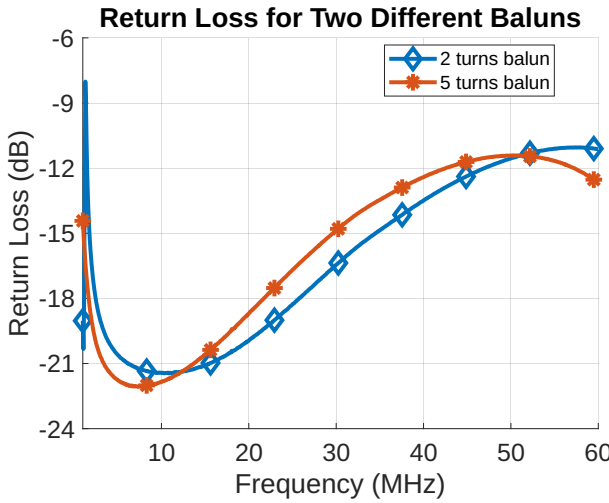


Figure 2.42: Impact of balun on return loss

It can be noticed that the balun with more turns performs better at lower frequencies, most likely due to higher inductive reactance, which more effectively chokes the common mode on the coax's shield. The balun with a smaller number of turns and the same TLT exhibits better return loss for higher frequencies. This is most likely due to lower capacitive leakage. Ultimately, the balun with a lower number of turns and thicker coax was used during further tests of the physical amplifier because of its better ability to handle high power.

## 2.5 Bias Supply

Field effect transistors (FETs) are voltage controlled devices in which drain current increases with the gate voltage and is proportional to  $((V_{GS} - V_{Th})^2)$ [23]. The amplifier is designed for class AB operation, in which the gate voltage is slightly above the threshold, allowing for idle drain current. This class provides higher gain and better linearity when compared to the zero bias used in class C, but, when compared to class A, it will always have more distortion [8]. The idle current of transistors (collector or drain) depends on many factors. MOSFET's drain current is quite sensitive to temperature changes, so the bias circuit needs to account for those changes so that the gate voltage is inversely proportional

to the temperature, with a ratio of approximately  $1\frac{mV}{^{\circ}C}$  to  $2\frac{mV}{^{\circ}C}$  [53]. In order to ensure stable and reliable operation of the amplifier, the relationship between transistor temperature and gate voltage should be characterized.

A proper bias circuit that can maintain a stable idle drain current of a LDMOS transistor can be characterized by low output noise and very low output impedance. An example circuit of a LDMOS bias circuit was prepared by Ampelon in their application report [54]. In their circuit, a general-purpose transistor is used as a temperature sensing device. This works because the voltage across the diode junction depends on temperature, so a temperature dependent voltage divider can be built using a PN junction. This also means that the simplest form of bias can be a divider that uses a silicon diode and a resistor or a resistor and a thermistor. However, this does not provide a low impedance output. For that, Ampelon suggests using an op-amp to achieve less than  $2.5 \Omega$  from DC to 100 MHz. The chosen op-amp in this report is also a high-current output op-amp so that a capacitive load can be driven with high stability.

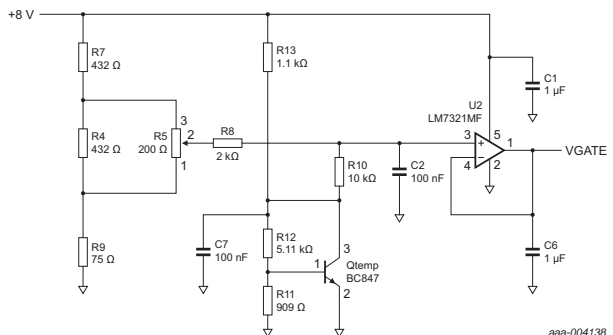


Figure 2.43: Ampelon's bias circuit

Another circuit for bias of LDMOS which ultimately was used in this project was described by Iulian Rosu[53]. This circuit was chosen because it uses very low noise linear regulator the LM723 which offers lower noise in comparison to commonly used 7805 regulator often used in this role.

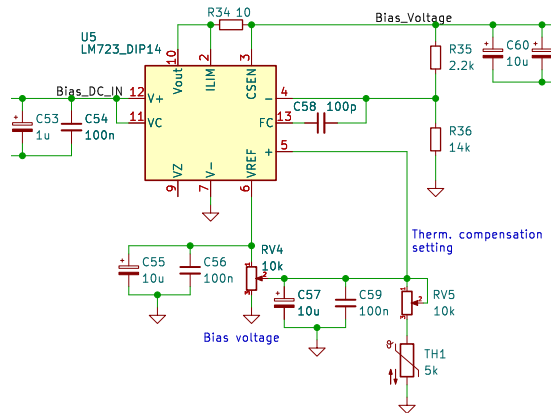


Figure 2.44: Used bias voltage circuit

In this circuit, a thermistor is used to sense the temperature, and together with a network of potentiometers, a reference voltage for the linear regulator is adjusted. Potentiometer RV4 sets the bias voltage, which should be adjusted for proper quiescent drain current, and RV5 sets the slope of the gate voltage to temperature.

Because of the manufacturing spread, which tends to be higher in FET devices [23], the elevated bias voltage is further split into two arms, each having an additional potentiometer so that the gate voltage is adjusted separately for each MOSFET. Resistors and potentiometers in those arms were chosen to be of lower value to minimize thermal noise while still maintaining a relatively low impedance output. Multiple decoupling capacitors were used to provide low impedance across the wide frequency range. Output resistors are included to ensure stability at the lower frequency of operation [54].

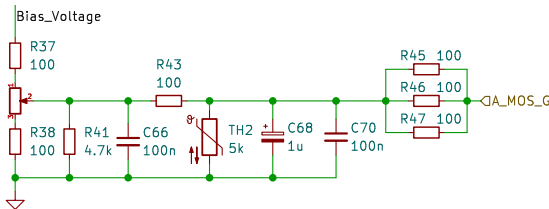


Figure 2.45: A gate bias supply network

The bias supply is switched on only during the transmission mode, similar to the drain voltage. The LM723 is supplied by the

12 V rail, which is switched by the MOSFET Q5 only when the *bias\_EN* signal from the control board is high and when the *HIGH\_SWR* flag from the directional coupler is high. This logic operation is independent of software and was implemented using an AND gate with two general purpose NPN transistors Q3 and Q4.

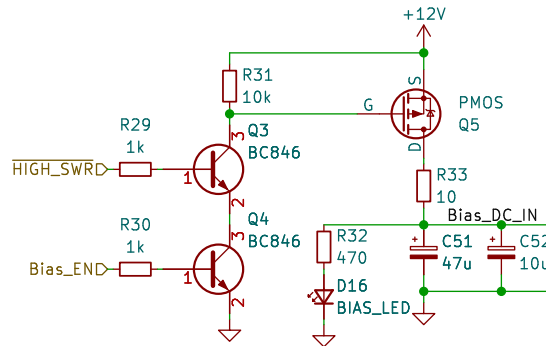


Figure 2.46: Bias enable circuit

In order to test the circuit across a wide temperature range and tune it for a desired slope, an assembled board without transistors was mounted onto a heat sink. Both gates were connected to ground using  $1\text{ M}\Omega$  resistors and parallel 100 pF capacitors. A DS18B20 thermometer was mounted on a brass lug screwed to the copper heat spreader plate. A simple data acquisition system was built using an Arduino Uno, which logged the temperature and converted the value from ADC to gate voltage. A hot air station was used to heat up the copper plate with the temperature sensor attached to it.



Figure 2.47: Bias circuit test setup

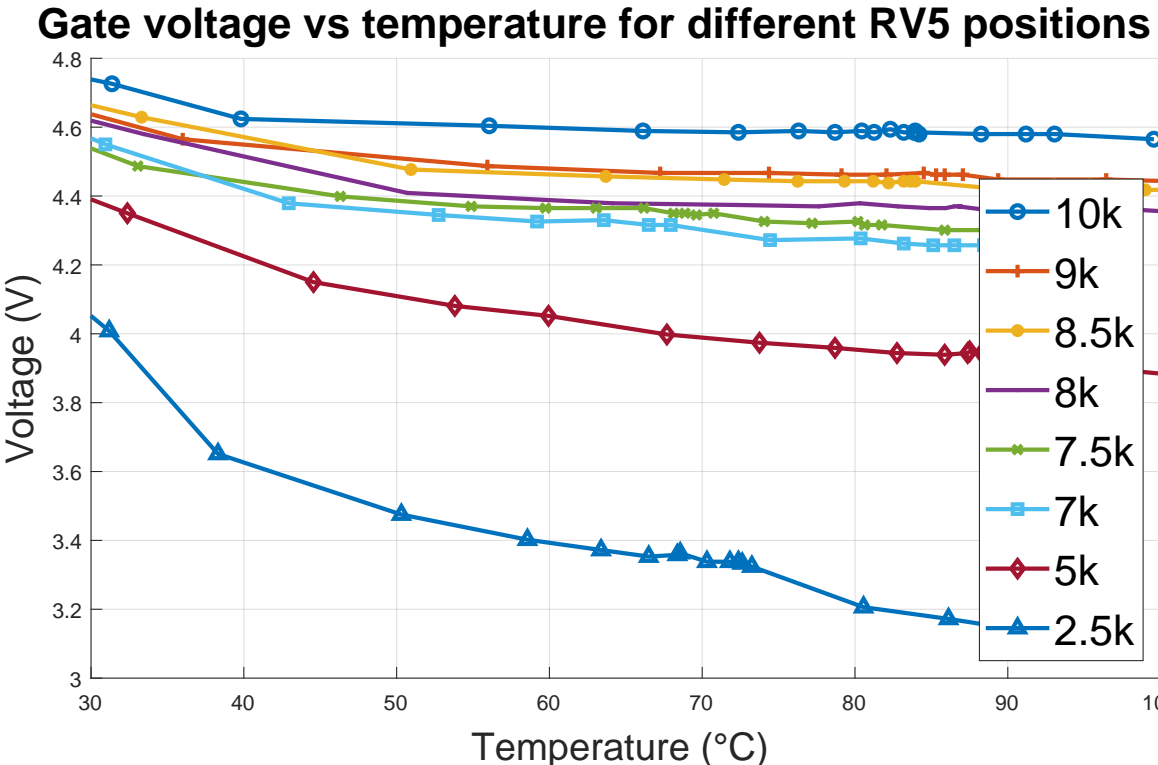


Figure 2.48: Bias circuit test

From the measured data, it can be seen that the relationship between gate voltage and temperature is nonlinear for lower operating temperatures and then becomes mostly linear. This is an acceptable result because the working amplifier very quickly heats up above 30 °C. Furthermore, Fig. 2.48 shows that for lower settings of RV5, the slope becomes steeper, giving a larger change in gate voltage for every °C compared to the high value of RV5.

The exact ratio of gate voltage change to temperature change should be chosen based on the LDMOS manufacturer's datasheet and design resources, similar to quiescent drain current, which will also depend on the desired output power.

For a future experimenter wanting to implement this circuit, a table 2.4 was prepared that gives exact ratios for different settings. These values were taken as the difference between two extreme points of the linear part of traces. These values represent the relationship between the gate voltage

and temperature change for different settings of RV5 in the tested bias circuit.

RV5 [kΩ]	$\Delta V_{gs}$ [mV]	$\Delta T^{\circ}C$	[mV/°C]
10	54	80.18	0.673
9	78	81.19	0.961
8.5	112	88.75	1.262
8	122	89.69	1.360
7.5	161	87.06	1.849
7	249	94.57	2.633
6.5	225	79.87	2.817
5	294	83.38	3.526
2.5	567	63.19	8.973

Table 2.4: Example settings of RV5 for given ratio of gate voltage change to 1 °C

For the amplifier designed during this project, a total quiescent drain current of 400 mA was chosen. The ratio of gate voltage to temperature change was chosen as  $1.25 \frac{mV}{^{\circ}C}$ , so RV5 was set to 8.5 kΩ according to table 2.4.

## 2.6 Feedback, Stability

Several methods are implemented in the amplifier to improve its stability. One of the most important is the use of a negative feedback circuit. This circuit samples part of the output signal from the drain of the MRF300s and feeds it back to the gates. Because the signal at the drain is  $180^\circ$  out of phase with respect to the gate, the feedback signal decreases the input signal, causing degradation of gain due to superposition.

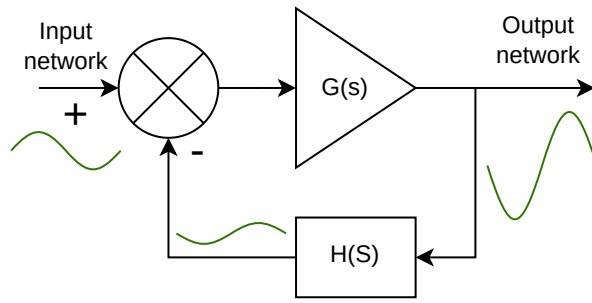


Figure 2.49: Negative feedback control loop

The reduction of gain also reduces efficiency however, negative feedback can improve the stability of the amplifier and flatten the gain over the spectrum of operation. For the feedback network, a solution tested by Razvan Fatu [20] was used. The network consists of a series DC blocking capacitor ( $C_{10}$  in Fig/ 2.50) and a  $560\ \Omega$  resistor  $R_{11}$  from drain to gate. The resistor is realized as a combination of two parallel  $1.2\ k\Omega$  non-wire wound resistors to reduce parasitic inductance and increase power handling.

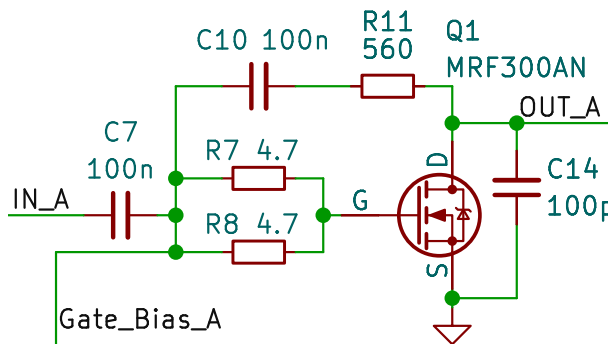


Figure 2.50: MRF300 connections

Another measure of ensuring stability was the addition of small resistance in series with the gates of MRF300s. Here, two parallel  $4.7\ \Omega$  resistors ( $R_7, R_8$ ) are used to prevent oscillations at high frequencies.

Presented in previous paragraphs network implements negative feedback that provides stability. Positive feedback, on the other hand, might lead to an increase in the in-phase signal at the input, leading to self oscillation. Positive feedback might be a result of transistor interelectrode capacitance and lead inductances, but it can also be caused by physical layout and magnetic coupling between amplifier stages [8].

To minimize this linear feedback effect, chokes were placed as close as possible to the drains to minimize the drain DC supply trace length, which should limit RF radiation from that part of the amplifier. Each drain has its own choke wound with 5 turns on a 43 material ferrite core (Fair-Rite 2643102002). Multiple parallel chip SMD capacitors are used to provide a low-impedance path for the RF that might leak through the choke. An additional choke,  $L_3$ , is placed at the input to the PA deck board ( $10\ \mu H$ ), followed by another bank of parallel capacitors. A bleeder resistor,  $R_4$  ( $47\ k\Omega$ ), is used in parallel with decoupling capacitors to discharge the larger electrolytic input capacitors.

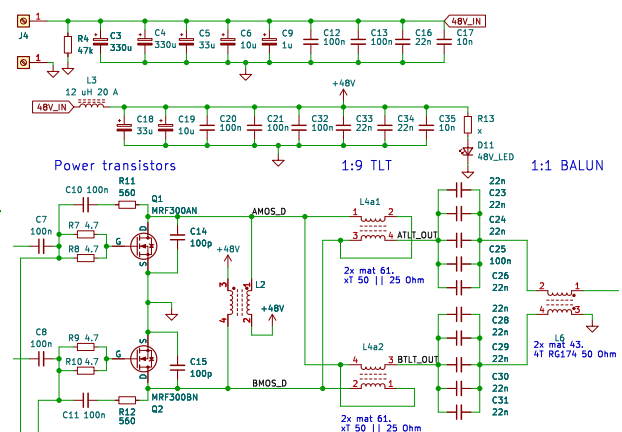


Figure 2.51: Schematic of output stage

## 2.7 PA Board

The PCB that contains power transistors, input and output matching, and the bias circuit also contains a power coupler identical to that presented in Sec. 2.2.3. This additional coupler can be used to detect high VSWR condition when a wrong LPF is selected or when the filter is damaged and causes a lot of reflection. Another reason for having a coupler before and after the LPF is to estimate the power lost in the

filter. This includes the power of rejected harmonics, which can be then used to detect an overdrive of the amplifier.

The PA deck PCB is a two layer board where the bottom layer is entirely a ground plane for the best RF performance and stability. The bottom solder mask was also removed to expose a conductive plane that is mounted onto a copper heat spreader, providing even lower inductance and the best possible ground plane.

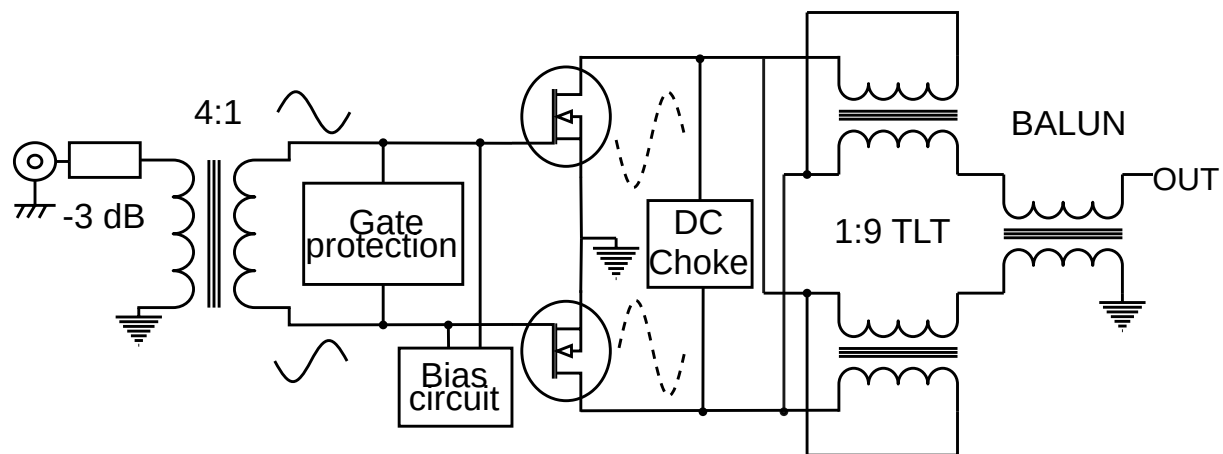


Figure 2.52: Diagram of the PA deck board

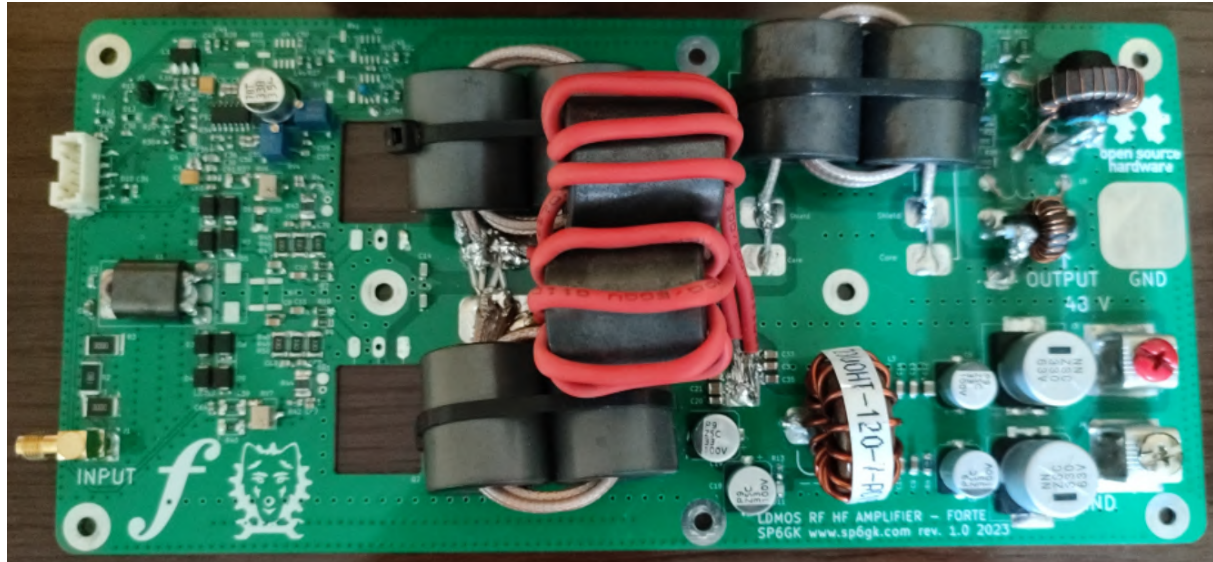


Figure 2.53: Assembled PCB without power transistors

## 2.8 Power Supply

The power amplifier board consumes up to 18 A DC at 48 V, which is 864 W. To efficiently deliver this power from mains, a switching mode power supply is used. The unit chosen for this project is a server power supply produced by Delta, model AWF-2DC-2100W. It provides one 12 V rail at 20 A and 48 V at 41 A for 200-240 V AC input or 20 A for 100-127 V AC input. The 48 V rail can thus supply a sufficient amount of drain current with a large margin, assuming a high-line AC supply.

Another possibility was to use an industrial power supply. However, units produced by generally respected brands such as Mean Well are expensive, and at the time of building, a power supply with sufficient capabilities was not in stock. Furthermore, on the second hand market, many clones with dubious specifications are common. Server power supplies are designed with high reliability and heavy duty use in mind.

Server power supplies are also notoriously loud because they are expected to work in separated and enclosed server rooms therefore, fans inside are designed for maximum airflow and not silent operation. In addition, such units don't have typical connectors, they often come in hot-swappable enclosures with quick disconnects. Therefore, some modifications had to be made.

First of all, the original fans were disconnected from the controller of the PSU and connected to the PWM of the control board. It is possible that fans could be controlled using the I<sup>2</sup>C interface provided at the back of the PSU however, no instructions were found on what commands should be used for that. The pin-out of the back connector allowed for an easy jump start of the PSU by shortening two wires without the PSU being inserted into any server frame. This jump starts only the 48 V rail since the 12 V rail is always on when the power supply is

connected to AC. The second major modification was soldering of AC and DC wires directly to the boards inside the unit.

During the modification of the Delta power supply unit, it was observed that high quality capacitors were used, with many of them being connected in parallel. Heatsinks were implemented as rectangular, thick aluminum bars, with some of them having additional thin copper heat spreaders. Since heatsinks are usually designed to maximize their surface, this hints at either very high efficiency or an expectation of high pressure airflow through the unit. Input protection in the form of varistors and ceramic fuses was also present. A large EMI filter was found inside, consisting of multiple common mode chokes with decoupling capacitors of X and Y class. The EMI filter itself was enclosed in a separate shielded area.



Figure 2.54: PSU under modification

The 12 V rail is used by all PCBs and modules, which then employ local regulation. All relays and fans are driven from 12 V. However, both LPF and TX/RX boards also have logic that is supplied from AMS1117-5 linear 5 V regulators. The control board also has an AMS1117-5 to supply its drain current sensor with a clean rail and an AOZ1280CI, which is an adjustable switching mode regulator that generates a 3.3 V rail for STM32 microcontroller. The front panel module is also supplied by the 12 V rail, but it has its own 7805 regulator for a 5 V rail.

# Chapter 3

## Mechanical construction

### 3.1 Enclosure

The enclosure for the amplifier was built from a modified industrial cassette tape recorder. The original enclosure had easy access from the bottom and top, with metal front and back panels being held by three perpendicular aluminum profiles on each side. Side metal panels were attached to those rails. Two 20x40 mm V-slot profiles were added perpendicular to the original profiles so that they ran parallel to the front and back panels. On those rails, a radiator and PSU were bolted from the bottom using M5 nuts.

Since the front and back panels had original holes, 3 mm thick aluminum sheets were prepared with new openings and were screwed onto the old panels, masking unnecessary holes. The case had some vent holes on the right side, this is where the main air intake for the PSU is now located. Other original vents are underneath the radiator and at the top of the case, allowing for conventional cooling. Modified front and back panels also have large rectangular vents with an aluminum perforated grid allowing for the intake of cold air from the front and the exhaust of warm air on the back of the amplifier.

Special care was taken to make the case EMI sealed. For this purpose, all panels had their paint stripped in places where they were touching another part of the case, en-

suring that all parts are conductive. Thin brass sheets were used to create improvised EMI fingers between profiles and panels, ensuring a low impedance connection is always present between the elements. Overall, the entire case is made out of conductive materials, mostly steel with holes that are much smaller than the highest possible wavelength, even accounting for harmonics. No EMI or RF problems were observed when using the amplifier with a real antenna on different bands.



Figure 3.1: Assembled profiles with mounted radiator (left) and PSU (right)

An IEC 60320 plug and 5x20 mm fuse holder were mounted on the back panel, a 250 V 14 A switch was installed on the front panel to control the mains power to the PSU. The bottom panel provides access to AC wiring, and low level signals, such as the IO for the LPF board and RF input signal. The top panel allows easy access to all the PCBs, facilitating repairs without necessity for disassembling the entire amplifier.

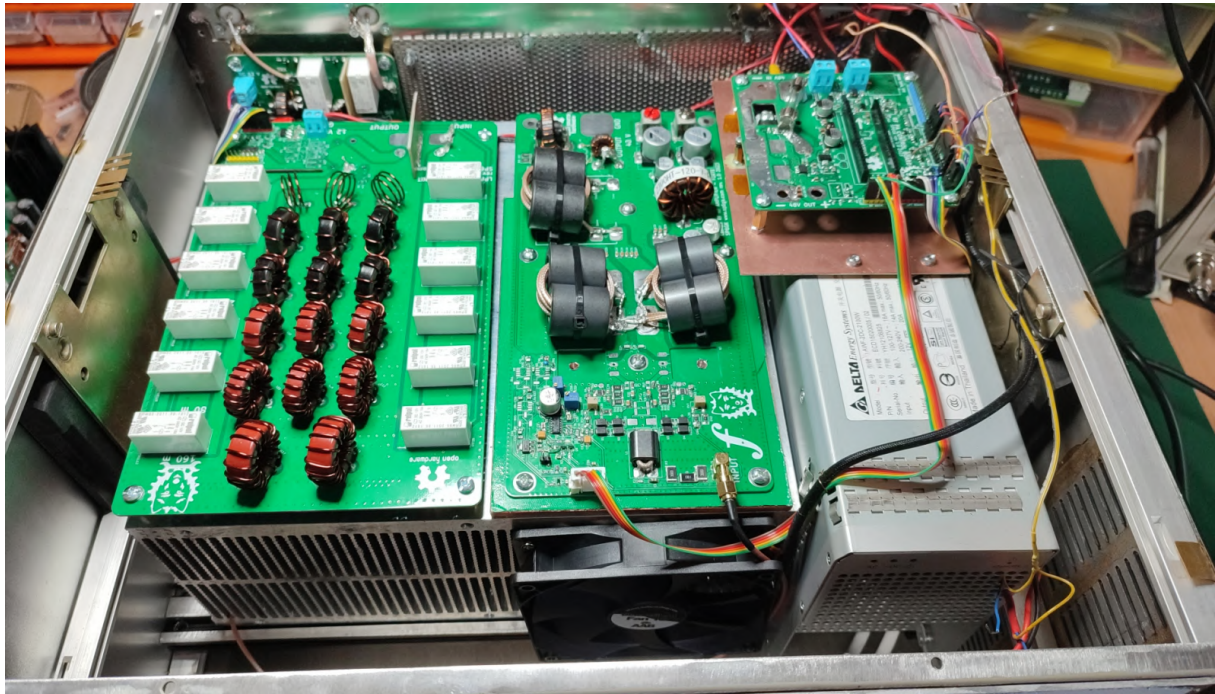


Figure 3.2: Top of the amplifier during assembly



Figure 3.3: Front of the assembled amplifier

## 3.2 Cooling System

MRF300s are not specified in terms of maximum drain current. For these RF transistors, NXP specifies the maximum thermal junction temperature. Operating close to this value can dramatically shorten the MTBF of the transistor. In order to keep the transistors within a safe temperature range at the junction, a proper system had to be designed to transfer the heat from the LDMOS package to the radiator, where it can be dissipated.

A large 215x144x133 mm aluminum radiator was installed in the amplifier. The MRF300 uses TO-247-3 package, and while they are designed for high power applications, the surface of the bottom source conductor is relatively small. To improve heat transfer from the transistors to the heatsink, a copper plate was used as a heat spreader. This plate is 5 mm thick and has dimensions of 200 x 120 mm, and is made out of copper for its high thermal conductivity. Because the bottom metal surface of the MRF300 is a source of LDMOS, which in this design is connected to ground, conductive thermal paste was used.

The TIM or thermal interface material used between the heat spreader and transistors is the Be Quiet DC2 Pro BZ005, which is a liquid metal type thermal paste with a thermal conductivity of 80 W/mK. Between the large area of the heat spreader and the radiator, a cheaper and non-conductive thermal paste was used, AABCOOLING TG5 with thermal conductivity of 12.5 W/mK. This thermal conductivity is still sufficient due to the much larger surface over which heat is being transferred. The second reason for using non conductive thermal paste between the aluminum radiator and copper heat spreader is that, because of the metal difference, a thermoelectric effect might cause a voltage difference to appear, which might lead to corrosion of the heatsink.

Two 120 mm 12 V PWM controlled fans were used for forced air cooling of the radiator. One fan pushes air on the front, and the second fan exhausts air from the back, working in a push-pull configuration. The PSU uses its two low-profile factory installed fans that are now PWM controlled by the control board. The air intake for the PSU is on the right side of the amplifier, and the exhaust is at the back so that the heat from the PSU does not affect the amplifier deck, and vice versa.

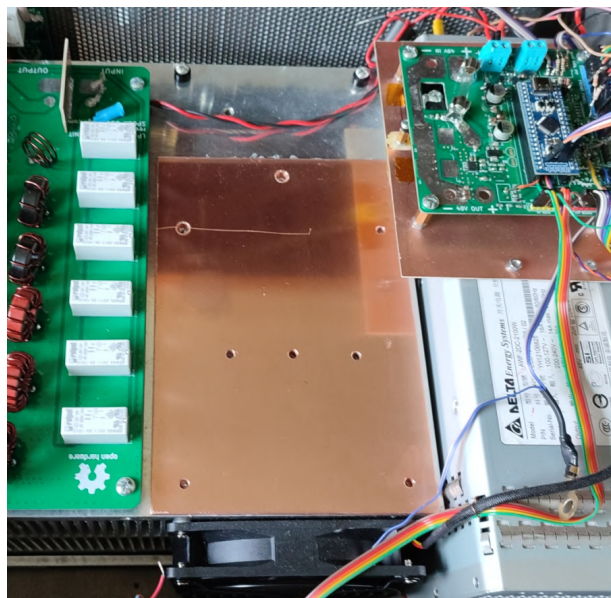


Figure 3.4: Amplifier during assembly without PA board, copper heat spreader and intake fan are visible



Figure 3.5: Right upper corner view of the amplifier, air intake options are visible

# Chapter 4

## Amplifier Tests

### 4.1 Measurement Setup

#### Dummy Load

In order to test the amplifier, a proper measurement setup had to be implemented. Important part of this setup was the  $50\ \Omega$  dummy load. This is a load that presents an excellent match to the amplifier output across a wide frequency spectrum and dissipates the RF power into heat. For that, a  $220\times140\times120$  mm aluminum radiator with special purpose low inductive RF resistors was used. In order to increase the power handling while maintaining low inductance, two parallel resistors were used. Each  $100\ \Omega$  resistor was made by Diconex and was rated for 400 W. Liquid metal TIM used previously between transistors and heat spreader was applied between resistors and heat spreader. Finally, both resistors and heat spreader were mounted to the radiator using M4 screws after threads were tapped in the radiator.



Figure 4.1: Inside of the dummy load

Resistors were connected using copper braid. This was done to minimize inductance because normal wire would be more susceptible to the skin effect due to a smaller surface area. Another reason for using copper braid was its elasticity. As the terminals of the resistors expand and contract with heat, a stiff connection might lead to the breaking off of the resistor terminal, resulting in a high VSWR.

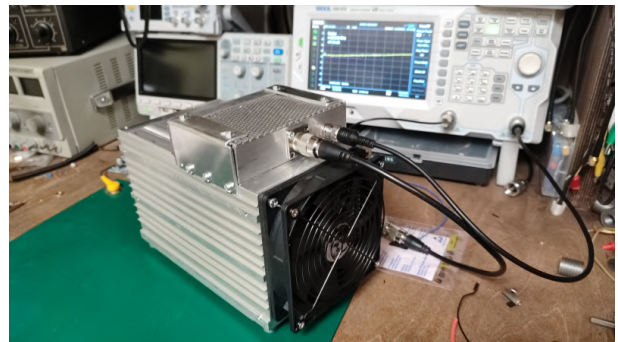


Figure 4.2: Dummy load and sampler.



Figure 4.3: Input (left) and output sample port (right)

The PL-239 connector was mounted on the front L-shaped profile alongside the BNC connector. To minimize RFI and improve safety, the exposed resistors were enclosed using aluminum sheets with perforated air vents on top. Steel or other ferrite material would be better to shield the magnetic field however aluminum was much easier to work with. The PL-239 was connected using RG-303 coax to the copper braid and parallel resistors. A BNC connector was added to provide an output for the built-in RF sampler. With the sampler output terminated in another  $50 \Omega$  load, a VNA was used to measure the return loss of the dummy load.

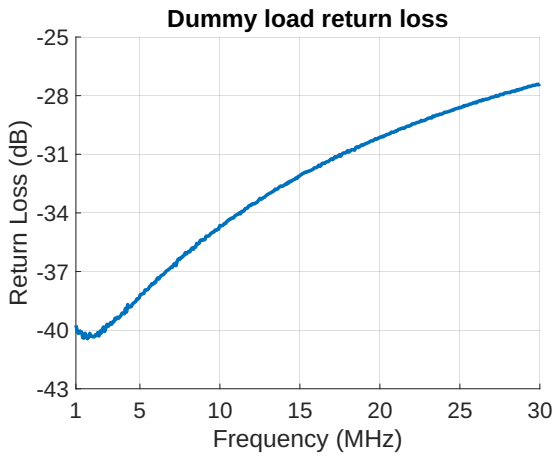


Figure 4.4: Dummy load return loss

## RF Sampler

The sampler was implemented according to the article by Don Jackson published in CCA Signal[55]. It outputs an RF signal that is 50 dB below the input. This signal can then be safely connected to a sensitive spectrum analyzer. Since the expected amplifier power is 600 W or 55.56 dBm, and the used spectrum analyzer's maximum input is 20 dBm, this means that using the sampler, a maximum of 5.6 dBm will be seen by the spectrum analyzer. Even with higher powers, this is a much safer solution because proper attenuators can be connected in series with the sampler's output port. The RF sampler was tested using a spectrum ana-

lyzer with a tracking generator in the range of 1 to 30 MHz and 1 to 120 MHz.

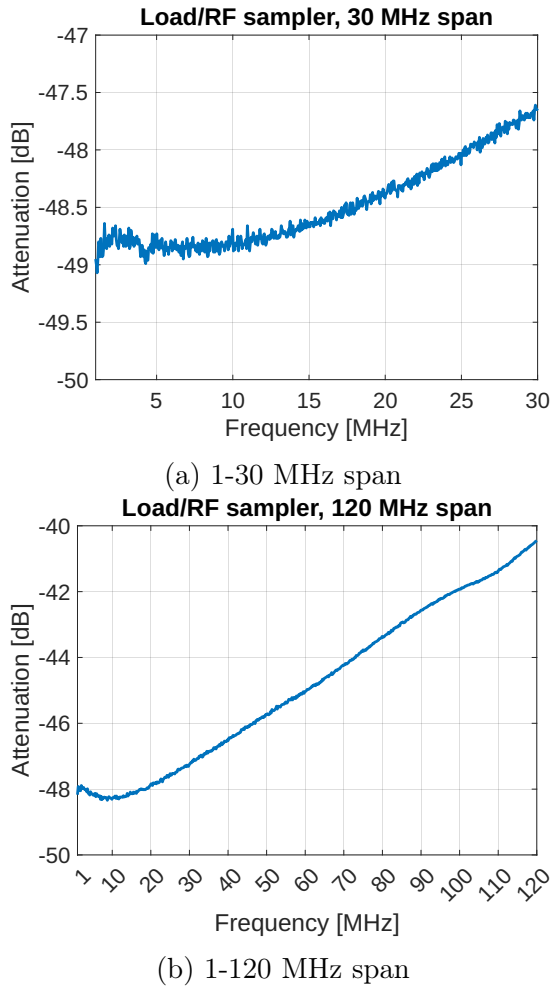


Figure 4.5: S31 measurement of RF sampler

In Fig. 4.5, it can be seen that for lower frequencies, the sampler provides attenuation very close to the desired 50 dB. However, as the frequency increases, the performance decreases linearly. This is due to the long length of the unshielded connection of the output port, which was necessary due to the mechanical design of a dummy load. This sampler is still valid for measuring amplifiers working below 30 MHz because, with knowledge of the sampler's characteristics, a correction can be applied after the measurement. Harmonics will, of course, be presented to the spectrum analyzer with lower attenuation than the fundamental however, due to their lower power by nature, the measurement instrument should be safe with the addition of an attenuator.

The constructed sampler works on the same principle as the RF coupler used to measure output and reflected power described in Sec. 2.2.1, except it does not detect the signal but simply takes a small portion of it to another port, and it has 3 ports instead of 4. Because the used coaxial cable acts as a single turn primary winding of a current transformer, its shielding is grounded only on one side to act as a Faraday shield. However, it is not a shielded transmission line anymore, so its length should be as short as possible for the best performance. The coupler visible in Fig. 4.1 has quite long connections, decreasing its performance (not flat line attenuation across a wide bandwidth) because it was an addition to a dummy load. A second, more compact coupler was built, using the same bill of materials and schematic.

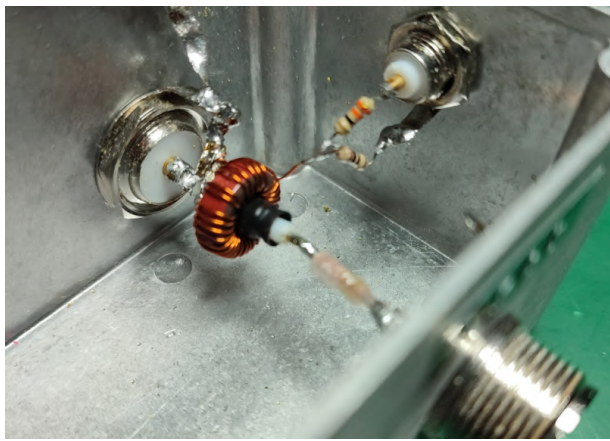


Figure 4.6: Another 50 dB sampler built in a smaller metal box

This sampler exhibits relatively flat coupling up to 90 MHz (see Fig. 4.7) and does not show significant capacitive coupling up to 180 MHz. However, in this project, a sampler built into the dummy load was used with calibration applied.

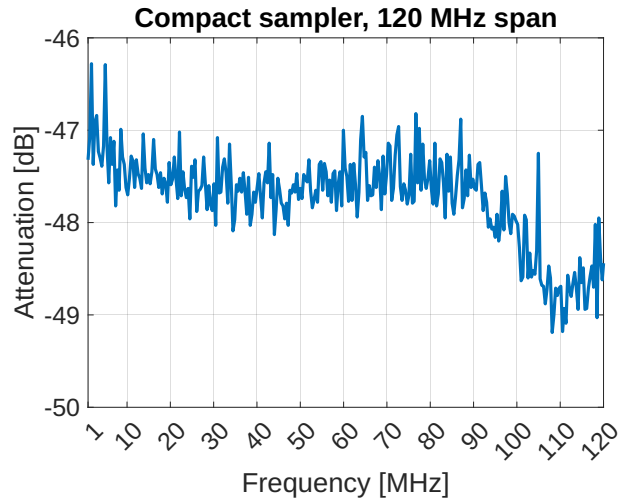


Figure 4.7: Compact sampler S31

### Inline Power Meter

The power meter used during testing was the Maas RX-600. This cross needle meter can measure forward power in three ranges: 30 W and 300 W with an accuracy of  $\pm 5\%$ , and 3 kW with an accuracy of  $\pm 7.5\%$ . Average power was measured in all the tests.



Figure 4.8: Power meter showing 600 W

### Spectrum Analyzer

For the analysis of harmonics and intermodulation products, a Rigol DSA 815-TG was used. Most measurements were carried out with 3 kHz or 10 kHz RBW, except for the IMD measurements, where a smaller RBW of 100 Hz was chosen. The detector was set to peak mode. Data from the device was saved to .csv file and then plotted using Matlab.

## Signal Source

For the signal source, a Xiegu G90 amateur radio transceiver was used. This transceiver can output CW, SSB, AM or FM signals from 1.8 to 30 MHz in amateur radio bands, with power ranging from 1 W to 20 W in 1 W steps. To achieve greater resolution, a 6 dB attenuator was placed in series with the transceiver and amplifier when the power going to the amplifier was smaller than 2 W.



Figure 4.9: Xiegu G90 transceiver

The testing methodology for the amplifier was adopted based on the test procedures of ARRL (American Radio Relay League)[56]. However, the most significant limitation to a proper test setup has proven to be a signal source for the IMD test, which requires two tones to be as clean as possible. For this purpose, the use of two signal generators with class A RF amplifiers is recommended. Alternatively, two 100 W transceivers can be used with reduced power and then coupled using, for example, a Wilkinson hybrid made out of coaxial cables. The second solution is generally considered difficult to achieve due to poor isolation of the combiner and presents a potential risk to the equipment used. The spectral purity of common transmitters has also been criticized, as most transceivers achieve up to 30 dBc IMD3 products[57].

## 4.2 Bias Setup

Initially, the amplifier was switched to TX mode with transistors in cutoff. Subsequently, the voltage of one bias arm was increased using a potentiometer until the idle drain current for that transistor reached 200 mA. Next, the second transistor was biased to achieve a total current of 400 mA, ensuring an even load shared between the transistors. Current measurements were taken using a DMM (Uni-T UT 60A) at the input to the PA deck board and using the ACS-712 sensor, which displayed a value of 0.4 A at the front panel at the end of the biasing procedure. The quiescent drain current was selected to balance between good efficiency and linearity. Higher quiescent current would improve power gain and linearity at the cost of decreased drain efficiency. However, both the gain power and drain efficiency differences decrease for higher output powers. This dependency is presented in the MRF300 datasheet, where values of quiescent drain current from 100 mA to 900 mA were tested[17].

## 4.3 Initial Test

First, the amplifier was tested with a 1:9 transmission line transformer made with 3 turns of 17 Ω coaxial cable on type 61 ferrite cores. The purpose of this test was to verify whether the amplifier is functioning correctly and whether the custom sampler provides accurate results. The amplifier was tested with a CW signal at frequency of 14.15 MHz, corresponding to the middle of the band to which it was optimized.

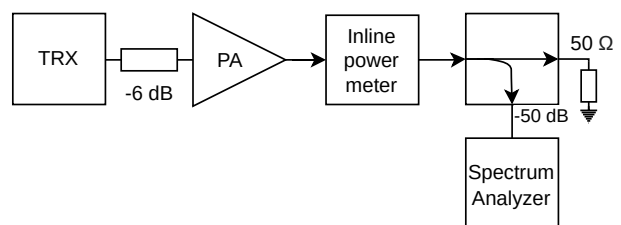


Figure 4.10: Test setup diagram

Pin [W]	Meter [W]	Meter [dBm]	SA [dBm]	$\Delta$ [dB]
0.25	50	46.99	45.17	1.82
0.5	100	50.00	48.26	1.74
0.75	147	51.67	49.84	1.83
1	185	52.67	50.6	2.07
1.5	260	54.15	52.16	1.99
2	355	55.50	53.67	1.83
3	450	56.53	54.76	1.77
4	515	57.12	55.27	1.85
5	580	57.63	55.45	2.18
6	590	57.71	55.66	2.05
7	600	57.78	56.05	1.73

Table 4.1: Initial test of the power amplifier and sampler. CW at 14.15 MHz

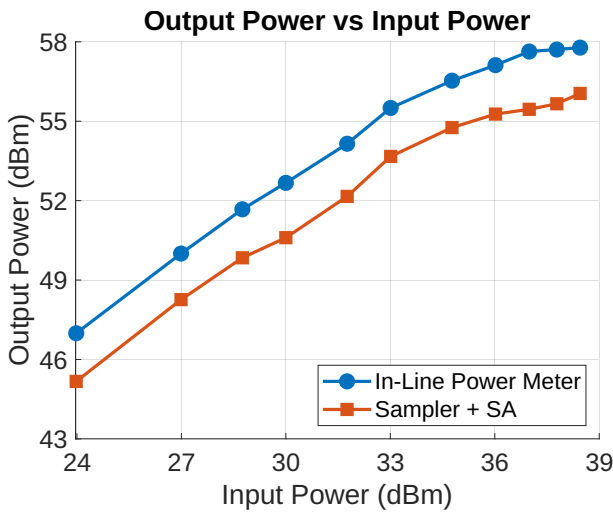


Figure 4.11: Output power measurement

In Table 4.1, it can be observed that the amplifier has reached the desired power level according to the meter. However, the custom built sampler connected to a spectrum analyzer did not indicate the same amount of power. The accuracy of the spectrum analyzer was ruled out because its amplitude uncertainty, specified by the manufacturer is 0.4 dB. While this accounts for the variation in the difference between steps of power (not a constant  $\Delta$ ), it does not explain the difference of an average 1.89 dB. Zero span was also used to measure the power at 14.15 MHz with a 10 kHz RBW however, very similar results were obtained,

but with much faster readings, as the heterodyne of the spectrum analyzer did not have to sweep the entire spectrum.

Another hypothesis considered was the presence of harmonics in the signal that could account for the additional power measured by the wideband inline power meter. The result from the spectrum analyzer in Table 4.1 represents the measured level of the fundamental signal (1st harmonic) with a RBW of 3 kHz. In contrast, the inline meter measures the integral of the power across the whole spectrum from 1.8 to 180 MHz.

To investigate whether a reasonable amount of harmonics accounts for this power, the level of first eight output harmonics was measured for an input power of 7 W. This implies that when the values from the spectrum analyzer are converted to Watts, then summed up, and converted back to dBm, the result should indicate the total power from 14.15 MHz to 113.2 MHz. The results of the harmonics measurement are shown in Table 4.2. The plot of the first eight harmonics is presented in Fig. 4.12. The effect of the push-pull amplifier on the second harmonic is apparent, as the second harmonic is lower than the third. This characteristic is advantageous when the amplifier has to conform to legal norms, as the second harmonic is more challenging to attenuate due to its proximity to the fundamental frequency.

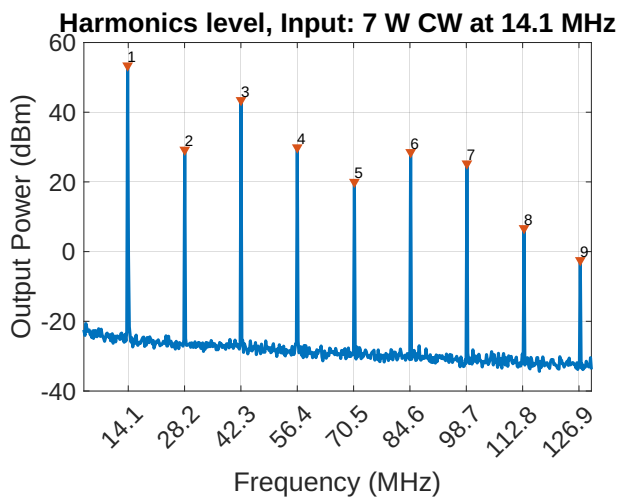


Figure 4.12: SA harmonics measurement

Harmonic	1	2	3	4	5	6	7	8
SA [dBm]	56.05	31.93	45.35	33.99	21.43	29.53	26.14	7.56
SA [W]	402.72	1.56	34.28	2.51	0.14	0.9	0.41	0.01

Table 4.2: Wide harmonic measurement using spectrum analyzer and sampler

From Table 4.2, it can be observed that the first four harmonics contain a significant amount of power, but the next four contain very little power. The inline power meter has measured forward power of 57.78 dBm or 600 W. The sum of the fundamental power and harmonics measured by the spectrum analyzer and sampler is 442.51 W or 56.46 dB.

- **SA total:** 56.46 dB dBm  $\pm > 0.4$  dB
- **Inline meter:** 57.78 dBm  $\pm 7.5\%$

This concludes that the harmonics do, in fact, constitute a part of the total power measured by the meter, but they don't account for the total difference. The resulting 1.32 dB difference is significant, and unfortunately, no other reference standard for such a high power measurement was available in the laboratory. A positive aspect of the experiment is that both the sampler and meter measurements have resulted in the same shape of traces in Fig. 4.11, indicating that the sampler works well with this level of power and maintains its characteristics. The only difference is its large offset. Another aspect lowering the accuracy of the sampler method is the uncertainty stacking. To calibrate the sampler reading, a tracking generator was initially used to normalize the generator to the input of the spectrum analyzer. Subsequently, the sampler S31 was measured and saved to a CSV file. After completing the measurement of the amplifier's output, the values from the calibration S31 of the sampler were added to the results. This introduces several points of possible error stacking. Ultimately, even though the results from the sampler are not accurate on their own, adding 1.3 dB should bring them to a reasonable approximation of real power levels at the specific frequencies.

What is more important is that the characteristic of the sampler matches the characteristic of the inline meter. Therefore, it was assumed that relative measurements in dBc are still valid.

## 4.4 Power, Gain, PAE

Power output and gain characteristics were measured for different amateur radio bands using three different output transformers. The first transformer was the 1:9 TLT wound with 3 turns of 17 Ω coax on 61 type material cores (see Fig. 2.35a). The second transformer was also a 1:9 TLT, wound with three turns of 50 Ω and 25 Ω coaxial cables connected in parallel on 43 type cores (see Fig. 2.35c). The third investigated option was the 1:4 transformer wound with 25 Ω coax on 43 type cores (see Fig. 2.35d). The goal of this section was to determine the maximal output power and 1 dB compression for each band, as well as the flatness of the gain and maximal power across the 1.8 to 30 MHz spectrum.

There are several ways to measure the efficiency of a RF amplifier. One method is to use the collector efficiency for BJT or drain efficiency for MOSFET, defined as the ratio of RF output power to the DC input power of the transistor. However, the collector or drain efficiency (usually denoted as  $\eta_C$  or  $\eta_D$ ) does not include the input power. Therefore, another measure known as power added efficiency (PAE) is also used. PAE is naturally smaller than drain efficiency, but it will be utilized in this project because it provides a more realistic measure, taking into account the necessary drive power.

$$PAE = \left( \frac{P_{OUT} - P_{IN}}{P_{DC}} \right) \cdot 100\% \quad (4.1)$$

#### 4.4.1 1:9 TLT, 3 Turns 17 $\Omega$ , Ferrite Material 61

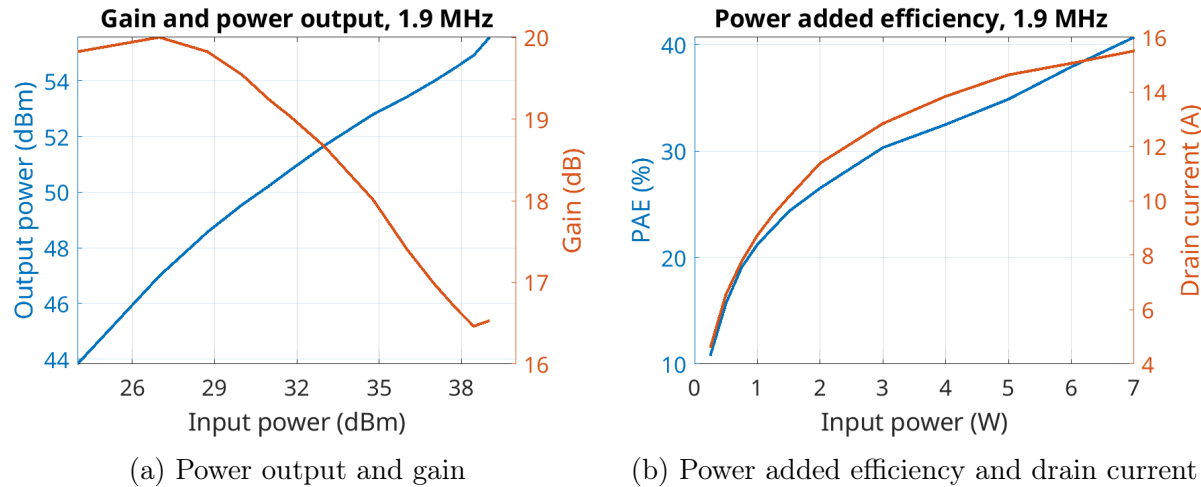


Figure 4.13: Measurement of amplifier at 1.9 MHz CW

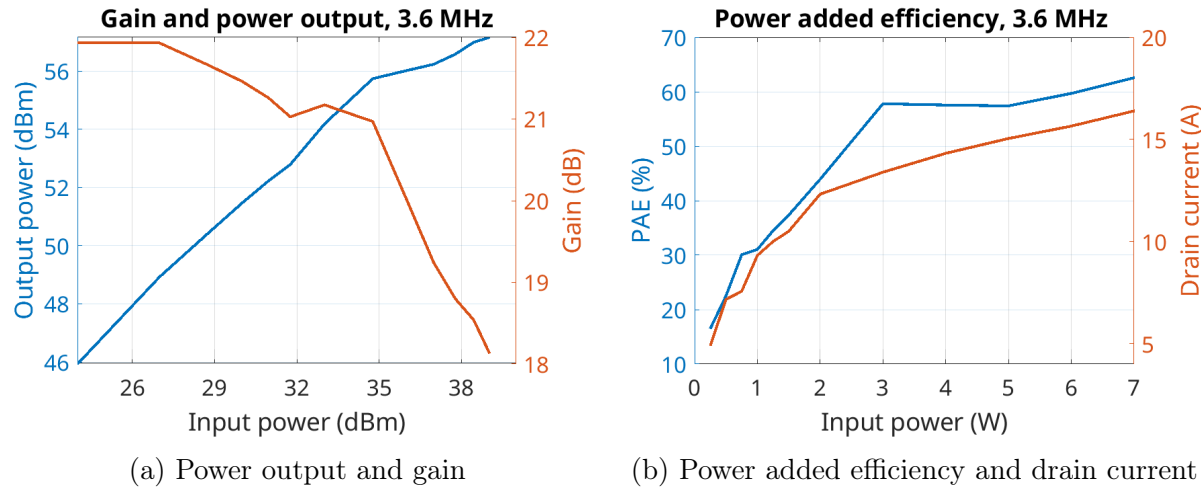


Figure 4.14: Measurement of amplifier at 3.6 MHz CW

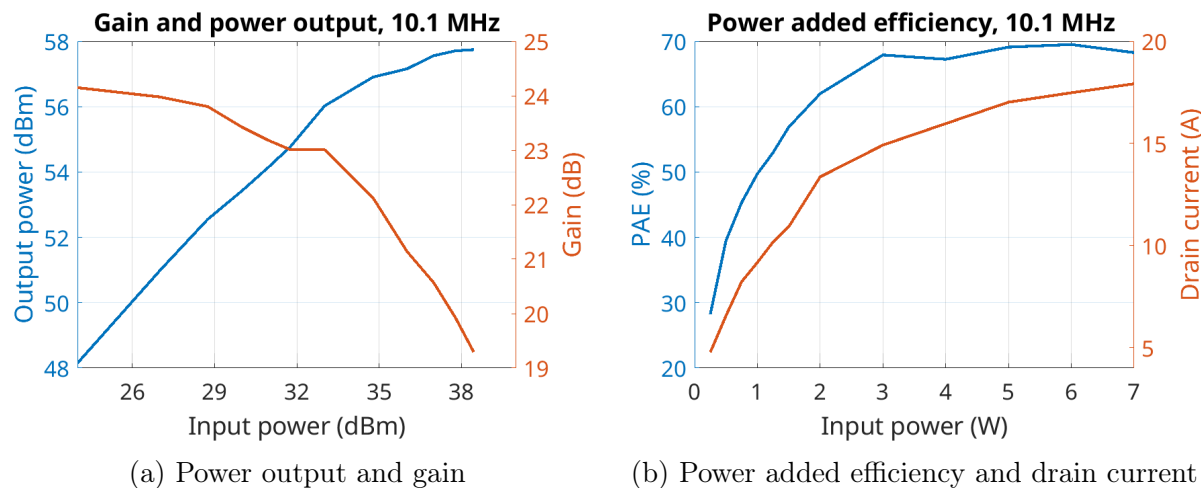


Figure 4.15: Measurement of amplifier at 10.1 MHz CW

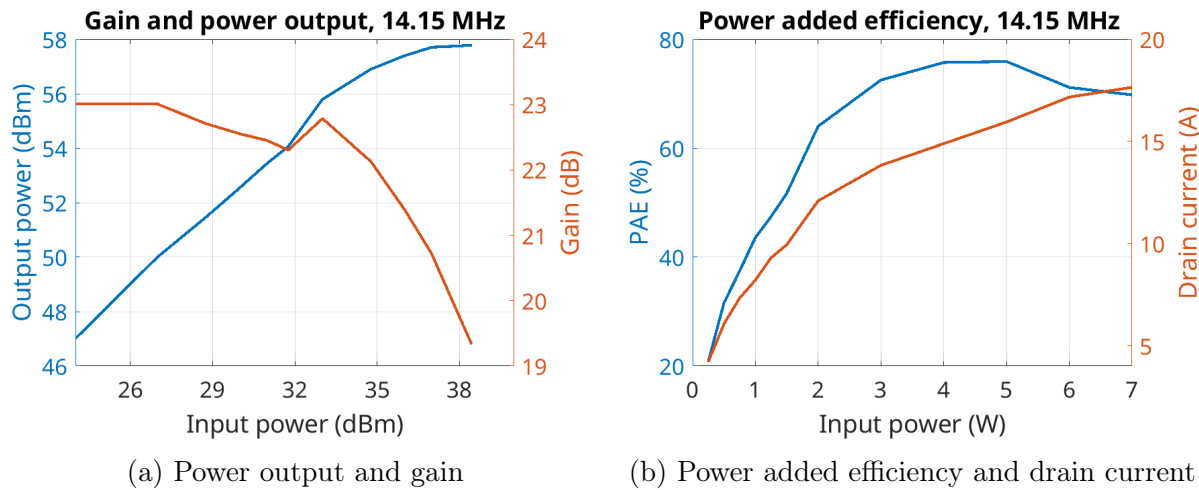


Figure 4.16: Measurement of amplifier at 14.15 MHz CW

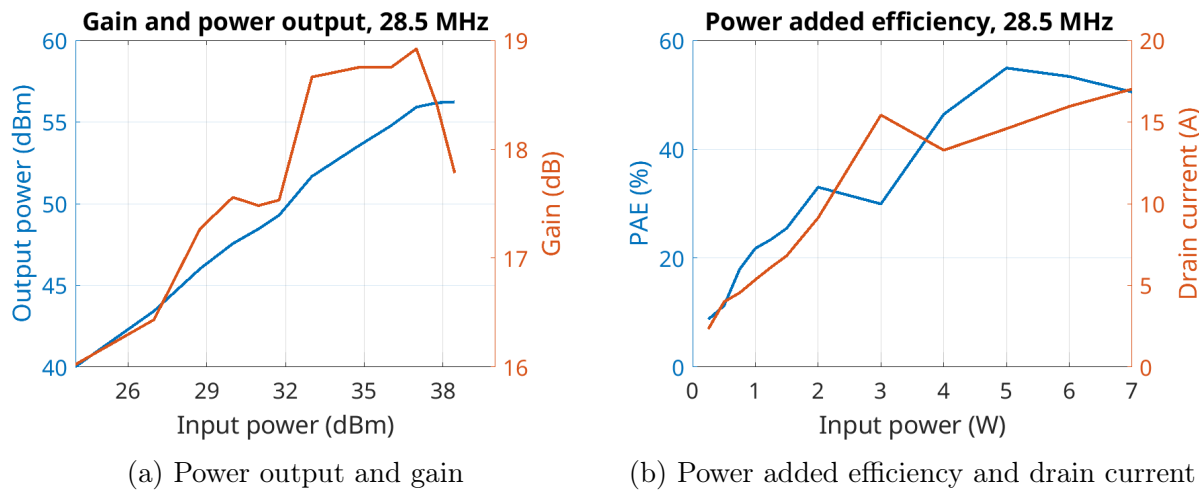


Figure 4.17: Measurement of amplifier at 28.5 MHz CW

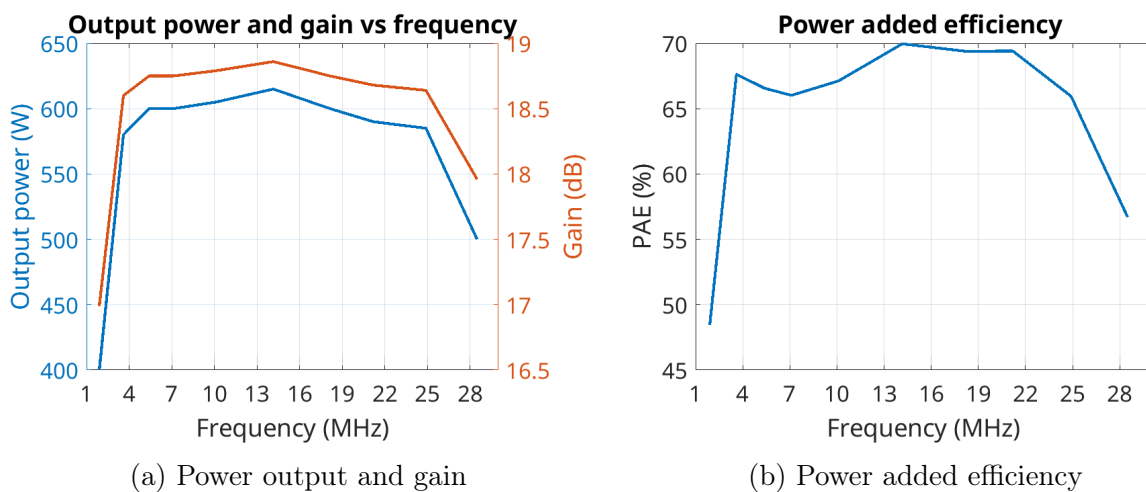


Figure 4.18: Across bands characteristic of amplifier with tested TLT

#### 4.4.2 1:9 TLT, 4 Turns $50\parallel 25 \Omega$ , Ferrite Material 43

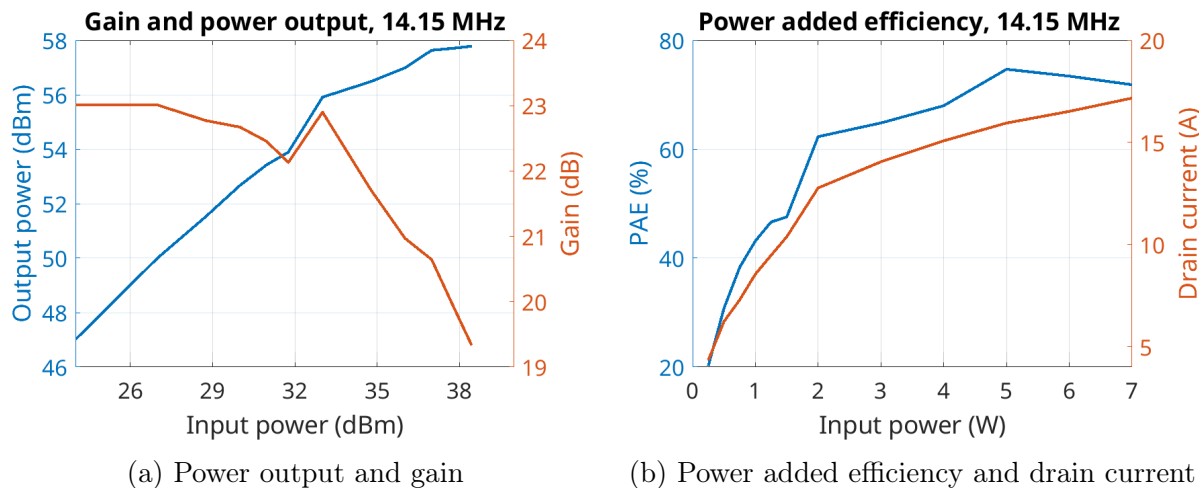


Figure 4.19: Measurement of amplifier at 14.15 MHz CW

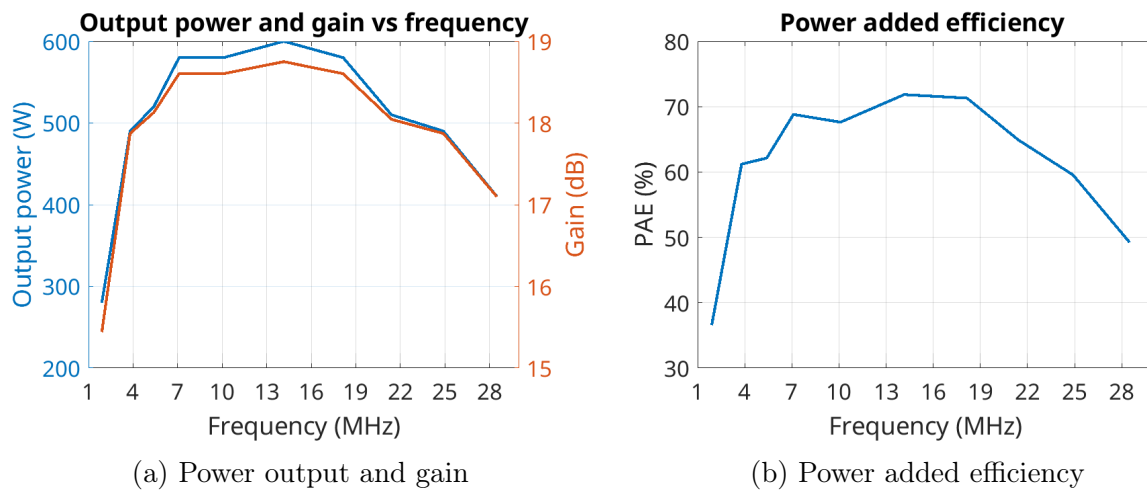


Figure 4.20: Across bands characteristic of amplifier with tested TLT

### 4.4.3 1:4 TLT, 5 Turns 25 $\Omega$ , Ferrite Material 43

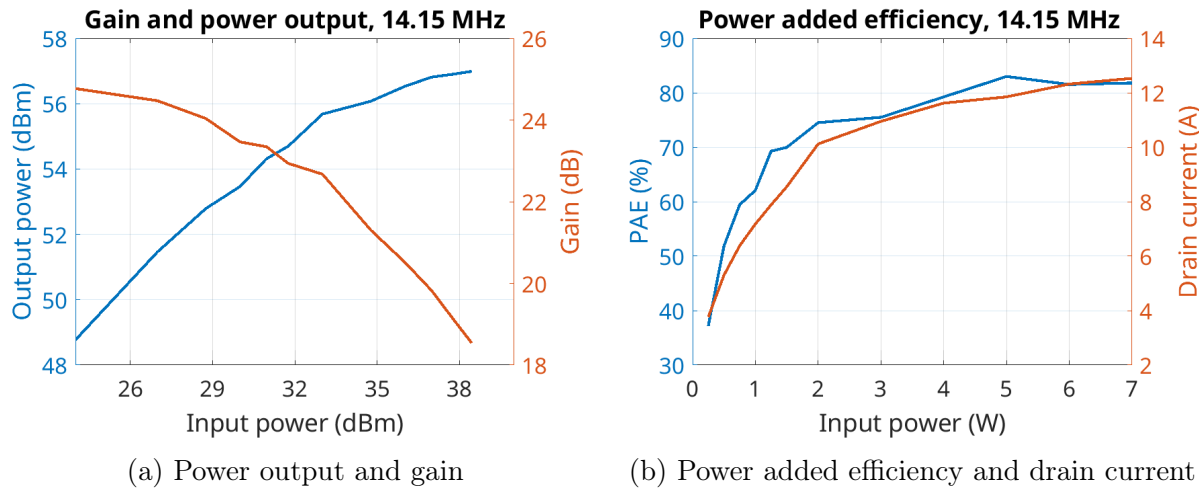


Figure 4.21: Measurement of amplifier at 14.15 MHz CW

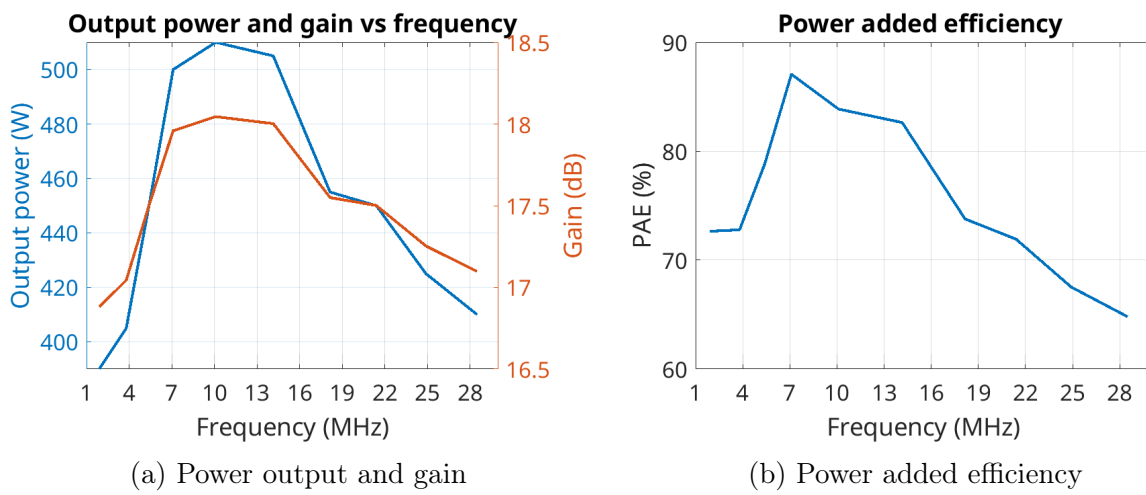


Figure 4.22: Across bands characteristic of amplifier with tested TLT

#### 4.4.4 TLT and Efficiency

In the above measurements, all three transformers were tested for peak power across amateur radio bands. Additionally, each configuration was tested in depth at 14.15 MHz, which was the center frequency for which the amplifier was designed.

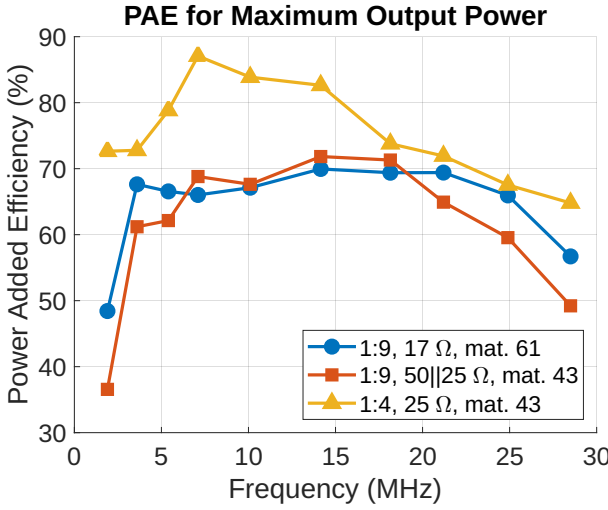


Figure 4.23: Comparison of amplifier's PAE for three TLTs across HF spectrum

The first 1:9 transformer wound with  $17\ \Omega$  coaxial cable represents an example of a transformer that utilizes special-purpose coax. The construction of this transformer was presented in Fig. 2.35a. It has reached a peak PAE of 69.96% at 14.15 MHz. Notably, this transformer achieved the most flat characteristic in Fig. 4.23), maintaining more than 65% PAE from 10 MHz to 25 MHz.

Observations indicated that the amplifier with this transformer exhibits a very similar PAE to a 1:9 TLT built using two parallel coaxial cables, as shown in Fig. 2.35c. Furthermore, it can be noted that the transformer with a  $17\ \Omega$  cable performs in a more predictable manner and, according to measurements, achieves approximately 7% better PAE for medium input power and only slightly worse PAE for high input power at 14.15 MHz (see Fig. 4.24) when compared to the improvised 1:9 TLT.

The transformer with a 1:4 impedance ratio managed to achieve the highest effi-

ciency out of the amplifier. The peak PAE was observed at 7.1 MHz with 87%. However, while this result is very good, the linearity of such an amplifier can be brought into question. Additionally, it can be noticed that this configuration achieves excellent efficiency of 72% at 1.9 MHz, which is most likely due to the larger reactive inductance of 5 turns on type 43 ferrite cores when compared to 1:9 transformers.

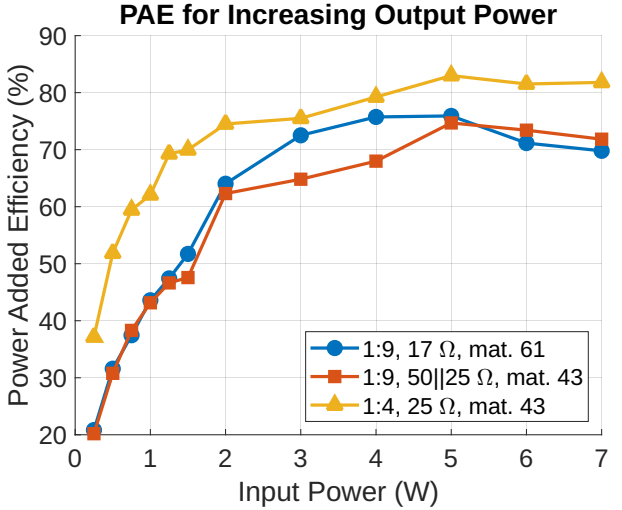


Figure 4.24: Comparison of amplifier's PAE for three TLTs for increasing input power

Both 1:9 transformers exhibited rather poor performance at 1.9 MHz. Even in the case of more turns on 43 type material (which has higher permeability), the results were almost identical. This confirms the information from the TLT handbook[45], where the problem of high reactive inductance required for lower frequencies was presented as a limiting factor in the practical application of this type of transformer. However, these tests also show that it is possible to create a 1:9 TLT using parallel transmission lines.

Ultimately, if efficiency is the primary concern, the 1:4 transformer is a good choice. As shown previously, it provides a safe return loss, and despite greater mismatch loss, the observed efficiency is higher. We hypothesize that this is due to lower temperature and much smaller current that

flows through the drains. Another consideration is the linearity of such a configuration.

#### 4.4.5 TLT and Output Power

For all three transformers, the output power was measured for increasing input power at 14.15 MHz and for 7 W CW input across different bands.

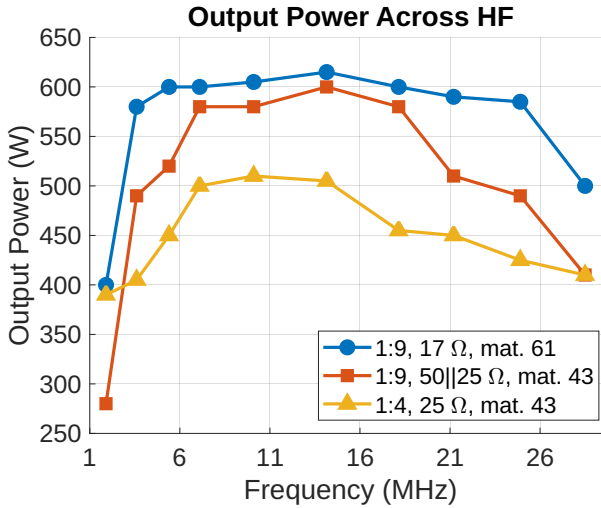


Figure 4.25: Output power for 7 W input

In Fig. 4.26, it can be observed that the 1:9 TLT made with  $17\ \Omega$  coaxial cable and 61 type ferrite cores provided the largest output power. A peak of 615 W was noted at the center frequency of 14.15 MHz, while a level of more than 580 W was maintained from 3.6 MHz to 24.9 MHz. This more expensive transformer also yielded the highest output power for both the low frequency of 1.8 MHz and the high end of the spectrum at 28.5 MHz. The improvised transformer that created a characteristic impedance of  $17\ \Omega$  using two parallel transmission lines of 50 and  $25\ \Omega$  resulted in a similar trace but with lower output power, especially at the bottom and upper end of the spectrum. For the medium frequencies between 7 and 17 MHz, the results are close to the more expensive 1:9 transformer but with a slightly lower peak of 600 W at 14.15 MHz. This alternative transformer also exhibits a much faster decrease in output power with frequency. This is very likely due to increased

stray capacitance of the two parallel transmission lines, which might be worsened by non-ideal winding since winding two parallel transmission lines was more challenging.

The cheapest and most available material wise 1:4 TLT, as expected from the power equation in Sec. 2.3.4, presented the lowest output power. Exceptions to that are at 1.8 MHz, where it performed better than the improvised 1:9 TLT with parallel coaxial cables, and at 28.5 MHz, where both improvised 1:9 and 1:4 TLTs achieved the same output power.

It is worth mentioning that even though in the midband, the power equation in the balanced system did provide lower output power, the minimum obtained power was very close to that calculated in Sec. 2.3.4. It is important to remember that the equation in Sec. 2.3.4 only considered the real part of the impedance to visualize the matching and possible power dissipation in the load. In this case, as shown in equation 2.3, the 1:4 TLT does not provide very good return loss because the impedance of the transistors is lower than the  $12.5\ \Omega$  used in the calculation, and the impedance changes with frequency. Because the 1:4 transformer presented the best efficiency for every band and allowed for the second-best output power for the lowest and highest bands, an argument can be made that it is the best choice for applications where wideband and high efficiency take priority over maximum power. Such an amplifier could also be more robust and less prone to failures. With higher efficiency and lower drain current, the transistors will produce less heat, leading to a longer mean time between failures.

Even though an output of 400 to 500 W using the 1:4 transformer might seem like a good choice, an argument for using the 1:9 transformer is not only its peak of 600 W but also a higher 1dB compression point. Fig. 4.26 illustrates the increase in output power in Watts for an increasing power in Watts. It can be observed that the 1:4 transformer saturates first, while both 1:9

transformers have very similar characteristics, but the single transmission line version is slightly more linear.

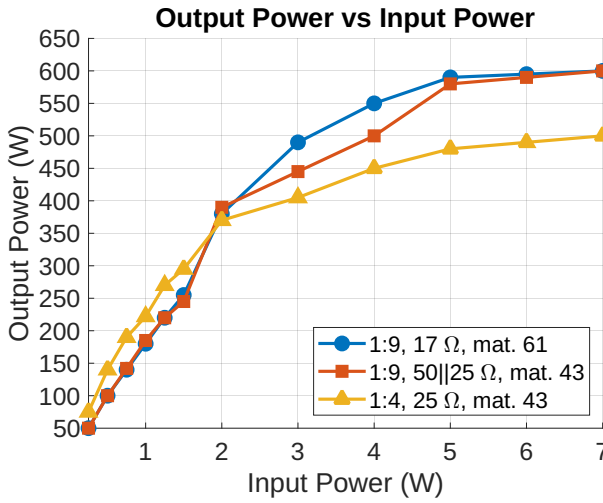


Figure 4.26: Increasing output power

In Fig. 4.26, it can be observed that for every tested TLT, the amplifier has a linear region after which it saturates. The input power for which the output drops by 1 dB compared to the extrapolated linear region is known as the 1 dB compression point. Above this point, the amplifier exhibits more nonlinear effects, resulting in an increase of spurious emissions.

## 4.5 Linearity

Although the data presented in the gain and power output measurements (Figs. 4.13a to 4.21a) is not always ideal due to the limitations of the measurement setup, the P1dB was determined for plots where it was possible to find such a point. Mainly, the 1:9 TLT with 17 Ω coaxial cable was investigated in this section. However, for its performance at 1.9 MHz, the 1 dB point was not possible to be determined because the maximum safe drain current was reached before the output power exhibited saturation. As the center design frequency was 14.15 MHz, all three tested TLTs were also measured for P1dB at that frequency.

P1dB was determined using Matlab. After importing the data into the script, coefficients for a first degree polynomial were calculated. Then, a fitted trend line was extrapolated using the polyval function. The blue continuous line in Fig. 4.27 shows the output measured from the amplifier, while the orange dashed line represents the extrapolation of the linear region of the tested amplifier. If the amplifier was ideally linear, this extrapolated line would represent its characteristic of output for all inputs, fulfilling the requirements of additivity and homogeneity from Sec. 2.2.3.

Finding the exact point where the difference of 1 dB occurs between the ideally linear trend line and the real amplifier output can be challenging. Therefore, a third dashed line (yellow color) was added, positioned 1 dB below the ideally linear line. This line intersects with the real output line exactly at P1dB, allowing for easy placement of a marker to read out the data.

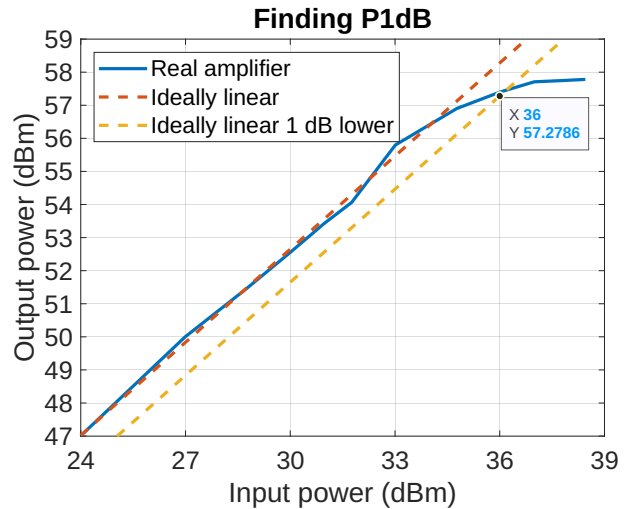


Figure 4.27: Plot showing the process of finding the 1 dB point

From Fig. 4.27, P1dB of 36 dBm or approximately 4 W can be read. For that point, the amplifier reaches an output of 57.27 dBm, which is 530 W. This measurement was done at 14.15 MHz with the 1:9 TLT that uses special 17 Ω coaxial cable.

From Figs. 4.13a to 4.21a, it can also be noticed that high power added efficiency is achieved for high output power. This is in contrast to linearity, the highest linearity is present well below the 1 dB compression point. This shows the inverse relationship between linearity and efficiency. Dependency of output power and linearity will be shown next using dual-tone IMD measurement.

<b>Test condition: 14.15 MHz CW</b>		
<b>TLT</b>	<b>P<sub>1db</sub></b> <b>[dBm]</b>	<b>P<sub>out</sub></b> <b>[dBm]</b>
1:9, 17 Ω, mat. 61	36	57.2
1:9, 50  25 Ω, mat. 61	35.4	56.8
1:4, 25 Ω, mat. 61	34.7	56

Table 4.3: P<sub>1dB</sub> for three tested TLTs at 14.15 MHz

<b>TLT: 1:9 17 Ω, mat. 61</b>		
<b>Frequency</b> <b>[MHz]</b>	<b>P<sub>1dB</sub></b> <b>[dBm]</b>	<b>P<sub>out</sub></b> <b>[dBm]</b>
3.6	36.3	56.1
10.1	35.6	57
14.15	36	57.2
28.5	37.5	56.2

Table 4.4: P<sub>1dB</sub> for 1:9 TLT at different bands

From tables 4.3 and 4.4, it can be seen that the amplifier with 1:9 transformer with 17 Ω coaxial cable presents the highest 1 dB compression point and highest output power out of all tested configurations.

It was also observed that with increasing frequency, the compression point is not constant, most likely because it depends on the gain of the amplifier, which is not flat. This could be improved with larger negative feedback. However, larger amount of feedback would lower the output power and thus efficiency.

## 4.6 Impact of TLT on Harmonics

The effect of operating the amplifier with input power beyond the 1 dB compression point is not only a decrease in gain and thus a smaller increase in output power but also increased spurious emission.

First, the even and odd harmonics were observed for different TLTs. The reason for this series of measurements was that the used topology of the push-pull amplifier should allow for the cancellation of the second harmonic because an ideal transformer will present a short circuit at two times the fundamental frequency [41]. Comparison of three transformers should reveal which one is the closest to being ideal by providing the largest SFDR between the fundamental signal (first harmonic) and the spurious second harmonic. The second and third harmonics of the amplifier with a 1:9 TLT made with 17 Ω coaxial cable were measured at increasing levels of a 14.15 MHz CW input signal.

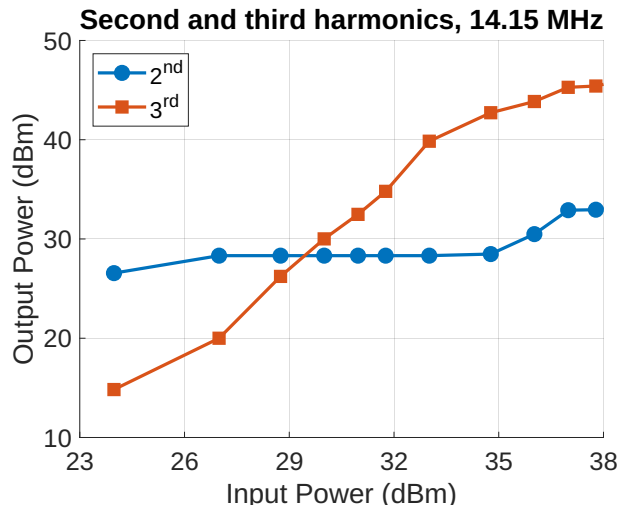


Figure 4.28: Power level of harmonics for increasing input power

It can be seen that the level of the second harmonic stays mostly constant, and for input levels above 29.75 dBm, it is actually lower than the third harmonic, which hints at the canceling effect of a balanced configuration. A second important observation from Fig. 4.28 is that the level of the sec-

ond harmonic started to increase only after 34.77 dBm of input power, right before the previously measured P1dB of 36 dBm. On the other hand, the odd third harmonic has consistently increased in power, similar to the first harmonic (fundamental), reaching almost 46 dBm or 40 W. Because different transformers presented different output power levels, the magnitude of harmonics was plotted as the level below the carrier in dBc.

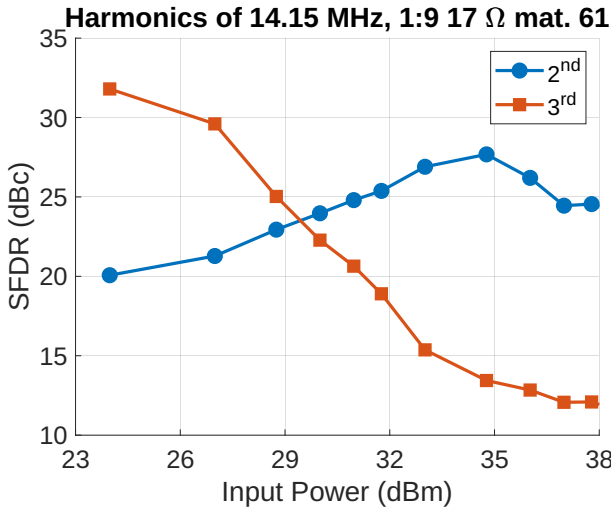
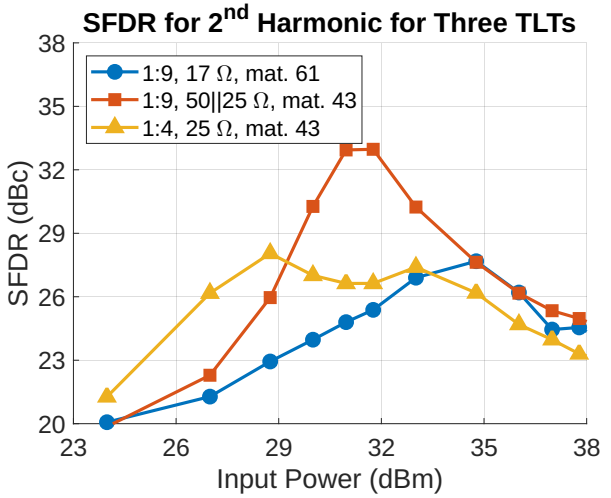


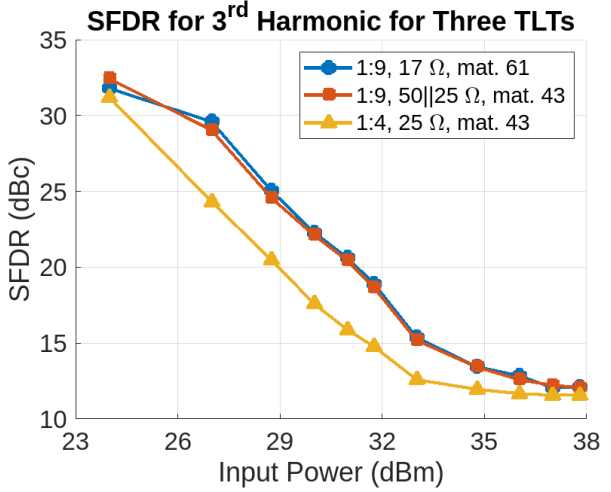
Figure 4.29: Spurious dynamic range between fundamental and harmonic

In Fig. 4.29, it can be seen that the Spurious Free Dynamic Range (SFDR) increases between the fundamental and the second harmonic up to 34.77 dBm of input power, after which the SFDR drops. This shows that after this point, the fundamental does not grow as fast as the second harmonic. This point, even lower than the P1dB compression, is worth considering when linear operation is critical. For maximum allowed input power, the third harmonic results in a SFDR of only 12 dB.

Next, all three TLTs were investigated for their impact on SFDR. Here, SFDR is defined as the spurious free dynamic range between the fundamental and a specific harmonic. When a specific order of harmonic is considered, the other harmonics are ignored, even if they would normally decrease the SFDR by standard definition.



(a) Second harmonic SFDR for three TLTs



(b) Third harmonic SFDR for three TLTs

Figure 4.30: Impact of TLT on SFDR

Second harmonic SFDR in Fig. 4.30a varies between different transformers. Even though the 1:9 TLT made with 17 Ω cable and parallel connection of 50 and 25 Ω cables had similar characteristics before, here a significant difference in performance can be seen. Surprisingly, the improvised 1:9 transformer with parallel coaxial cables has exhibited the best suppression in the range from 29 dBm to 34.77 dBm of input power with a peak SFDR of 33 dBc. Although the characteristic is not flat, this is a very good result. The transformer made with custom 17 Ω cable, on the other hand, has performed relatively poorly in comparison to the other transformers except above 34.77 dBm input, where it was better than the 1:4 transformer by 1.47 dB, but it was

almost identical to the improvised transformer. This was not expected since the improvised transformer had most likely larger leakage capacitance and its windings were less organized because of difficulties during winding of two parallel cables at the same time. Perhaps two parallel transmission lines have minimized the losses leading to a better cancellation effect, or perhaps this is an exception occurring at 14.15 MHz. The cheapest transformer, the 1:4 TLT, has also provided very good results, with a wider range of attenuation higher than 26 dB. Although this transformer performed the worst for inputs above 34 dBm, it has outperformed every other construction between 24 and 28 dBm. This once again shows that this transformer, despite poor RL, has some advantages for MRF300s.

For the third harmonic, the difference in SFDR between the two 1:9 transformers was negligible. On the other hand, the 1:4 transformer presented an SFDR better by about 5 dB until the input power reached 33 dBm, after which it converged to the result of the 1:9 transformers. From the plot in Fig. 4.30b showing the SFDR between the fundamental and the third harmonic for increasing power, it can be noticed that the SFDR for large input power is much smaller than in the case of the second harmonic, demonstrating the proper behavior of the push-pull amplifier.

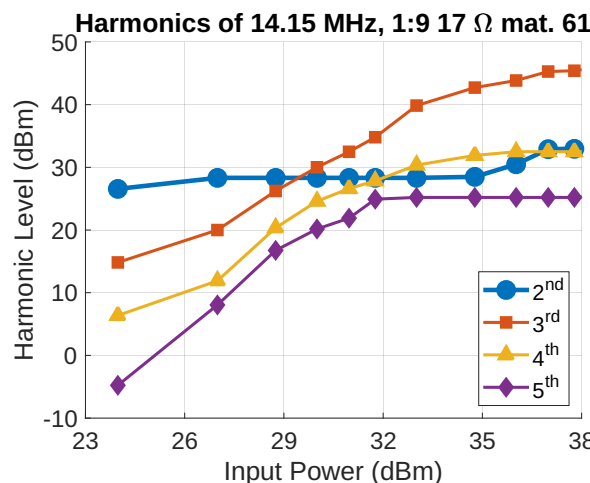


Figure 4.31: 4th and 5th harmonic level

The increase in power of the fourth and fifth harmonics was also measured and plotted in Fig. 4.31. This test used the 1:9 transformer wound with 17 Ω cable on type 61 material cores. As expected, a decrease in harmonic power was observed with increasing harmonic number.

Finally, for the same transformer, the SFDR of the second harmonic was observed for different frequencies. The plot is presented in Fig. 4.32.

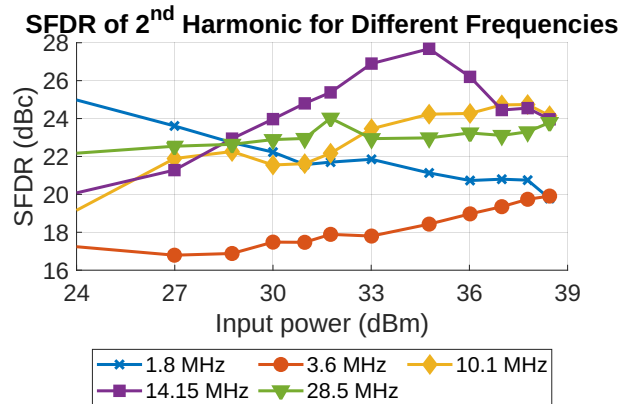


Figure 4.32: Second harmonic cancellation at different frequencies.

It can be noticed that the overall best result is present at the center of the spectrum. It was expected that the performance would decrease for higher frequencies due to capacitive leakage however, the suppression of the second harmonic at 28.5 MHz is almost constant and is comparable to that of the 10.1 MHz fundamental. On the other hand, the worst suppression was achieved at 3.6 MHz and 1.8 MHz. This again hints at the fact that TLTs loose performance at lower frequencies. Variation between the bands was not expected to be this significant.

It is possible the transformer presents worse balance at 3.6 MHz. For the lowest test frequency of 1.8 MHz, the trace resembles that of the third harmonic, which is not constant, and its SFDR always decreases with input power (see Fig. 4.30b).

## 4.7 Harmonics with LPFs

### 4.7.1 LPF Measurement

Although the previous section has proven the method of second harmonic cancellation, the level of harmonics present in the output RF spectrum is not sufficient to pass any regulatory compliance tests. In order to ensure further suppression of harmonics, low pass filters are used. The design procedure, schematic, and theory behind the LPF board were presented in Sec. 2.2.3.

First, the VNA was used to perform two port measurement for all the filters. Collected data was saved to a .s2p Touchstone file format, and then in AWR Designer, the N-port block of S parameters with the file import option was used. This allowed for precise plotting of S11 and S21.

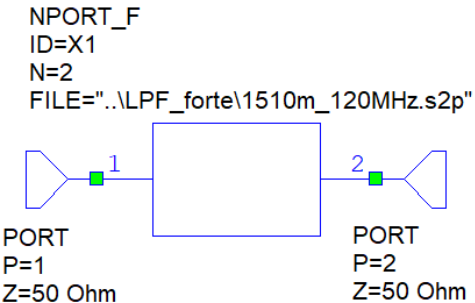


Figure 4.33: AWR designer schematic

Markers were placed at the end portions of one of the bands that the filter was designed for in order to determine the insertion loss in the passband. The point of -40 dB was also marked because from our harmonic measurement we know that the worst case SFDR was about 17 dBc for the second harmonic, so adding 40 dB of suppression should give much more than 50 dBc of total SFDR. One marker was also placed in the region of the designed band to mark the specific return loss. Following band frequencies are given for IARU region 1.

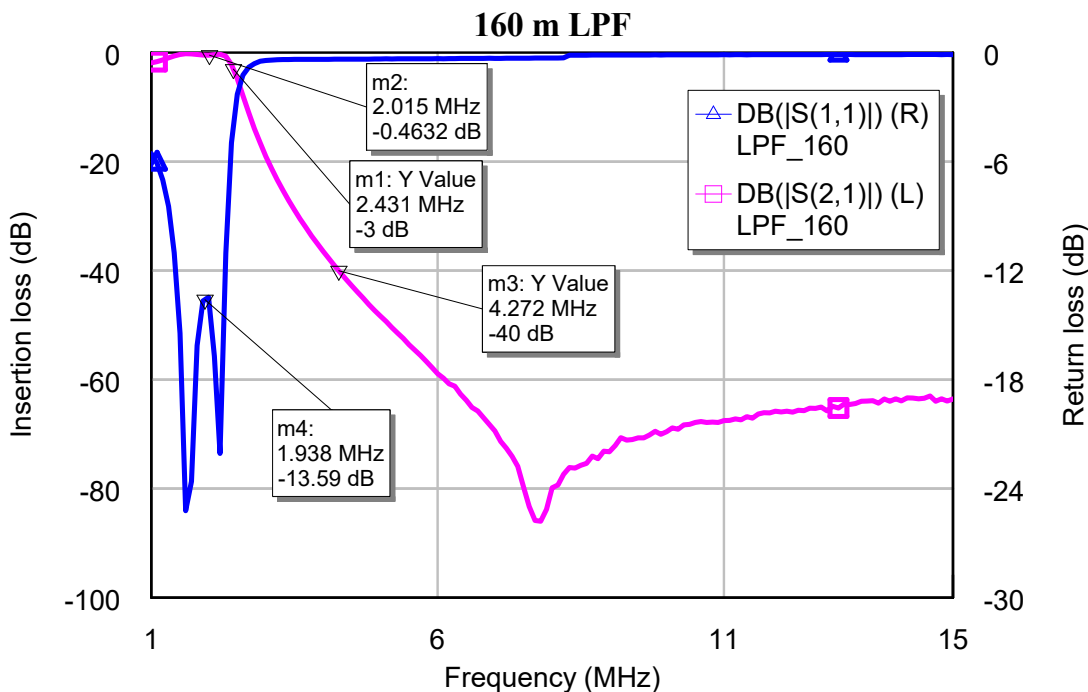


Figure 4.34: For the 160 m (1.8-2.0 MHz) LPF, the octave of the lowest allowed frequency is 3.6 MHz but the -40 dB marker is at 4.285 MHz, still this filter should be sufficient to attenuate the second harmonic below 50 dBc. Next harmonics will be attenuated even more, however, at some point, capacitive coupling causes the filter to decrease in performance.

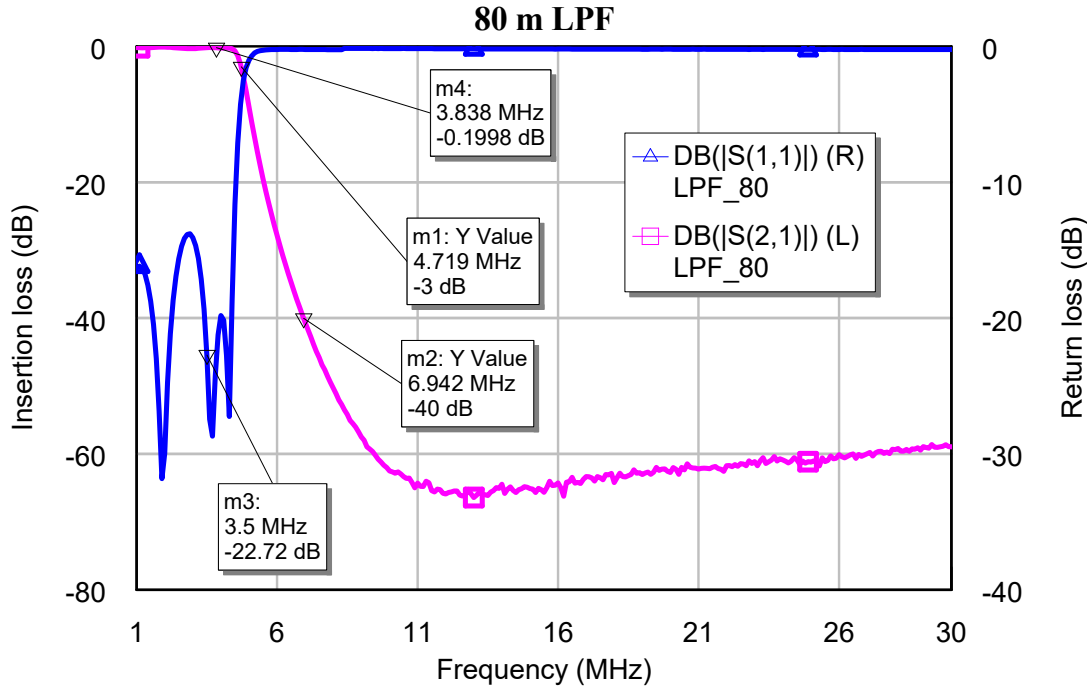


Figure 4.35: 80 m (3.5-3.8 MHz) LPF, an octave apart from 3.5 MHz is 7 MHz. It can be seen that -40 dB was achieved for that frequency. Insertion loss is very small, and excellent return loss of more than -20 dB was achieved.

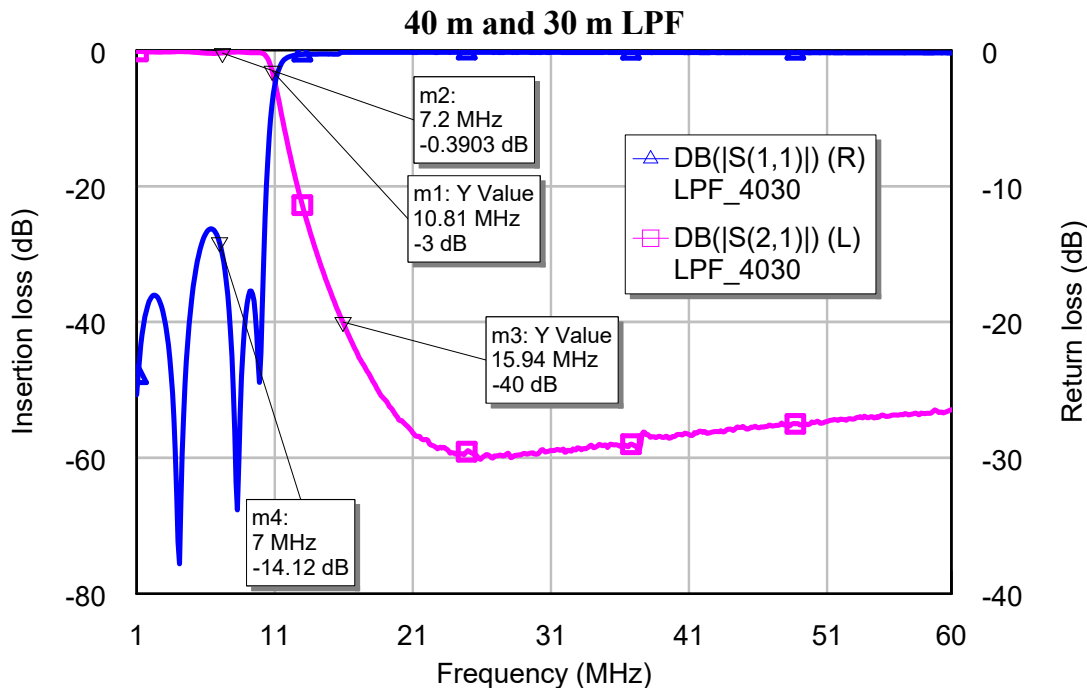


Figure 4.36: 40 m (7.0-7.20 MHz) and 30 m (10.1-10.15 MHz) LPF, the octave frequency of the lowest operating point is 14 MHz, and the -40 dB marker is on 15.9 MHz, quite close. Insertion loss is smaller than 0.4 dB, and the return loss for the worst case is -14.12 dB, presenting a good match.

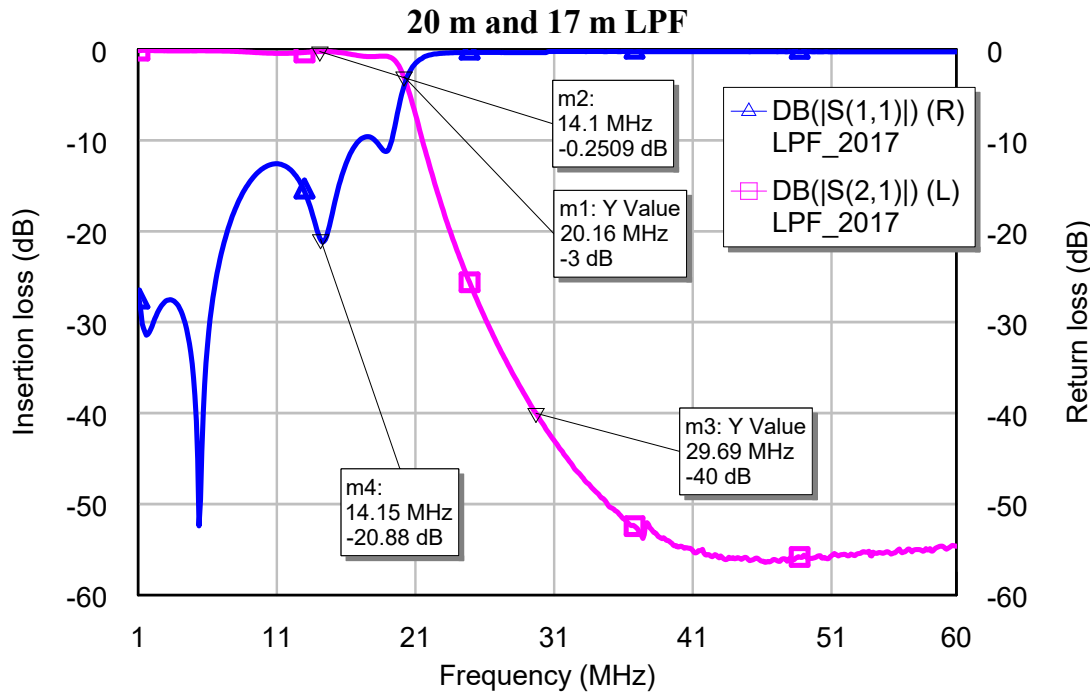


Figure 4.37: 20 m (14.0-14.35 MHz) and 17 m (18.068-18.168 MHz) LPF, this filter has the lowest frequency octave at 28 MHz, and the -40 dB marker is at 28.8 MHz. This filter represents good return loss, of about -20 dB for 20 m band and better than -10 dB for 17 m. Higher insertion loss might be due to the T80-10 cores used instead of T80-6, which would have a higher Q and lower losses at this frequency range.

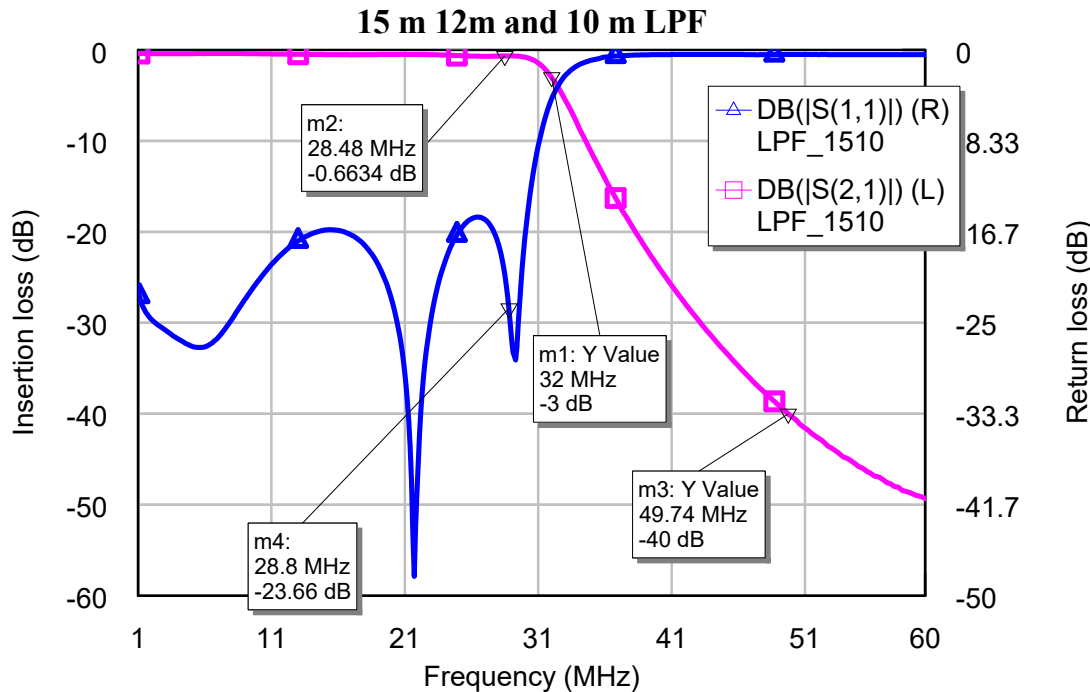


Figure 4.38: 15 m (21.0-21.45 MHz), 12 m (24.89-24.99 MHz), and 10 m (28.0-29.7 MHz) LPF, this filter fulfills the -40 dB octave requirement for 10 and 12 m but not for 15 m. However, the mentioned requirement had a significant margin of error, so the filter still might be good enough. Return loss is again excellent for all three bands.

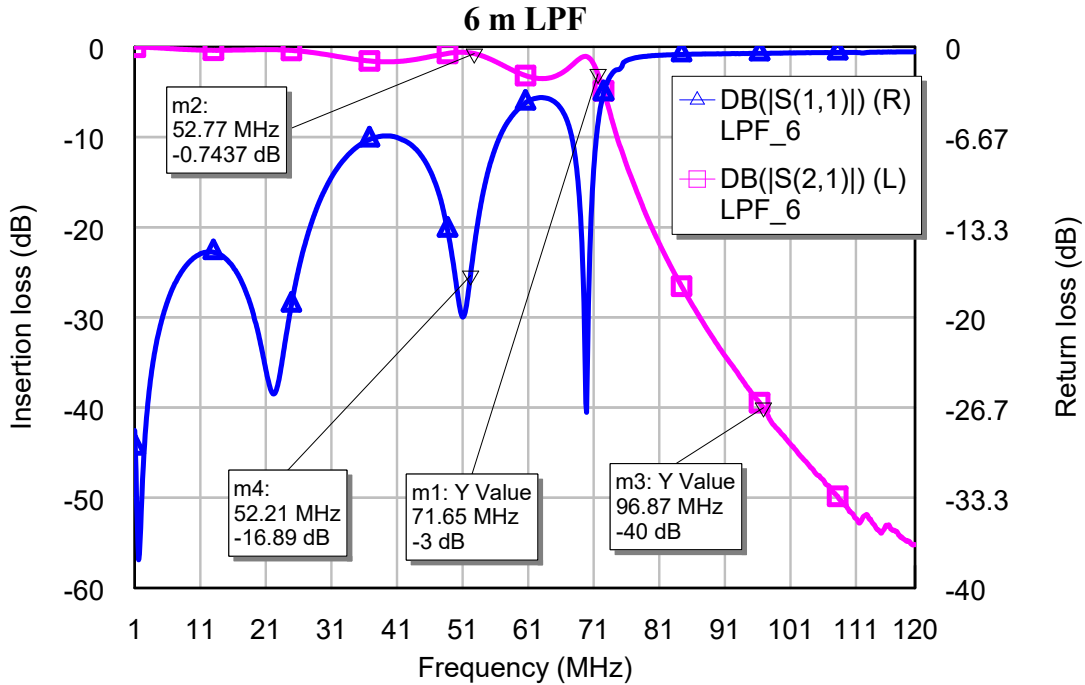
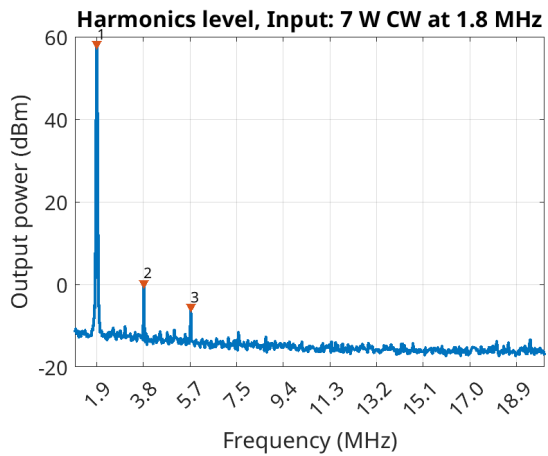


Figure 4.39: 6 m (50-54 MHz) LPF, high ripple is visible in the filter however, the frequencies of the 6 m band are within one of the peaks, providing an insertion loss of -0.75 dB. The marker of -40 dB is 3 MHz before the octave of the lowest frequency of operation, ensuring sufficient suppression. Return loss is very good, around -16 dB, providing a VSWR better than 1.4.

## 4.8 SFDR Measurement

The goal is to achieve a spurious free dynamic range (SFDR) of at least 50 dBc for the worst case harmonic emission according to ITU recommendations [2]. An amplifier with a LPF board was fed with a 7 W CW input signal, which was determined to be the maximum safe signal level for all the bands. Using a spectrum analyzer with an RF sampler and dummy load, the spectrum containing at least three harmonics was saved to a CSV file. A Matlab script was written to find the peaks and display the data from the spectrum analyzer with the fundamental frequency as the step of a major grid. This script has also produced the peak tables so that the SFDR in dBc can be easily identified for each case. While calibration was applied, it was shown in the previous section that the measurement with the sampler does not provide the best accuracy for the amplitude level.

Despite the limited accuracy, relative measurements should still produce reliable results, as it was shown in Sec. 4.1.



Peak Number	F [MHz]	[dBm]	[dBc]
1	1.8866	57.37	0
2	3.7866	-0.32	57.69
3	5.6866	-6.17	63.54

Figure 4.40: Output with LPF, 160m band

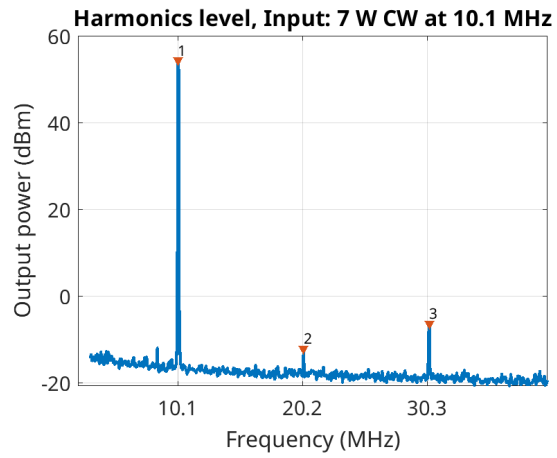
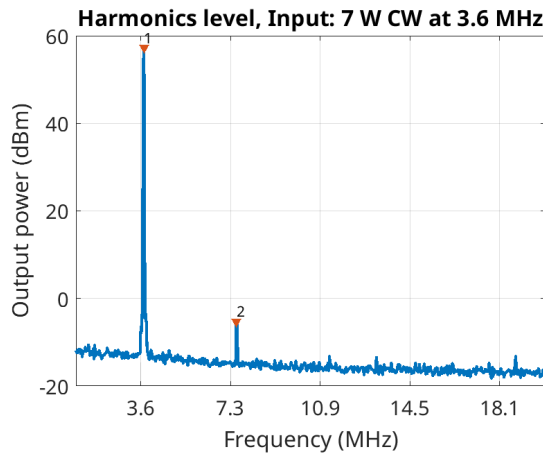


Figure 4.41: Output with LPF, 80m band

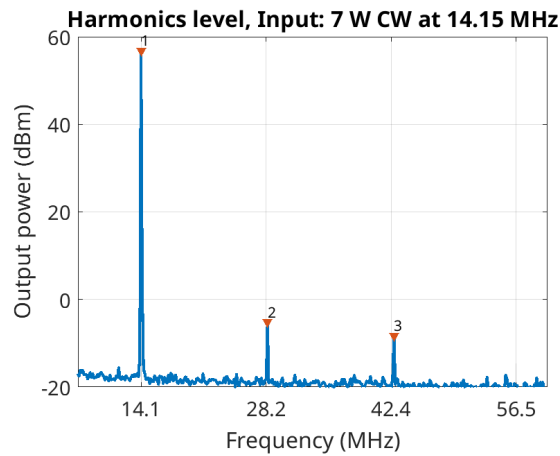
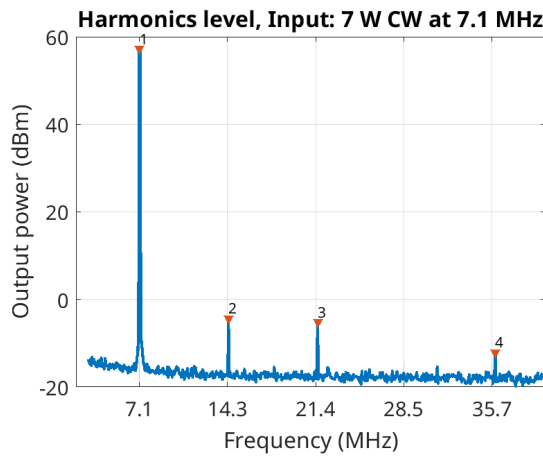


Figure 4.42: Output with LPF, 40m band

Figure 4.44: Output with LPF, 20 m band

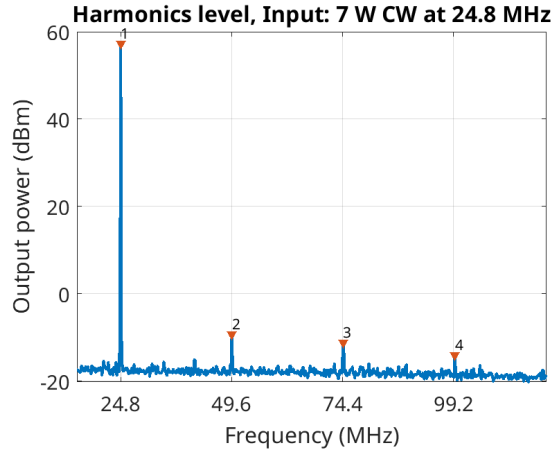
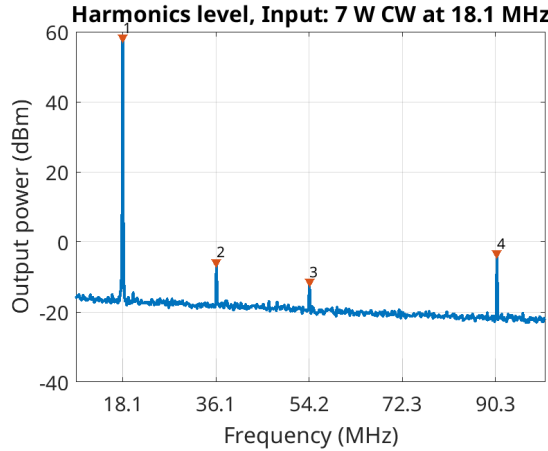


Figure 4.45: Output with LPF, 17 m band

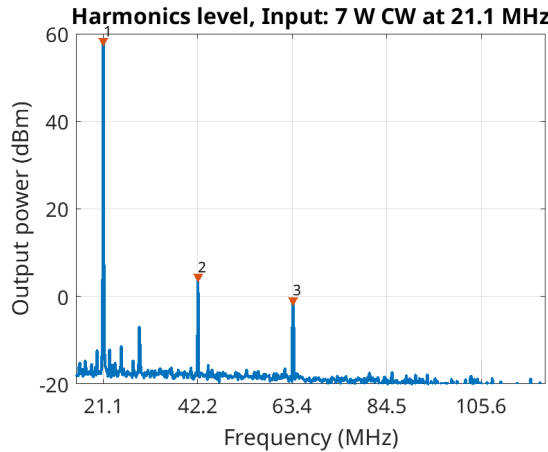


Figure 4.47: Output with LPF, 12 m band

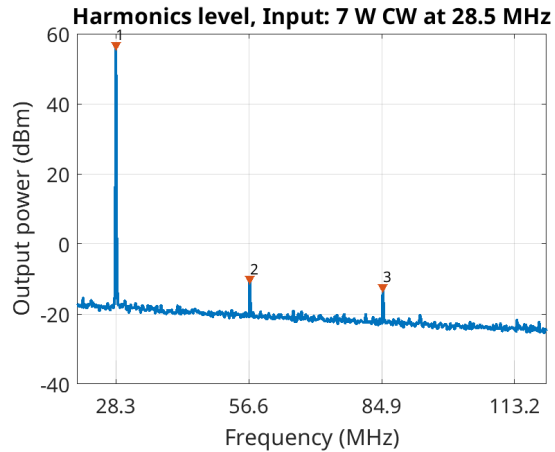


Figure 4.46: Output with LPF, 15 m band

Figure 4.48: Output with LPF, 10 m band

The 6 m band was not tested due to a lack of a proper signal source with sufficient drive power at that frequency.

Amplifier has passed the requirement of at least 50 dBc of harmonic suppression with the worst result being 53.89 dBc noted at 21.1 MHz. All the other bands achieved even larger attenuation of harmonics.

## 4.9 IMD

The previous section has dealt with harmonics of fundamental signals that arise due to the nonlinear behavior of the amplifier. Using low-pass filters and cancellation methods, it was possible to mitigate those spurious emissions. However, there are also spurious products created due to nonlinear effects that are much closer to the fundamental signal. In all the previous experiments, a continuous wave signal was applied at the input. This signal contained only a single sinusoidal tone (ideally) however, most other modulation schemes use multiple tones at the same time. Because of inherent nonlinearities, the amplifier also acts as a mixer, where both input tones and their harmonics mix together, creating sums and differences in the frequency domain, which is known as intermodulation or IMD.

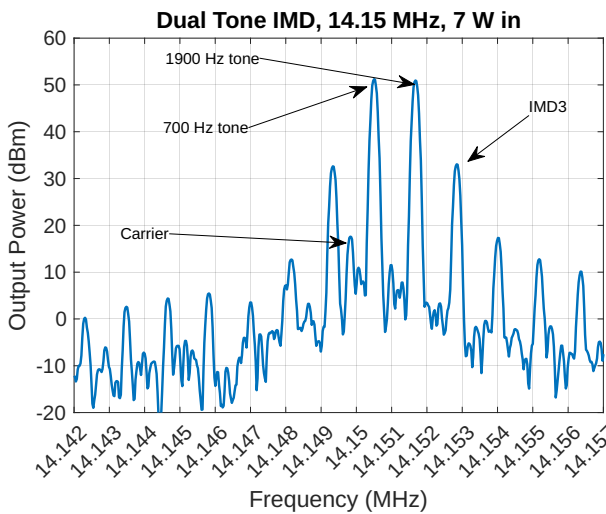
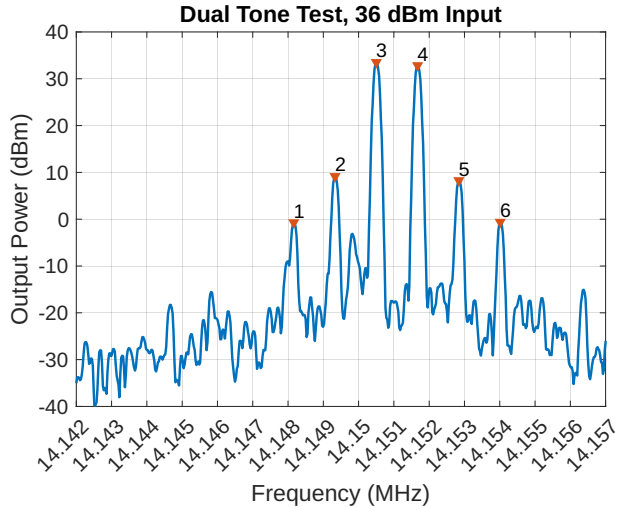


Figure 4.49: Example of IMD produced by the amplifier, it can be seen that each peak is lower than in case of CW because total power is spread over more peaks.

A common test to determine the linearity of a RF amplifier is the measurement of third-order intermodulation products (IMD3). This can be done using a dual-tone test, where a signal containing only two tones that are not multiples of each other frequency are input to the amplifier, and the increase of IMD3 or Spurious Free Dynamic Range (SFDR) is mea-

sured. In the presented test, the tones were chosen according to the recommendation of ARRL and they were 700 Hz and 1900 Hz. Both are within the bandwidth of a typical SSB window (2.7 KHz), and they are not harmonics of each other. Because the dual-tone input must be very clean without its own IMD products, this measurement is quite difficult and requires either two separate CW signals coupled with a 3 dB hybrid with high isolation or a single SSB source with excellent linearity[56]. Dual-tone input requires IMD3 of the input to be much greater than 30 dBc, a result that is difficult to achieve even in modern amateur radio transceivers, as reported by Rob Sherwood[57]. Due to limitations in laboratory equipment, a Xiegu G90 was used. Custom made isolated adapter was used to connect a computer sound card to the microphone input. The dual-tone signal was generated using a PC with a 24-bit 48 KHz sampling sound card. The signal source was measured for its own IMD3.



Peak Number	F [MHz]	[dBm]
1	14.14816	-0.71
2	14.14933	9.16
3	14.15050	33.52
4	14.15167	32.85
5	14.15284	8.28
6	14.15401	-0.61

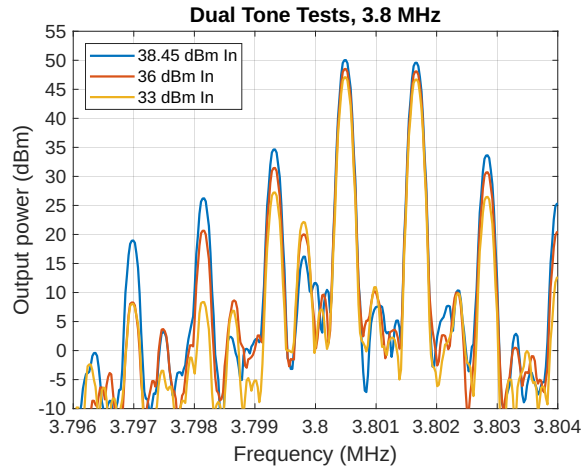
Figure 4.50: The dual-tone test of the signal source shows a far from ideal input to the amplifier.

In Fig. 4.50, it can be seen that the dual-tone input to the amplifier has its own IMD3 products, making the whole measurement not conform to standard procedures. However, this setup represents a realistic environment in which such an amplifier might be employed, so the data is still useful. The SFDR of the input in the worst case is 24.36 dBc at 14.15 MHz USB (upper side band). The audio input to the transceiver was adjusted so that the ALC meter was reading 100%, and the output power meter indicated 7 W. The frequency difference between the two tones in Fig. 4.49 and 4.50 is 1200 Hz, but the peak table in Fig. 4.50 might not reflect the exact frequency because the peaks have an assigned frequency with resolution corresponding to the RBW of the spectrum analyzer. For these tests, a RBW of 30 Hz was used.

Section 4.6 presented that increasing input power leads to an increase in harmonics and their levels. In the case of IMD three measurements for three frequencies were carried out. The input power of the dual-tone input signal was first set to 7 W, which was the maximum input power, then to P1dB, which was previously determined as approximately 36 dBm or 4 W for the used TLT (1:9 with three turns of  $17\ \Omega$  coaxial cable on 61 type cores), and lastly to 2 W, so 3 dB lower.

Besides the third-order product, a fifth order product was also included in the following plots. This allows for better observation of adjacent channel power ratio (ACPR). SFDR for a 5 KHz channel bandwidth includes IMD3 products on both sides, and SFDR for a 7 KHz bandwidth includes IMD5 products on both sides. For less stringent requirements or a wider channel, values of SFDR for a 7 KHz wide bandwidth can be utilized. However, for amateur radio service, the narrower bandwidth should be applied so that adjacent channels, which are 2.7 KHz wide, are not interfered with.

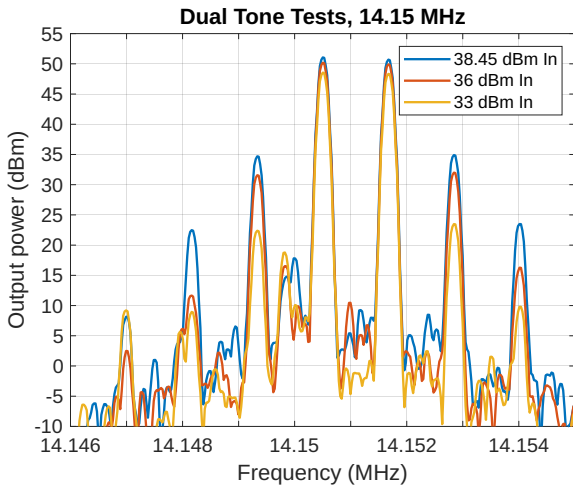
### IMD3 3.8 MHz



Input [dBm]	SFDR 5 KHz [dBc]	SFDR 2.7 KHz [dBc]
38.45	15.92	24.38
36	17.05	27.87
33	19.87	38.72

Figure 4.51: Comparison of 8 KHz spectrum for three levels of input power at 3.8 MHz.

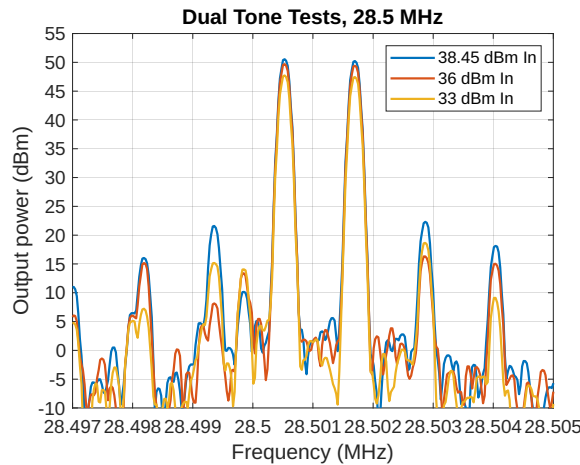
### IMD 14.15 MHz



Input [dBm]	SFDR 5 KHz [dBc]	SFDR 2.7 KHz [dBc]
38.45	16.37	28.58
36	18.68	33.92
33	25.95	38.542

Figure 4.52: Comparison of 8 KHz spectrum for three levels of input power at 14.15 MHz.

## IMD 28.5 MHz



Input [dBm]	SFDR 5 KHz [dBC]	SFDR 2.7 KHz [dBC]
38.45	29.03	34.5
36	33.49	34.51
33	32.55	40.8

Figure 4.53: Comparison of 8 KHz spectrum for three levels of input power at 28.5 MHz.

For the series of three measurements it can be seen that with decreasing input power the IMD3 products are decreasing much faster than the fundamental signals. This shows that amplifier should be operated below P1dB for a linear characteristic. What is more it appears that with increasing frequency the IMD decreases and SFDR increases. For the 28.5 MHz (see Fig. 4.53) the SFDR of 29 dBc for 5 KHz bandwidth is actually quite good result. While still not ideal, this worse case scenario for 10 m band is often considered an industry standard and most solid state 100 W transceivers according to Rob Sherwood achieve this or close to this level of IMD with 6 dB lower overall output power. In case of 14.15 MHz and 3.8 MHz tests the IMD3 is quite poor unless amplifier is operated with power that is well below P1dB. This test was to demonstrate the increase in IMD products when the amplifier is overdriven. A proper dual-tone test should include a much cleaner signal source. With such a setup, the linearity

of the amplifier could be better characterized. Besides further investigation of intermodulation for lower frequencies, the intercept points could be then determined. The intercept point of the third order is a theoretical point that describes the input power level at which the intermodulation product of the third order achieves the power level of the fundamental signal. A high value of IP3 is almost always desired since it indicates higher linearity. IP3 is determined similarly to the P1dB shown in Fig. 4.27. Extrapolation of the fundamental power trace and IMD trace in the linear region is necessary to find the intercept since it is just a mathematical concept. Here, even if IP3 was determined, it could not be treated as a valid measurement due to a non-linear source.

### 4.9.1 IP3

In order to demonstrate the IP3, the linear region of 14.15 MHz fundamental and its third harmonic was extrapolated, and intersection point was noted. In this case we can read from Fig. 4.54 that the IP3 = 42 dBm. Such a point can be determined based on harmonics or IMD3 products, however since we deemed our results of dual tone test not fully compliant with standards only an example of IP3 determination for single frequency was shown.

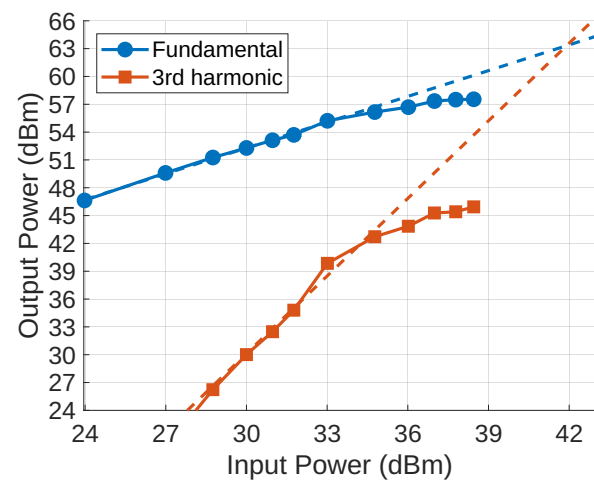


Figure 4.54: IP3 for 1:9 TLT made with 17  $\Omega$  coaxial cable on 61 type ferrite

# Chapter 5

## Software

### Microcontroller

The main microcontroller of the amplifier is located on the control board STM32F103C8T6, it has 64 KB of ROM. In this project, it uses an internal oscillator for a master clock of 64 MHz, although a maximum of 72 MHz is possible with an external crystal. The software was written in C language using STM32CubeIDE, which allowed for easy peripheral configuration and code organization thanks to CubeMX. During development, the size of the chosen microcontroller has proven to be a challenge, and most of the possible pins of the LQFP48 package were utilized.

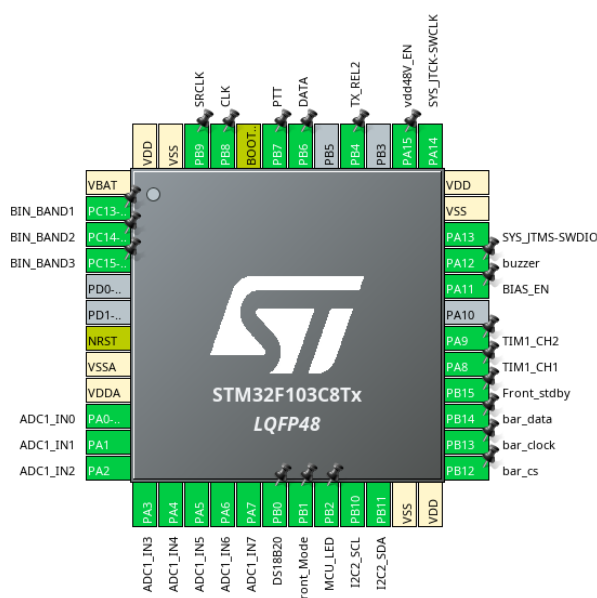


Figure 5.1: CubeMX diagram of pinout

Further expansion of the software for the amplifier controller was stopped because of the small number of pins on the chosen microcontroller and insufficient flash memory to implement a more advanced graphical display. The final version utilized 55.86 KB (87.27%) of flash memory and 8.91 KB of the available 20 KB (44.57%) RAM.

### Real Time Operating System

Because some aspects of the amplifier control system are more important than others, instead of a round-robin and sequential architecture, a real time operating system was used to give different priority levels for specific tasks. FreeRTOS is a real time operating system with a kernel designed for embedded applications, and it is also included as a software pack for STM32F103 in CubeMX. Implementation of FreeRTOS allows for running concurrent tasks, synchronization of those tasks, and communication between them.

In this project, normal priority was assigned to the tasks that performed operations on data from the analog to digital converter and the tasks that performed transmit and receive switching. This is to ensure a fast response to potential fault conditions and allow for responsive switching into transmit mode. Priority below normal was assigned to the band switching task, which implements the logic that, based on the chosen mode of band switching and specific

band selection signal, drives the 74HC595 shift register on the LPF board. Low priority was assigned to the display task. This process handles the drawing of data on the 16x2 display by sending I2C commands to the PCF8574 expander. The display task also maps readings from ADC values to the bar graph display and performs serial communication with MAX7219.

In order to observe the task scheduler behavior, one pin was toggled inside each task, and its status was observed using an oscilloscope. Fig. 5.2 shows an example of a high priority task switching an LED.

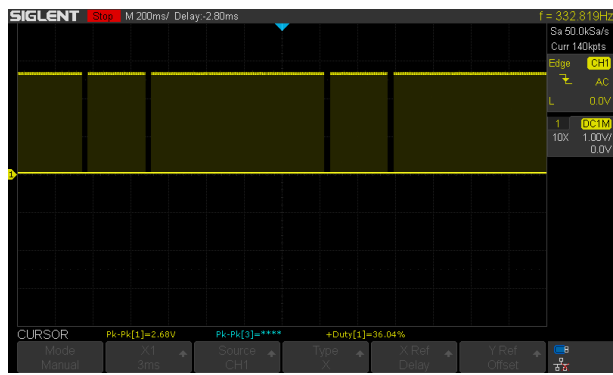


Figure 5.2: GPIO switching by the ADC task shows frequent execution of this code with low downtime, hinting at high priority. Observed low periods show the time where other tasks are executed.

With this simple method, it was determined that with 16 times averaging, the ADC task executes every 36 ms, which is more than 27 Hz. Temperature reading is obtained every 122 ms thanks to added counter. The display task takes 65 ms however, it has an additional non blocking delay at the end to limit its execution. Other tasks are much smaller, like the band switching and TX/RX switching tasks, where only 3 ms was measured. This might be limited by the time of the context switching, which is the time it takes for the kernel to switch from execution of one task to execution of another task.

## Analog to Digital Converter

To achieve the most efficient utilization of system resources, the ADC uses direct memory access (DMA) so that values from the converter are written in the background constantly to a buffer. When the buffer is full, it can be used by the ADC task. The DMA buffer has 8 elements, each representing a separate channel of the ADC. Since the microcontroller does not have 8 ADCs onboard, it uses a multiplexer to switch between channels. This limits the sampling rate however, it is not a problem since the real-time window in this application is rather long. More focus was put on the precision and dynamic range of the data.

Since the STM32F103 has only a 12-bit ADC, averaging of 16 was implemented. This technique is also known as decimation, and it divides the sum of n samples by n, which is equivalent to a low pass filter[58]. Decimation was discovered to be especially efficient in the removal of noise peaks, which, without filtering, often caused fail-safe mechanisms to trip.

The ADC buffer for improved efficiency was implemented as a collection of unsigned 16-bit integers. However, since it is easier to represent values of physical quantities such as voltage, power, or current using floats, conversion functions are called by the ADC task after each time a new average is calculated.

This software also presents an easy option for the calibration of directional couplers used in the amplifier. It was shown in Sec. 2.2.1 that the implemented couplers are non-linear. Therefore, a polynomial function is used to assign the proper value to the forward power variable.

In addition, one could create a look-up table with calibration for different frequencies, which would be applied based on the selected band, allowing for even better accuracy of measurement since the output for the tandem match circuit will change slightly with frequency.

The ADC task also performs reading from the digital thermometers on the one-wire bus. Since this interface is rather slow, a counter was added. On every iteration of the task, its value is increased by one, and if the counter value reaches 100, then additional code is executed in which sensors are polled. The code can detect many sensors on the one-wire bus, and after detection and reading of the DS18B20 ROM sector, it will call a function that sets the duty cycle of a 16 KHz PWM signal generated by timer 1 according to programmed fan and temperature curves. Minimal duty cycle of fans, temperature at which fans start to ramp up, maximal duty cycle and temperature to which fans can ramp up are set in the software.

Finally, the ADC task compares the obtained results from the ADC and other sensors with defined maximal values, and if an anomaly is detected, a fault handler with a specific error code is called. This function can halt the execution of other tasks and put the amplifier in a safe state. The exact resolution of the fault depends on the error code.

## DMA and Interrupts

The STM32F103 has only one simple DMA controller with multiple channels. Channel 1 was used for readings from the ADC peripheral to memory (ADC buffer) so that the CPU does not have to switch its context at the end of every conversion, but rather it can use the already prepared buffer every time the ADC task is ready to calculate the new average. With more strict time constraints, full and half callback interrupts are available in the CMSIS library so that sequential code can be executed after filling the buffer by the DMA. However, here, the buffer is filled in a circular mode, and whenever, due to the OS scheduler, the execution of the ADC task starts, the software can use the buffer in its current state.

No concurrency problems are expected to occur since all other tasks only read from the buffer, which alleviates the synchronization problems.

Because I2C for the front display also needs to send a significant amount of data, the I2C is also configured to use DMA. Channel 4 is used for transmission from memory to the peripheral, and channel 5 is used for receiving from the peripheral to memory.

In addition, interrupts are used to serve the PTT and band mode switching. Those two GPIO pins are configured as external interrupts with rising edge trigger detection. A special function is defined which takes as its parameter an interrupt number and provides a short sequential code that serves the interrupt.

In the case of PTT, it changes the flag to 1 so that the higher priority TX/RX task can switch the relays on the transmit relay PCB. Then, after a small delay, it enables the bias and 48 V rail to the amplifier board. This sequence, in older amplifiers was realized by a separate analog circuit often called a sequencer. Digital implementation is easier since the delay can be precisely adjusted both for when the voltages should be enabled and when the relays should be released after PTT goes back to the receive state. This is important especially for CW operation or digital modes where PTT is controlled by a Morse key in case of CW or sound card of the computer in case of digital modes. In addition, FreeRTOS provides non-blocking delay which causes a pause in the execution of one task, but the scheduler can run other tasks in the meantime.

# Chapter 6

## Conclusions

The final version of the amplifier has met all the design goals outlined in Sec. 1.1. The power amplifier board has reached a peak CW power of 600 W from 5.5 to 18 MHz and was able to deliver more than 500 W from 3.6 to 30 MHz, maintaining a power added efficiency from 56.7% to 69.96% in the HF spectrum.

While both the improvised 1:9 TLTs made with two parallel transmission lines and the well-made 1:9 TLT with special purpose 17  $\Omega$  coaxial cable have shown similar characteristics, both in terms of return loss and circuit performance, the 1:9 TLT with special purpose coaxial cable performed better. It presented higher output power across all the bands, and at the bottom and end of the spectrum, it achieved better power added efficiency. This improved PAE at the ends of the spectrum was the main factor why it was chosen as the final TLT installed in the amplifier. The improvised 1:9 TLT made with parallel coaxial cables has shown decent performance for a narrower spectrum. If the engineer wants to design an amplifier working only in specific bands, this study shows that the utilization of a well characterized transformer with two parallel transmission lines is feasible. However, if broad bandwidth with good characteristics across the whole spectrum is desired, we recommend the use of special single transmission line cable with a characteristic impedance that is the geometric average of the input and output impedance.

The robustness and relatively low price of LDMOS transistors produced in recent decade gives RF engineers a very good opportunity for designing reliable and efficient high-power RF amplifiers that outperform tube amplifiers in terms of efficiency, which is an important aspect of the modern electronics industry.

Proper IMD tests could not be conducted due to limitations of the measurement setup. A rudimentary dual-tone test has shown the intermodulation products for the LDMOS amplifier. While non ideal, these results can be considered sufficient when the amplifier works with power input below 1 dB compression point. While the linearity for lower bands was not very good, the free spectral range of 29 dB for a 5 KHz bandwidth at 28.5 MHz dual-tone test with a rather non clean input signal at P1dB represents a very good result. Further improvements could be made by implementing active predistortion techniques, which are offered by some of the modern software-defined transceivers.

Overall, the designed amplifier presents the advantages of both LDMOS technology and TLT matching, resulting in broad bandwidth operation with good power added efficiency. The designed low pass filters make the amplifier compliant with local regulations, and the designed controller provides digital monitoring over all aspects of the amplifier.

# Chapter 7

## *forte 600 Operation Manual*

*rev 1.0 March 2024, by SP6GK*

### 7.1 Introduction

Forte 600 is a linear solid state high frequency amplifier that operates from 1.8 to 30 MHz with maximum output power of 600 W. This amplifier utilizes two MRF300 LDMOS transistors in a push-pull class AB configuration, providing a robust power amplifier deck with good efficiency. Monitoring and controls of the amplifier are provided by a 32 bit STM32 microcontroller running a real-time operating system. Most important informations are displayed on LCD screen and LED bargraph.

### 7.2 Specification

- **Operating bands<sup>1</sup>:** 160, 80, 40, 30, 20, 17, 15, 12, 10 [m]
- **Output power:** 600 W CW max (no LPF) ≈400 W CW max (with LPF)
- **Input power:** 7 W maximum, P1dB ≈ 4 W
- **Worst case harmonic suppression:** -53.89 dBc at 21 MHz
- **Transmission modes:** CW, SSB, AM, FM, Digital
- **RF input and output ports:** 50 Ω unbalanced, Teflon SO-239
- **Connections:** IEC AC power connector, PTT - RCA phono, Analog band selection - RCA phono, ALC - RCA phono, Data - RJ-45.
- **AC power:** 200-240 V AC at 5 A max, Fuse 5 A 250 V slow
- **Weight:** 26 kg
- **Dimensions (W, H, D):** 455 x 260 x 430 [mm]

---

<sup>1</sup>60 m is not covered because of limitations in allowed power on that band. 6 m band operation is possible and LPF is included, but this band was never tested.

### 7.3 Front Panel

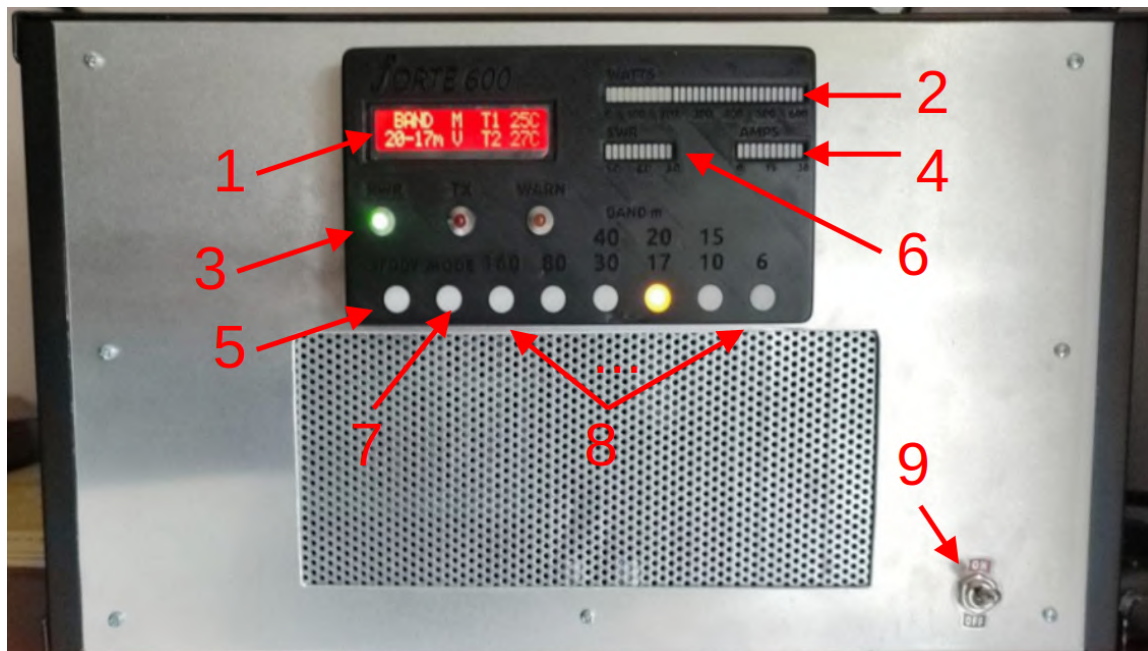


Figure 7.1: 1 - 16x2 Liquid Crystal Display (LCD), 2 - Output power bar graph, 3 - Status LEDs (from left to right: AC power (PWR), transmit mode (TX), fault detected (WARN)), 4 - Total drain current bar graph, 5 - Standby (STDBY) button, 6 - Standing Wave Ratio (SWR) bar graph, 7 - Band switching mode button (MODE), 8 - Manual band selection buttons, 9 - AC power switch

### 7.4 Rear Panel

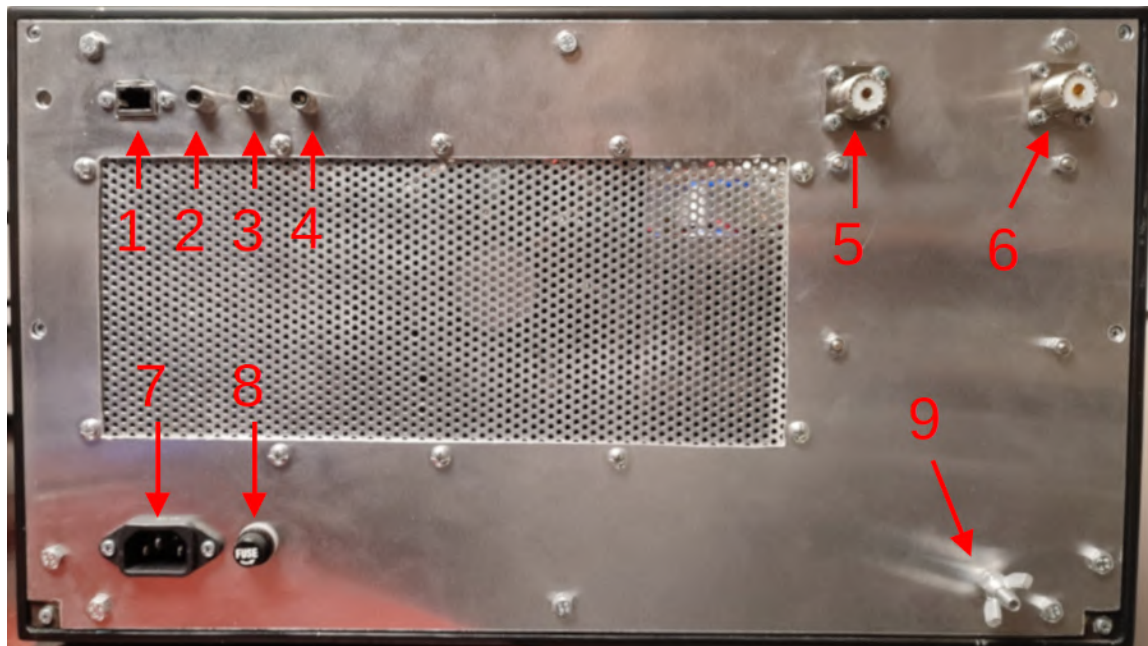


Figure 7.2: 1 - Digital band data, 2 - Analog band data, 3 - PTT, 4 - ALC (option), 5 - RF output, 6 - RF input, 7 - AC input, 8 - Fuse (slow 5 A), 9 - Ground

## 7.5 Installation and First Start

1. Ensure that the amplifier's AC switch is in the OFF position and that the power cable is disconnected.
2. Connect the PTT input of the amplifier to the transceiver's PTT output.
3. Connect a  $50 \Omega$  load or antenna to the RF output of the amplifier.
4. Leave the amplifier's input unconnected or terminate it with a  $50 \Omega$  load if possible.
5. Set the transceiver to LSB or USB mode on the 20 m band, and set the power level to minimum. Terminate the output of the transceiver into a  $50 \Omega$  load.
6. Connect the amplifier to the mains using an IEC cable.
7. Turn on the amplifier using the AC switch on the front panel.
8. When the amplifier goes through its startup procedure, a single one-second beep should sound, and after about 4 seconds, the front LCD should display the current band, temperature, and mode of operation.
9. Switch the amplifier to manual mode of band selection and switch to 20 m band. The button below 20/17 m should light up and LCD should show the same band.
10. Press the PTT on the transceiver side.
11. Observe the meters.

The amplifier should switch into transmit mode, and the LCD should display a drain current of 0.40 A and a drain voltage of 48 V. A difference of 0.04 A and 0.5 V from the nominal values is acceptable. The forward and reflected power should indicate 0 W.

If anything appears abnormal, please refer to Sec. 7.7.1. If the displayed values are correct, it indicates that the amplifier has also passed its self-test, and you can proceed to the next section.

## 7.6 Operation

In order to prepare the amplifier for normal operation after initial setup (Sec. 7.5), follow these steps:

1. Switch off the amplifier and transceiver.
2. Connect the RF output of the transceiver to the amplifier's input port using a  $50 \Omega$  coaxial cable.
3. (Optional but recommend) Choose one of the methods for automatic band selection from Sec. 7.6.1.
4. Switch on the transceiver and amplifier.

5. With the transceiver still in LSB or USB mode and with minimum output power, try changing the band to 15 or 40 m on the transceiver in receive mode. If one of the automatic band selection methods was used, the LPF section should switch automatically. Display should be updated, and you should hear the click of relays inside the amplifier.
6. Set the transceiver to CW and key the transmitter on one of the allowed bands while the  $50\ \Omega$  output load or antenna is connected. Increased output power should be noted. At this stage input power of 1 W is recommended.
7. Release the CW key and increase power by 1 W or the minimal step on the transceiver. Remember that maximum input power is just 7 W.
8. Repeat step 6 until you reach 7 W of input power, at least 400 W should be observed at the output by now.
9. For normal SSB operation, it is recommended to use a maximum of 4 W of input power for linear operation.

**NOTE:** It is highly recommended to use automatic band switching if possible.

If manual band switching is selected and the operator forgets to change the amplifier settings, two cases might occur. Either the amplifier will transmit full power with a low-pass filter with too high of a cutoff, leading to illegal spurious emissions, or the cutoff of the LPF will be too low, resulting in the full power being reflected back to the transistors, which might shorten the lifespan of the output transistors or destroy them.

**NOTE:** Reduce the power further for transmission modes with high duty cycles.

Amplifier can work with high duty cycles, but its durability was not tested extensively since it heavily depends on the modulation type. For modes such as AM, FM, or digital modes, you should closely monitor the temperature. If it increases very quickly, you should lower the power. It is recommended to stay below 50° C.

### 7.6.1 Band Switching Modes

Forte 600 allows one of three band switching modes to be selected. The currently selected mode is indicated by a letter displayed under the 'M' letter on the LCD display when the amplifier is not in transmit state:

**M** : Manual

**V** : Voltage (analog)

**B** : Binary

In order to change the mode of band switching, press the MODE button on the front panel (7 in fig. 7.1). It allows you to cycle between modes. With each press, the mode will change in the following order:

Manual → Voltage → Binary

After reaching the binary mode, the next press will cycle back to the Manual mode. The currently set band is displayed on the LCD screen, and the button representing the band is also illuminated by an LED. The amplifier will remember the last used mode even if power gets disconnected.

When the amplifier is in transmit mode, the option to change the band or band selection mode will be blocked until the amplifier returns to receive mode.

### Manual Band Selection

Forte 600 allows for manual band selection by pressing any of the buttons on the front panel. To do this, set the mode to manual (M). If the manual mode was lastly selected, the amplifier will remember the last chosen band even if power was disconnected.

### Automatic Band Selection

Forte 600 can also switch bands automatically if a connection between it and the transceiver is established. Two methods of automatic band switching are provided:

#### Analog Voltage Band Switching

This method utilizes a RCA phono jack at the back of the amplifier, where the center of the connector is the positive and the outer side is the ground. The amplifier measures the analog voltage on this connector and selects the band according to the voltage ranges presented in table 2.2.

#### Binary Band Switching

This method utilizes an RJ-45 connector at the back of the amplifier. For the pinout of the connector, see the schematic in Fig. 2.13. This amplifier uses a three bit binary to represent the necessary 6 bands of LPF. See table 2.1 for the assignment of bands.

When a cable with 3 bit binary data is connected to the amplifier, manual mode selection should not be used since the controller handling the manual selection uses the same 3 bit wide bus.

For transceivers using a 4 bit binary output to represent the current band, a translation layer needs to be provided for this version of the amplifier.

#### 7.6.2 Stand By Mode

Pressing the STDBY button will cause the amplifier to be put into standby mode. If the amplifier is in standby mode, the STDBY button will light up green. In standby mode, the amplifier acts as a pass through connection between the antenna and the transceiver, and the PTT will have no effect on the amplifier. To return to normal operation, press the STDBY button once more. This mode should be used when antenna requires tuning to  $50 \Omega$  with extenal antenna tuning unit (ATU) that is connected after the amplifier.

### 7.6.3 Antenna Recommendation and ATUs

It is highly recommended to operate the amplifier with a maximum SWR of 1.8 if an output of more than 300 W is used. While the amplifier has many protections against high SWR and temperature, a good match is still necessary for efficient operation and to avoid the fail-safe mechanisms from tripping.

**NOTE:** When tuning the antenna, put the amplifier into standby mode and use the minimal power possible.

Do not attempt to measure the SWR input of the amplifier using sweep feature on your transceiver, out of band emission might occur.

## 7.7 Protection

Forte 600 includes a modern digital controller that provides real-time software protection against:

- High temperature, temperature sensor not detected
- Drain overcurrent and overvoltage
- Excessive input power
- Too high output reflection
- Too high output power
- Excessive LPF loss or reflection (wrong filter selection or filter damage)

In addition, there are also analog mechanisms to protect the amplifier from:

- Too high input power comparator - switches TX/RX
- Too high output SWR comparator - switches off bias and TX/TX
- Temperature compensating bias circuit - drain current is regulated as temperature increases to prevent thermal runaway and instability

If any abnormality is detected, the amplifier will be put in a warning mode (WARN LED will light up). The response of the controller depends on the fault or abnormality detected. An error code will be displayed on the LCD, and the buzzer will sound in a specific way. In case the user encounters a problem, the error code should be read and checked with the manual.

### 7.7.1 Error Codes

#### 1. MAX Id CURRENT! Problem: Drain current has exceeded the maximal value.

**Note:** This error has a counter, the controller has to detect this problem a few times in a limited time span to trigger the protection. This mechanism prevents noise from tripping the protection.

**Action taken by the amplifier:** Disables the PA board, goes into RX, pauses for 10 s, and resets.

**Recommended action for the user:** Disconnect the power to the amplifier, open the top cover, disconnect the 48 V rail from the PA deck. Measure the resistance from drains to ground, it should be in the range of  $M\Omega$ . Measure the resistance from the 48 V rail (on the controller 48 V output) to ground, it should be more than a few hundred  $\Omega$ . If you did not find a short and readings are normal, connect the 48 V rail back to the PA board, connect the power, and turn on the amplifier. With the top cover removed, measure the 48 V rail on the input to the controller, it should be present in receive mode. With the amplifier connected to a matched load and no RF input, key down the amplifier into TX mode. The LCD panel should indicate a current of 0.4 A, and 48 V should be present at the drains. If up to this point, no abnormalities were detected, then the protection was most likely tripped by noise or improper operation, and the amplifier is good for use. Otherwise, troubleshoot the section close to where the abnormality was detected. See the section on difficulties for more details around current sensor.

## 2. MAX Ud VOLTAGE! Problem: Too high voltage detected on the 48 V rail.

**Note:** This error has a counter, the controller has to detect this problem a few times in a limited time span to trigger the protection. This mechanism prevents noise from tripping the protection.

**Action taken by the amplifier:** Disables the PA board, goes into RX, pauses for 10 s, and resets.

**Recommended action for the user:** Switch off the amplifier, open the top cover, and disconnect the 48 V rail from the PA deck. Key down the amplifier and measure the voltage at the 48 V rail output from the controller, 48 V should be measured. If the voltage is too high, then the PSU is damaged otherwise measure values of the 48 V rail divider resistors.

## 3. MAX TEMPERATURE!

**Note:** Reading on one of the temperature sensor has exceeded  $65^{\circ}C$

**Action taken by the amplifier:** The amplifier disables the PA board, goes into RX mode, pauses for 30 seconds with fans sped up to the maximum, and then resets.

**Recommended action for the user:** If the error did not occur rapidly and occurred when the amplifier was operated in a hot environment for a longer period of time, the recommended action is to wait until the temperature drops below  $40^{\circ}C$  before transmitting again. If the temperature rises too fast during normal operation (room temperature of  $24^{\circ}C$  and maximum P1dB input power into matched load for ICAS operation), the condition of the fans and thermal paste should be checked. If the temperature difference between T1 and T2 sensors is larger than  $5^{\circ}C$ , it is highly recommended to check the mounting of temperature sensors to the transistors, the application of thermal paste might also be uneven.

## 4. Out Power limit!

**Note:** Output power has exceeded 600 W

**Action taken by the amplifier:** Disables the PA board, goes into RX, pauses for 10 s, and resets.

**Recommended action for the user:** Check the amplifier according to startup guide again. Use lower input power, otherwise check the input attenuator and ouput couplers.

## 5. In Power limit!

**Note:** Input power has exceeded 7 W

**Action taken by the amplifier:** Disables the PA board, goes into RX, pauses for 10 s, and resets.

**Recommended action for the user:** Lower the power output on the transceiver side. If it's not possible to set a lower output power, consider using an attenuator. If the error occurs even when the power is lower than 7 W, check the input coupler and its output voltage when 7 W of CW is applied.

For a matched source with 7 W of input power the forward input voltage should be approximately 0.9 V.

## 6. High out SWR!

**Note:** High standing wave ratio detected at the output of the LPF board (output of the amplifier to the antenna).

**Action taken by the amplifier:** Disables the PA board, goes into RX, pauses for 10 s, and resets.

**Recommended action for the user:** Check if the antenna is tuned properly. If so, switch off the amplifier, disconnect AC power. Desolder the coaxial cable from the PA deck to LPF, connect VNA to the input of the LPF and output of the amplifier (SO-239). Disconnect the RF input to the amplifier and terminate the transceiver. Connect the amplifier to AC and turn it on, key it down on the band where the error occurred. Perform S21 measurement of the LPF and RX/TX switch. If error occurred during antenna tuning with ATU, ensure standby mode is used while tuning. If error occurs on startup, check connections between LPF and controller board PCBs, make sure ADC inputs are not floating.

## 7. High in SWR!

**Note:** The RF source is not well matched to 50 Ω.

**Action taken by the amplifier:** Disables the PA board, goes into RX, pauses for 10 s, and resets.

**Recommended action for the user:** If possible, check your input cable with a VNA. Switch off the amplifier and disconnect it from power. Disconnect the PA deck from the LPF board and connect the PA deck to the dummy load. Connect the VNA to the input port, only one port is necessary to perform the S11 measurement. Connect the amplifier to the power and switch it on. Measure the return loss in the range from 1 to 30 MHz, it should be better than -10 dB. Make sure that S11 sweep is made in the range of the selected LPF.

## 8. Mismatch LPF!

**Note:** The PA deck board output coupler has detected a large reflection.

**Action taken by the amplifier** Disables the PA board, goes into RX, pauses for 10 s, and resets.

**Recommended action for the user:** If using manual band switching, ensure that the correct band is selected. When using automatic band switching, refer to the High SWR section and troubleshoot the LPF and RX/TX section.

Make sure that the LCD is showing the same band as your transceiver.

## 9. LOSS PWR in LPF!

**Note:** A large difference between input power to the LPF and output power from the LPF was detected. This might indicate damage in the LPF section.

**Action taken by the amplifier:** Disables the PA board, goes into RX, pauses for 10 s, and resets.

**Recommended action for the user:** Refer to the High in SWR error code and measure the S21 of LPF and RX/TX sections. Make sure insertion loss in pass band is close to that specified in technical documentation (Sec. 4.7.1).

#### 10. TEMP SENS ERROR.

**Note:** The controller board did not detect at least two sensors on a One Wire bus.

**Action taken by the amplifier:** Disables the PA board, goes into RX, pauses for 10 s, and resets.

**Recommended action for the user:** Switch the amplifier off and disconnect it from power. Open the top lid and check the connections of the temperature sensors to the controller board. Temperature sensors are screwed on the top of the MRF300 packages.

**NOTE:** You can connect the ST-Link to the SWD port of the microcontroller and use the debug feature in a compatible IDE to step-by-step analyze what is happening with the amplifier. When debugging, proceed with caution if the PA deck is connected to the 48 V rail or RF input since real-time software protection might not be applicable.

## 7.8 In Case of Difficulty

### Maximum drain current or drain voltage error code is detected upon a startup.

Check the connection of the other PCBs to the controller board. Ensure that the input to the ADC channels of the controller board is not floating with high input impedance. Such a situation will cause a large charge to accumulate on the ADC input, leading to a high input voltage being read, which can trigger the fail mechanism immediately during the startup check.

### Exceeded drain voltage error occurs spontaneously during transmission.

Check the decoupling capacitors that filter the input to the ADC. High noise may be present on the drain voltage divider, potentially leading to false positive detection.

### The LCD and bargraph display experience glitches during transmission.

Check the grounding of the front panel electronics. Use shields grounded on both sides of SPI and digital bus connections. Ensure that decoupling capacitors for the 5 V front panel regulator are properly mounted. Also, confirm that front panel cables are not routed close to the high-power RF path.

### The temperature sensor reading is constant

It is possible that stray RF has corrupted the configuration of the DS18B20 thermometer. Ensure that sensors are connected properly with short grounded cable on both sides. Ensure that decoupling capacitors are not damaged.

## 7.9 Warnings

**Electrical Hazard!** This device operates on mains electricity, which can lead to lethal shock. Do not operate the device near water and avoid exposing it to moisture. Before performing maintenance and service, always remove the power plug.

**Heat warning:** During operation, certain parts of the device may become hot. To prevent damage, ensure proper ventilation around the vents of the device. Avoid placing the device near heat sources.

**Cleaning:** Use a soft, dry cloth to clean the exterior of the device. Do not use abrasive cleaners or solvents.

**Environment Considerations:** Dispose of the device responsibly according to local regulations. Do not dispose of it in regular household waste. Consider giving it to someone new to the hobby or keeping it for spare parts.

## 7.10 Service and Repair

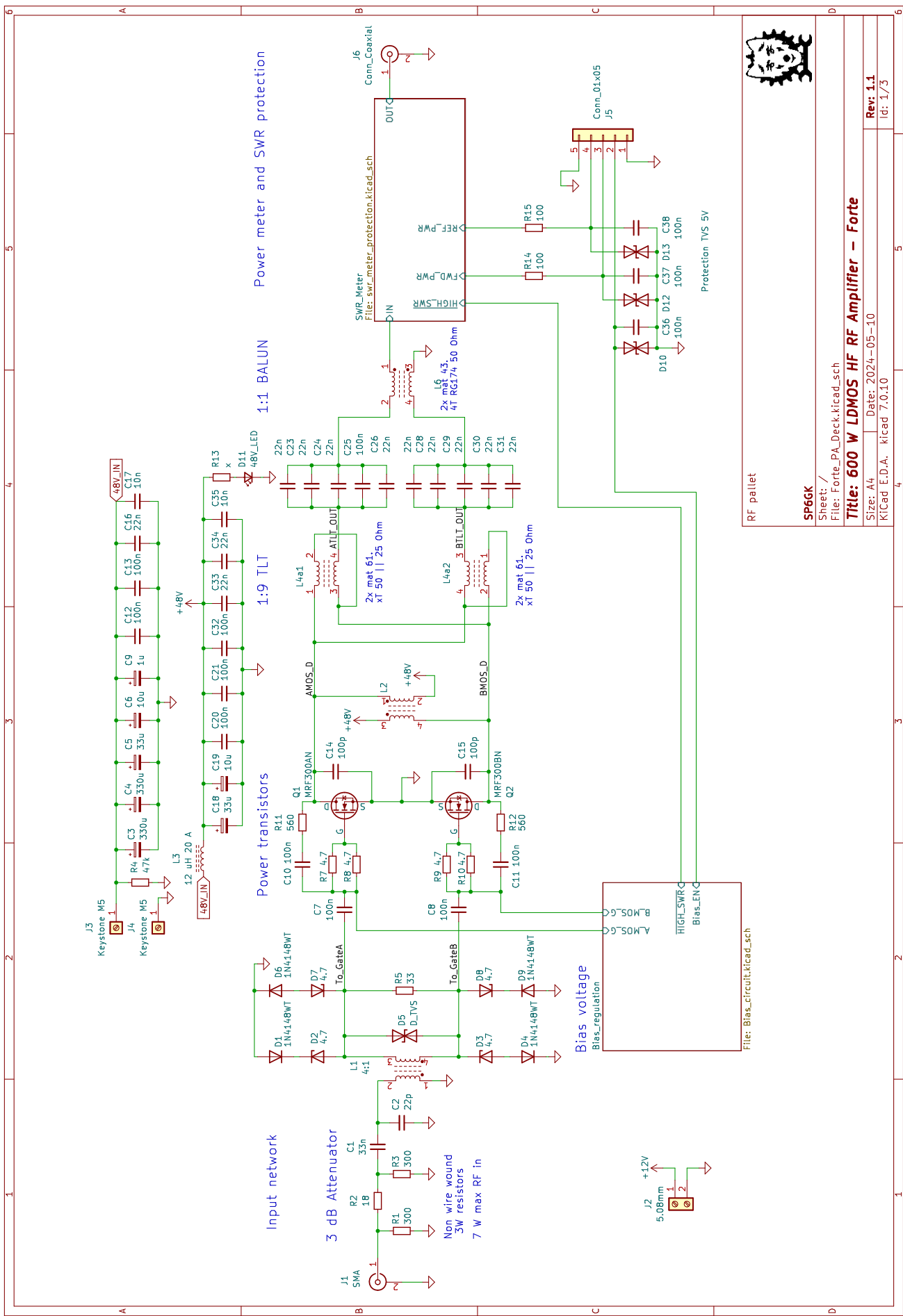
It is your device, absolutely attempt to disassemble or repair it if you have the proper tools and knowledge. Schematics are provided below!

**Remember about proper ESD protection!**

## 7.11 Schematics

Schematics follow on the next pages.

### 7.11.1 PA Board Main Schematic



RF pallet

SP66K

Sheet: /  
File: Forte\_PA\_Deck.kicad\_sch

Title: **600 W LDMOS HF RF Amplifier – Forte**

Size: A4 Date: 2024-05-10

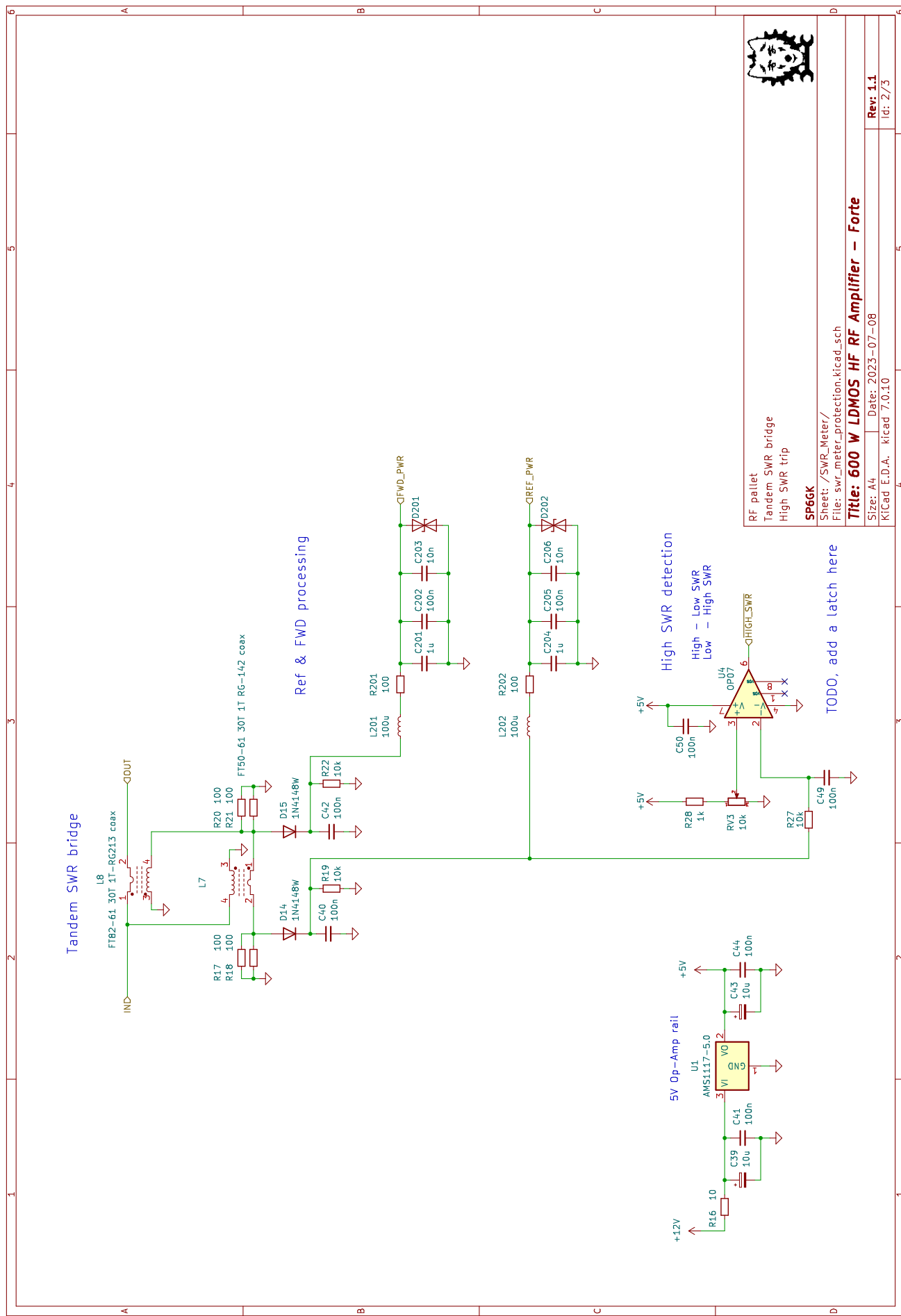
KICad E.D.A. Kicad 7.0.10

Rev: 1.1

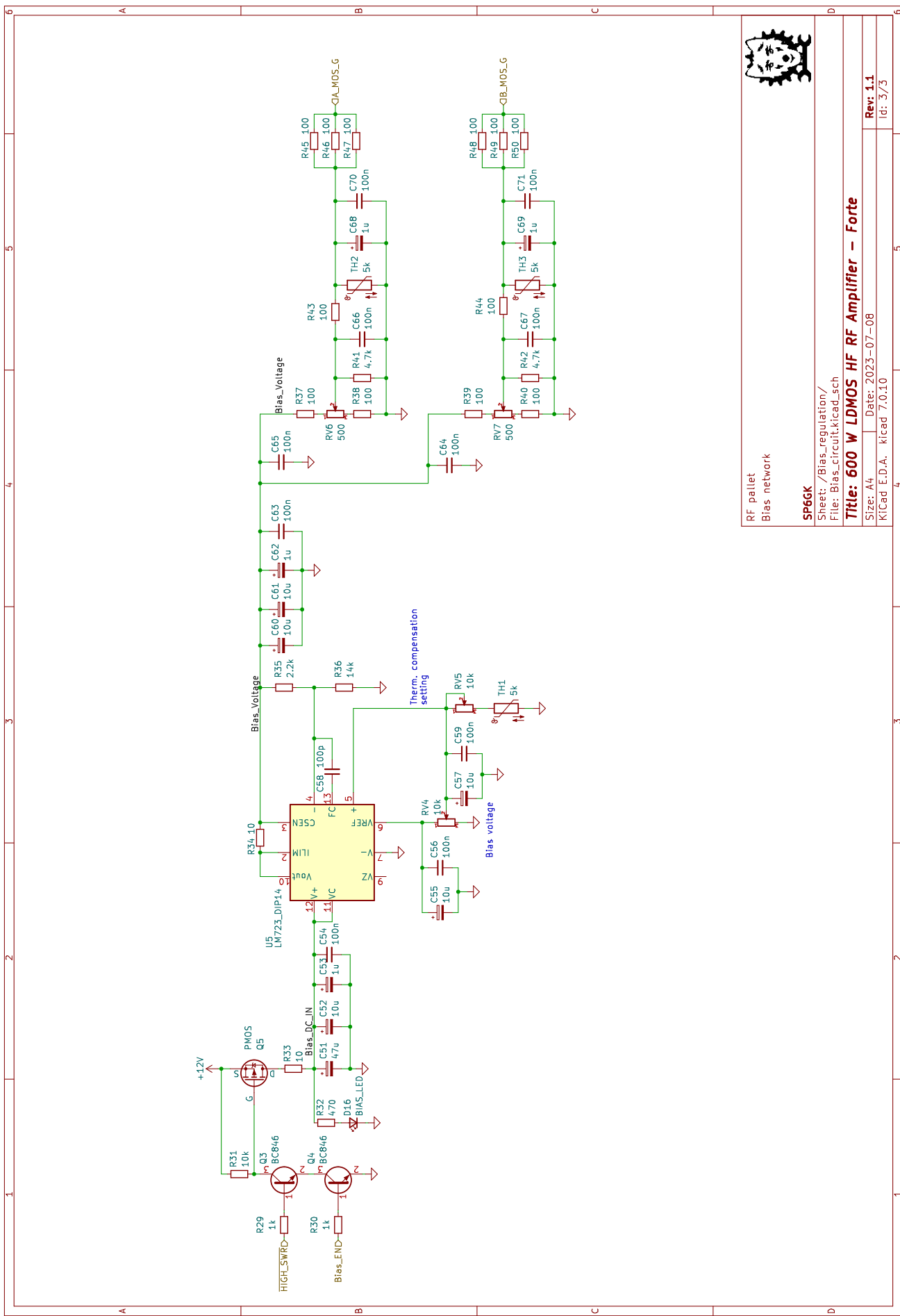
Ed: 1/3



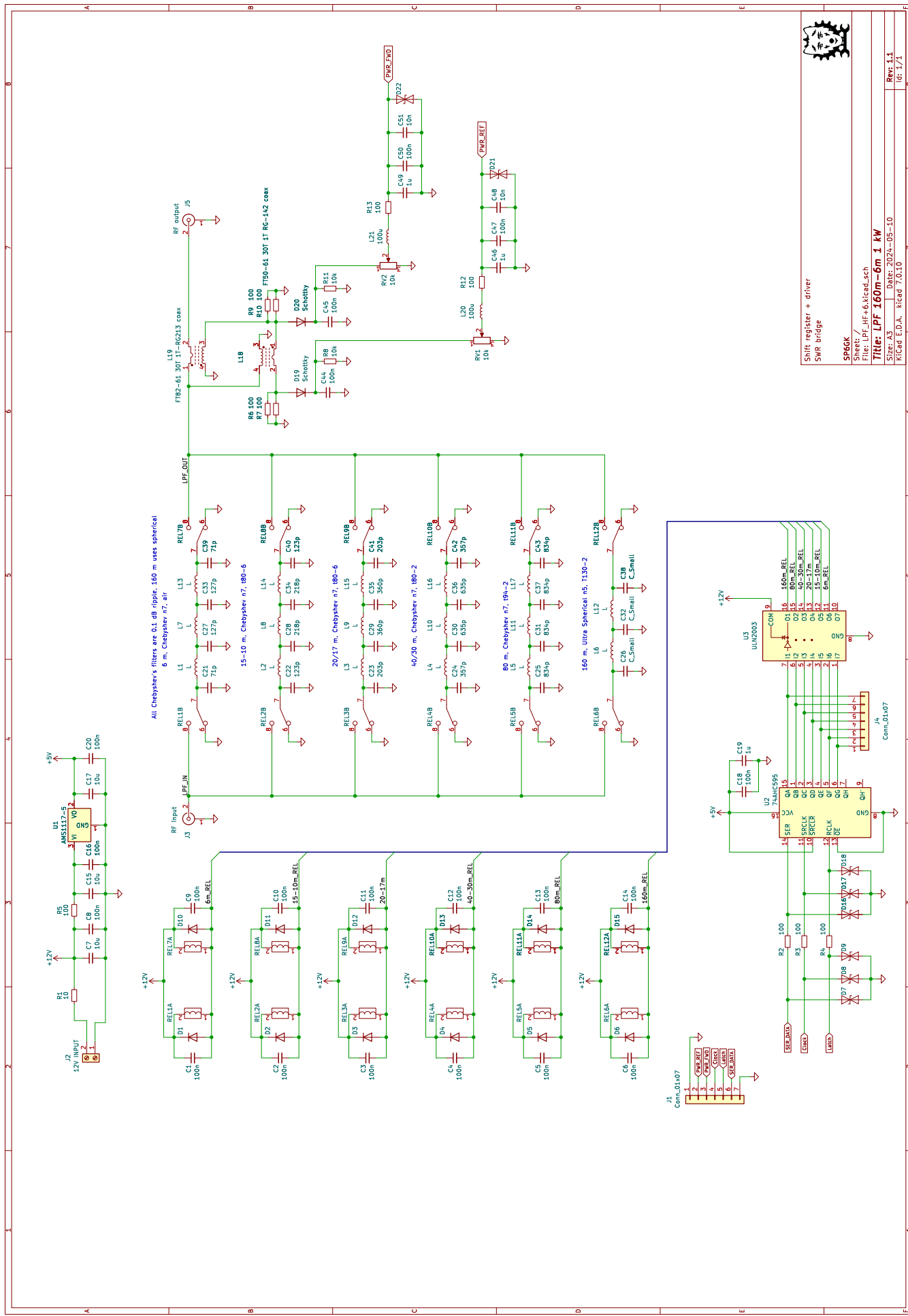
# PA board Directional Coupler



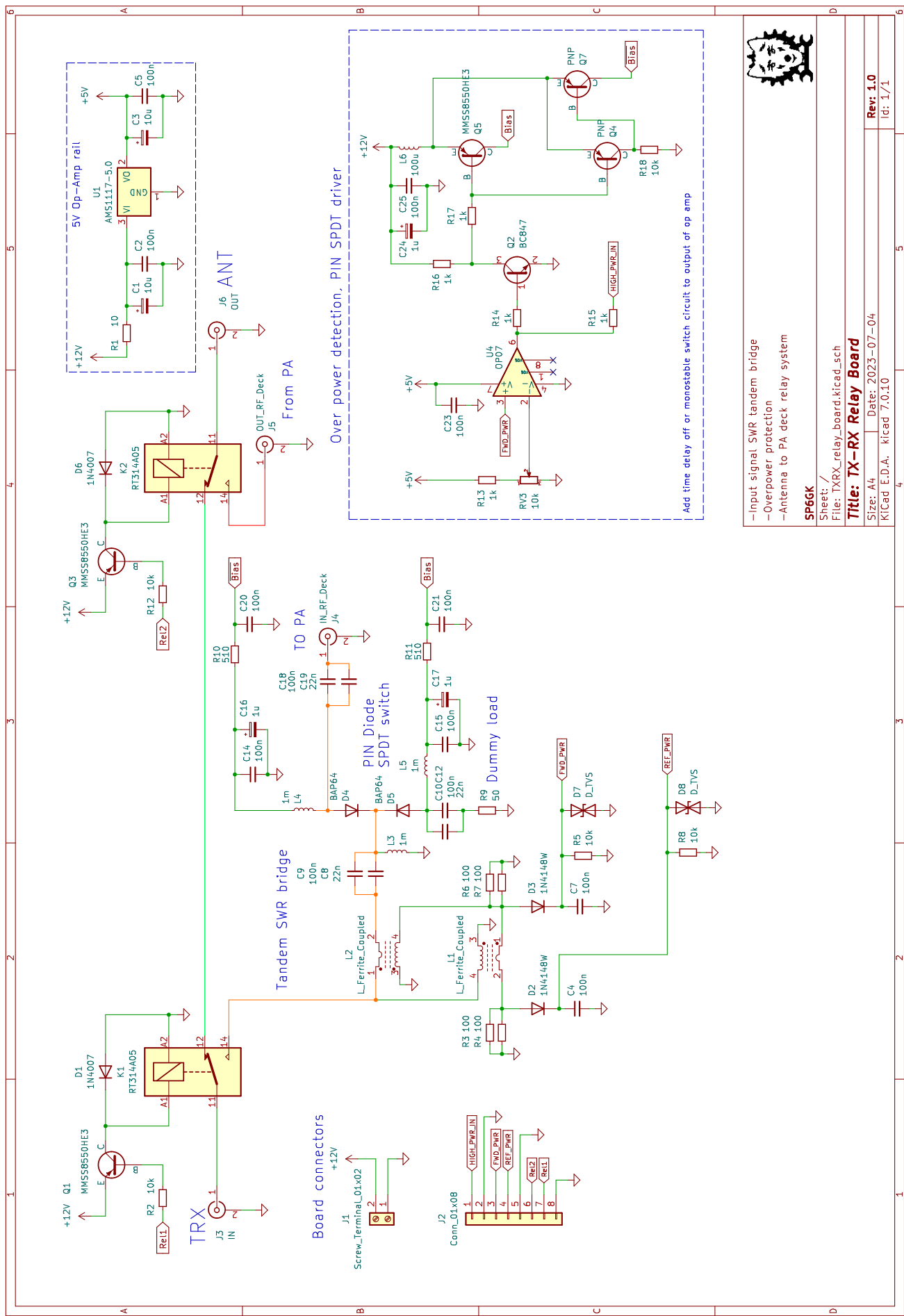
# PA board Bias Circuit



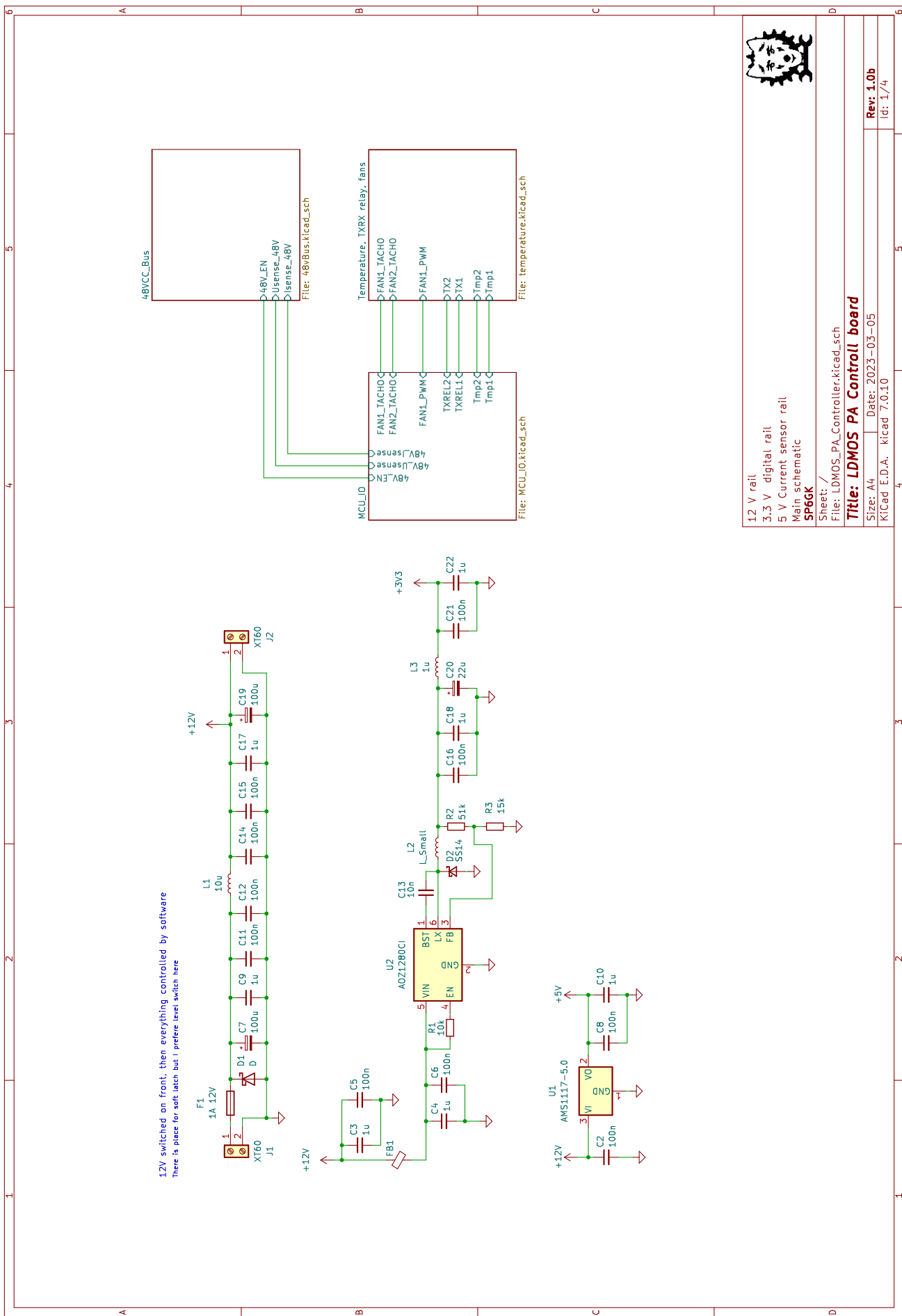
## 7.11.2 LPF Schematic



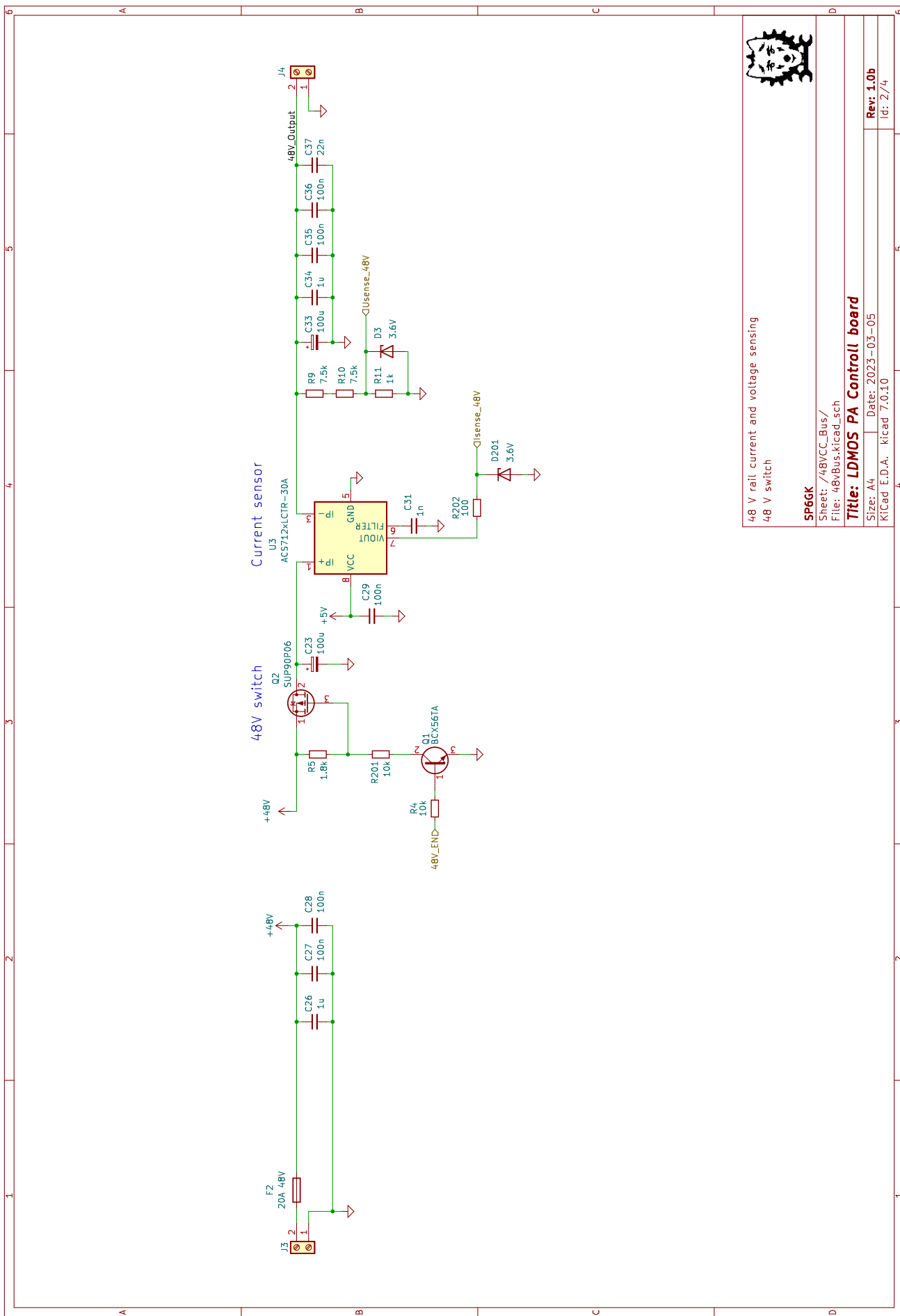
### 7.11.3 TX/RX Schematic



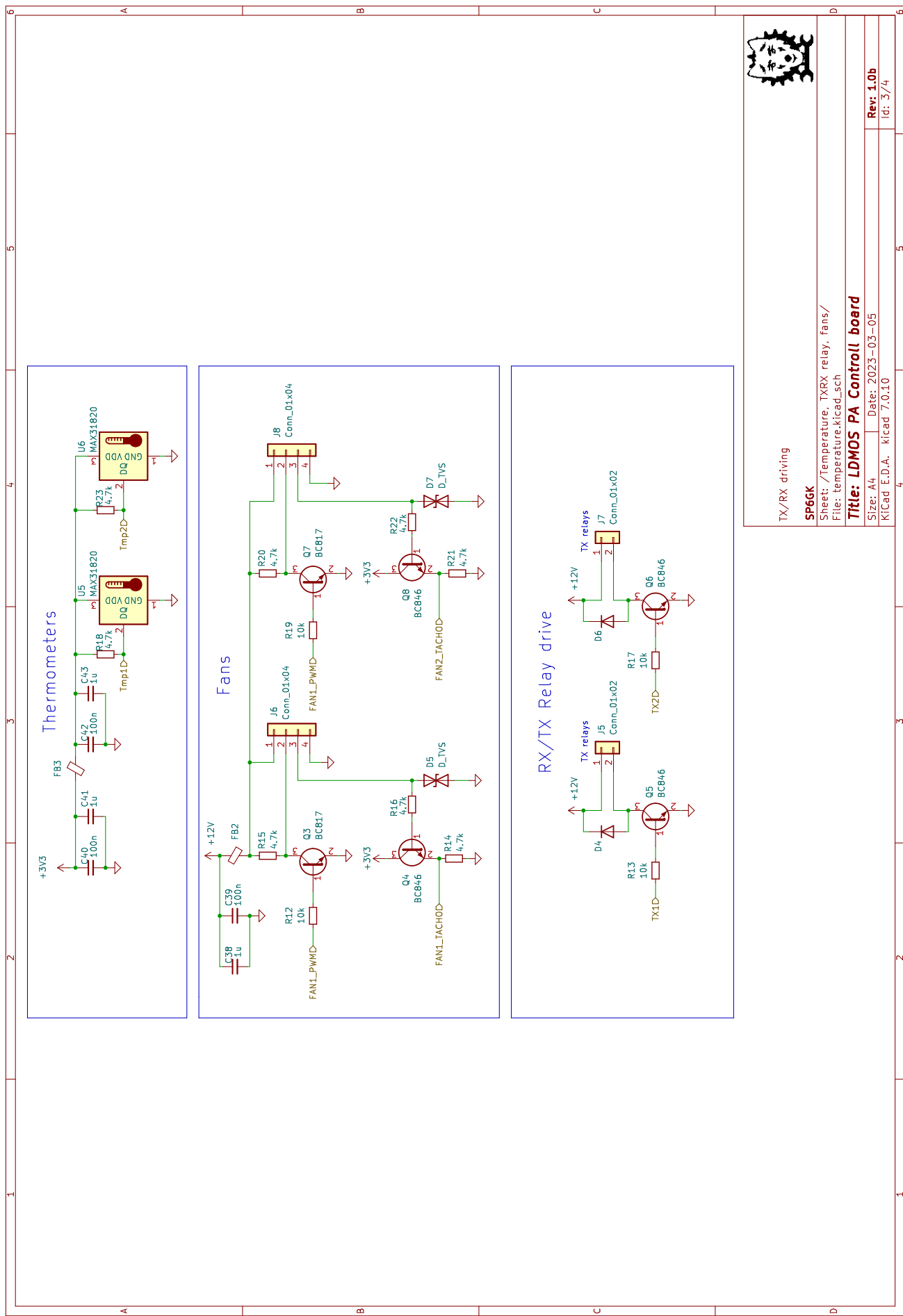
## 7.11.4 Controller Schematic



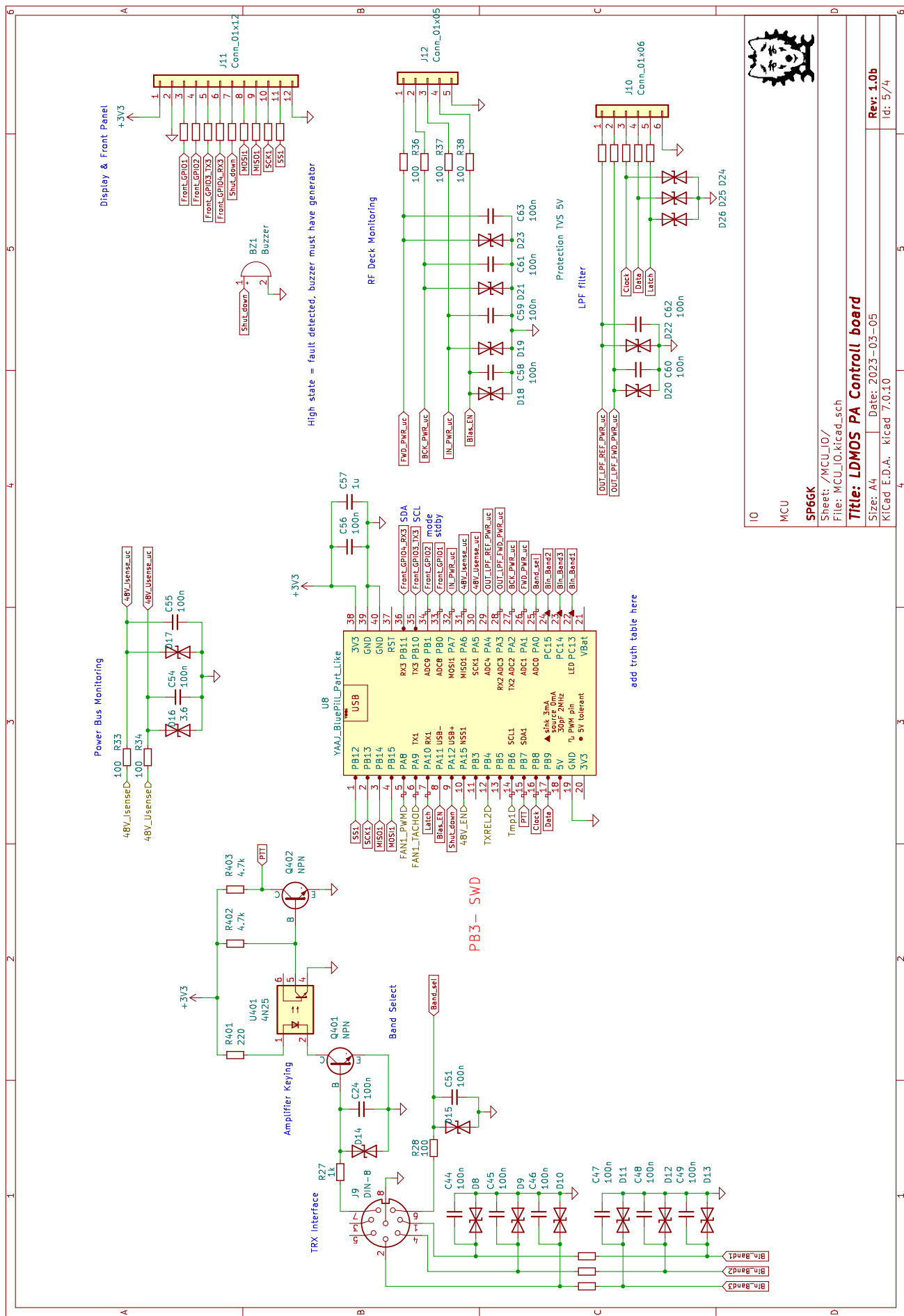
# Controller Schematic, 48 V Rail



# Controller Schematic, Temperature Sensors, Fans, Relays



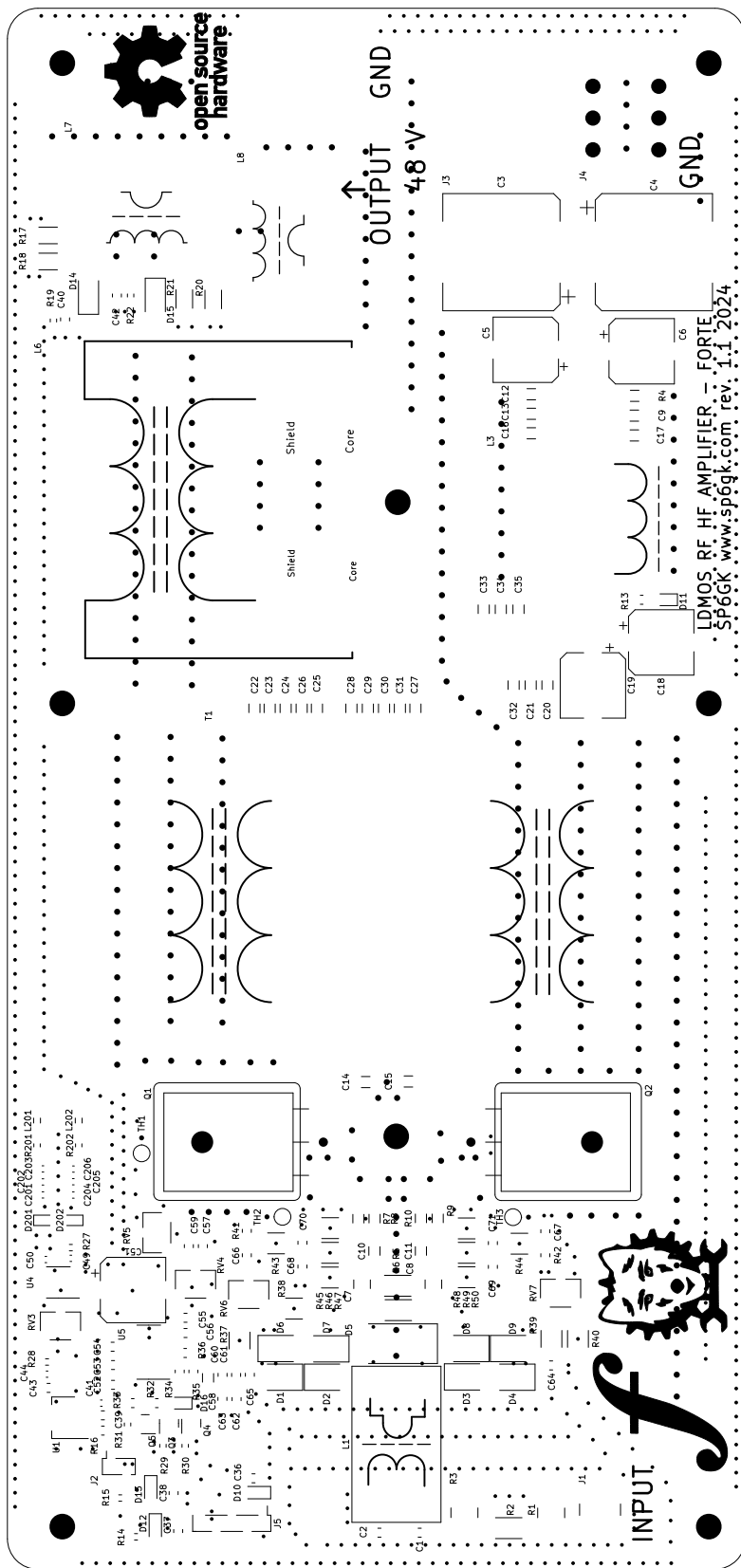
# Controller Schematic, Microcontroller



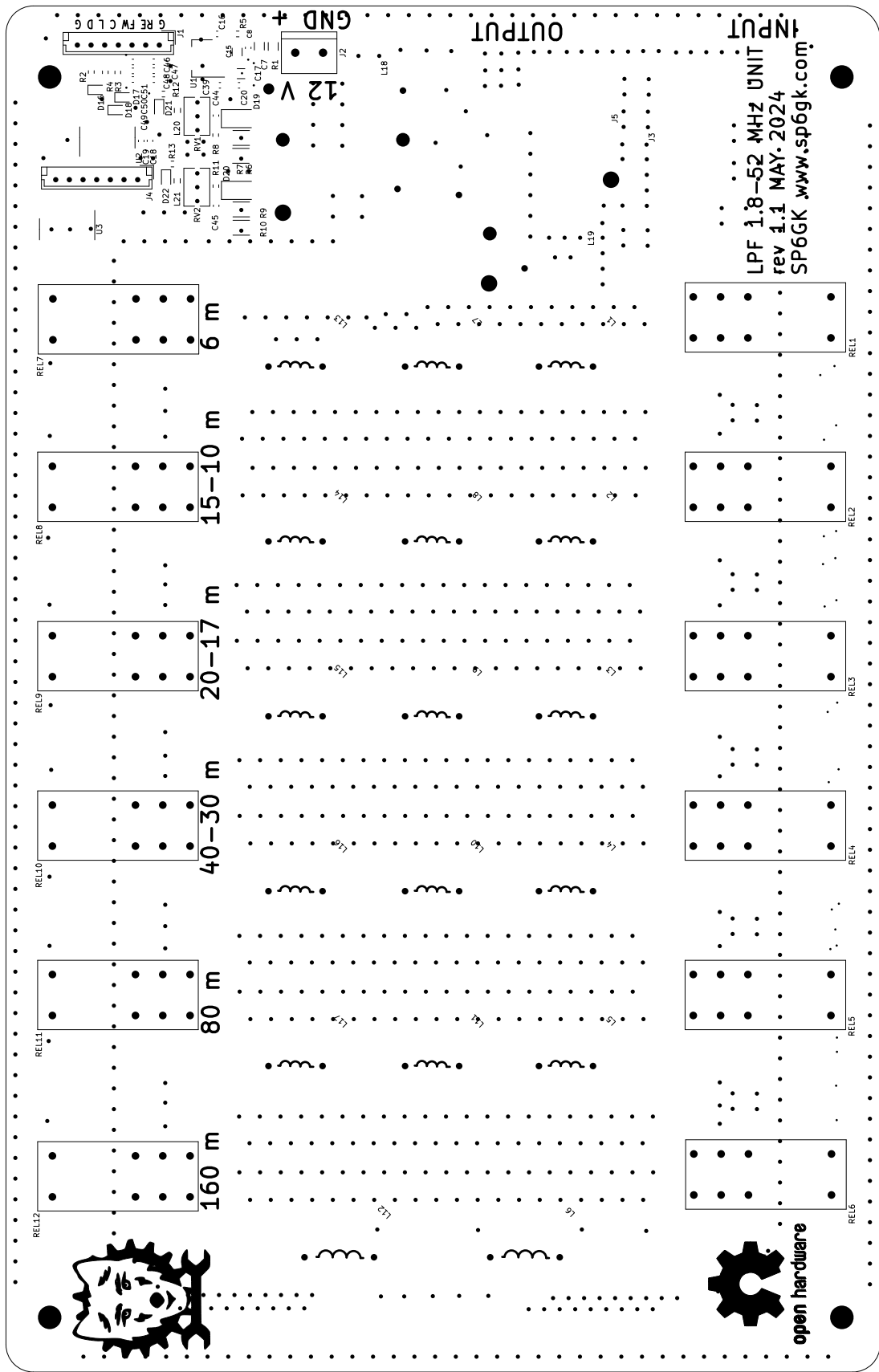
## 7.12 PCB Silkscreens

Presented silk screen layers are not to scale.

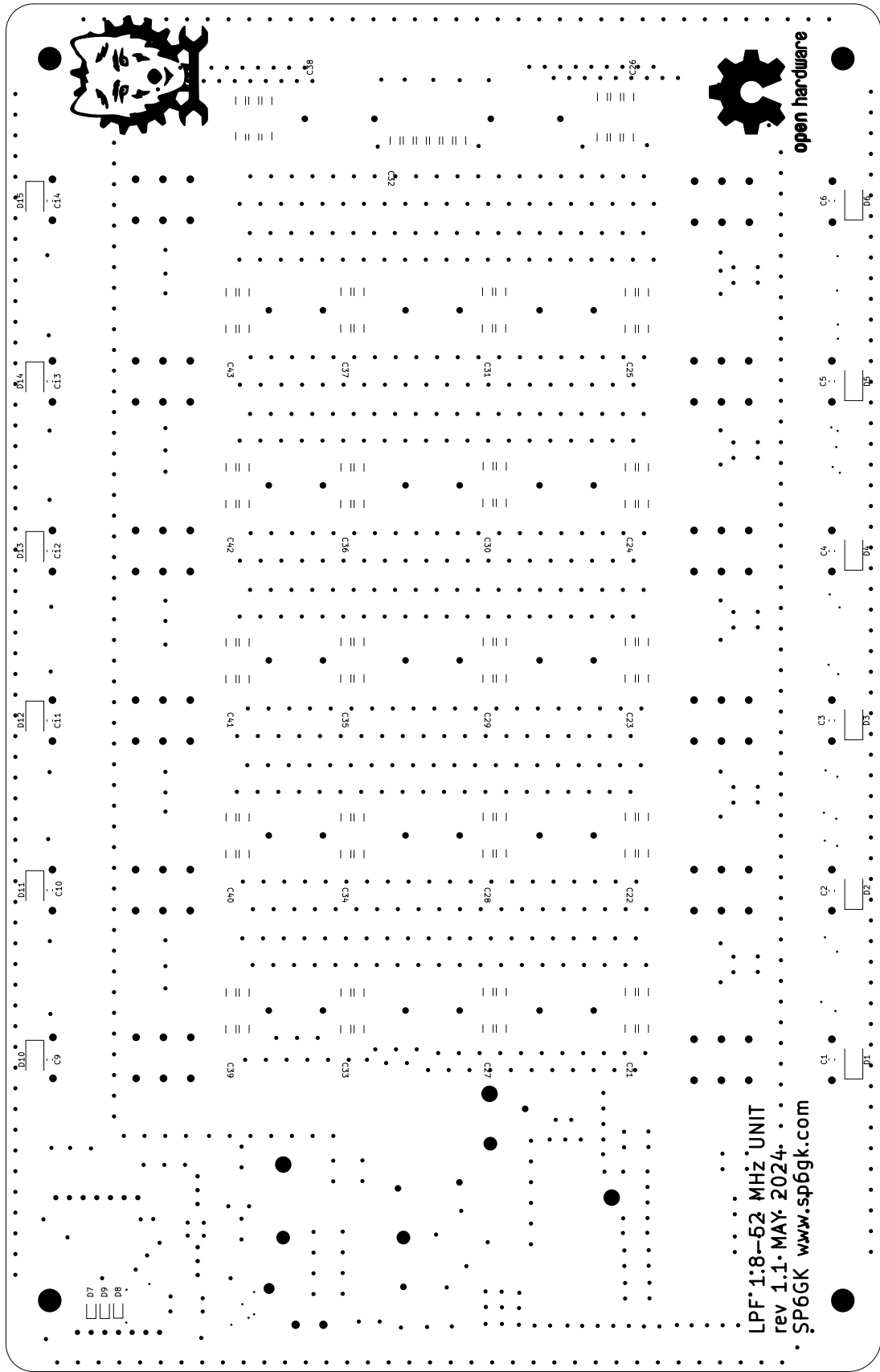
PA board Front Silkscreen



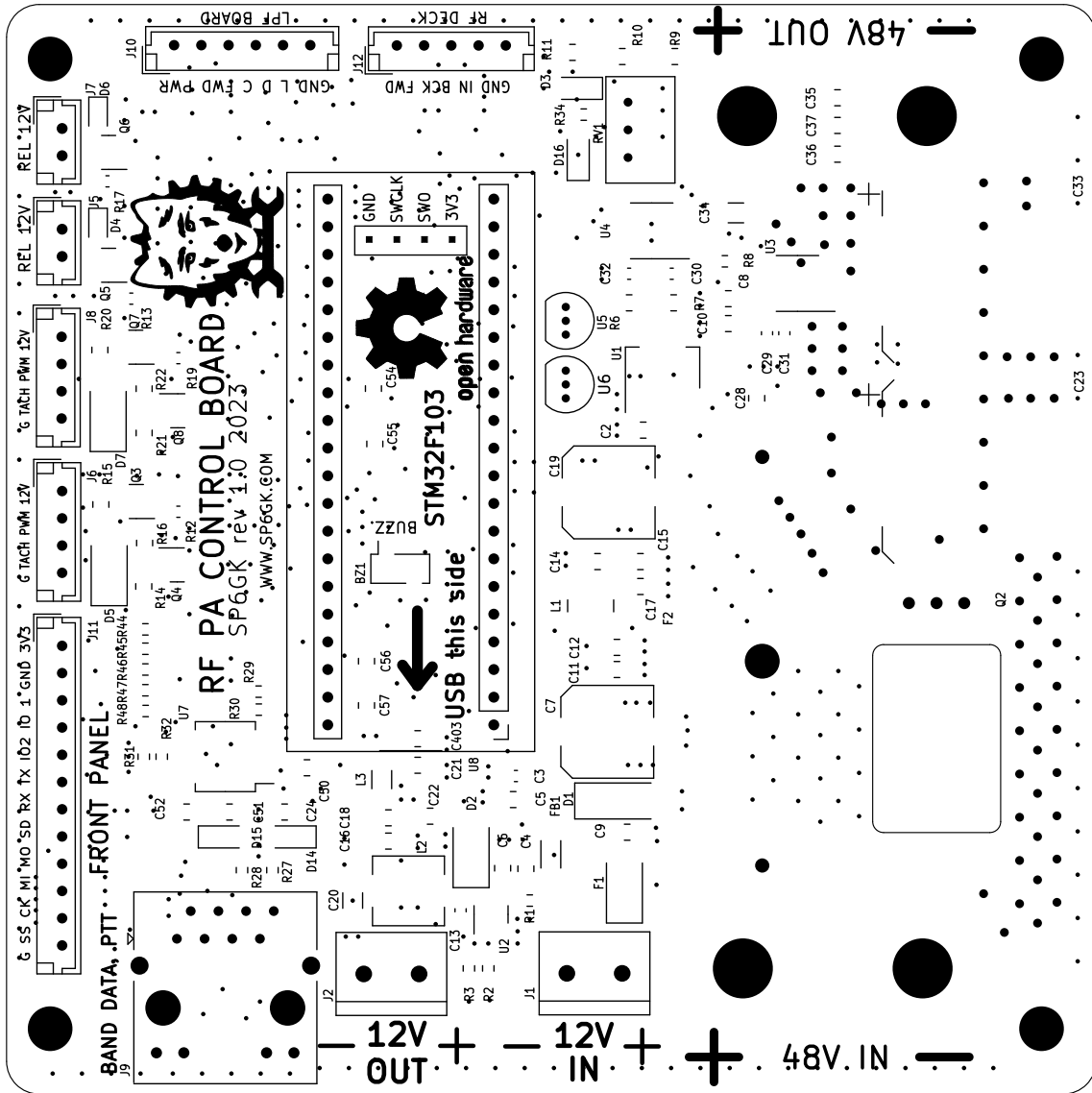
### 7.12.1 LPF Board Front Silkscreen



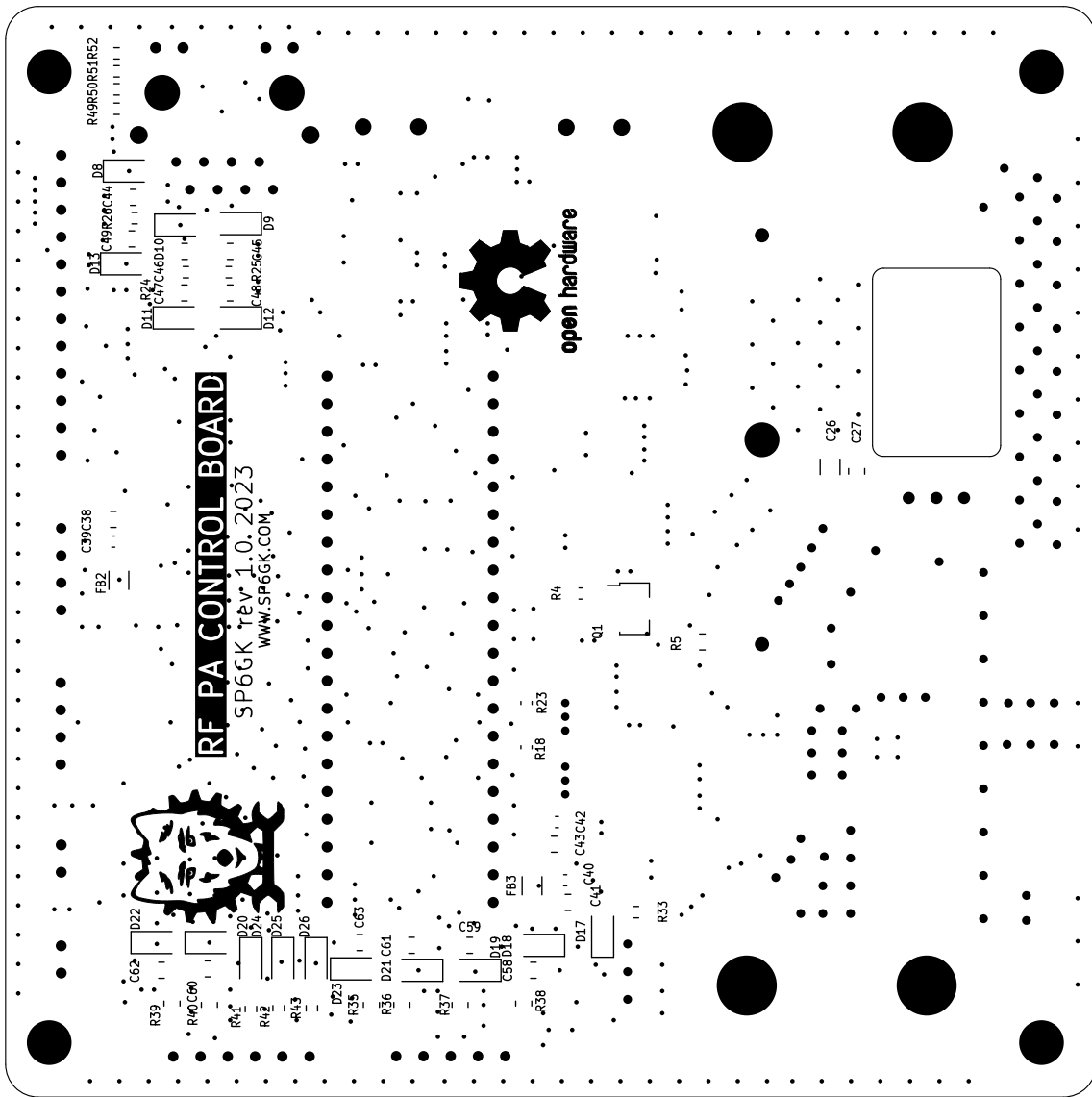
## 7.12.2 LPF Board Back Silkscreen



### 7.12.3 Controller Board Front Silkscreen



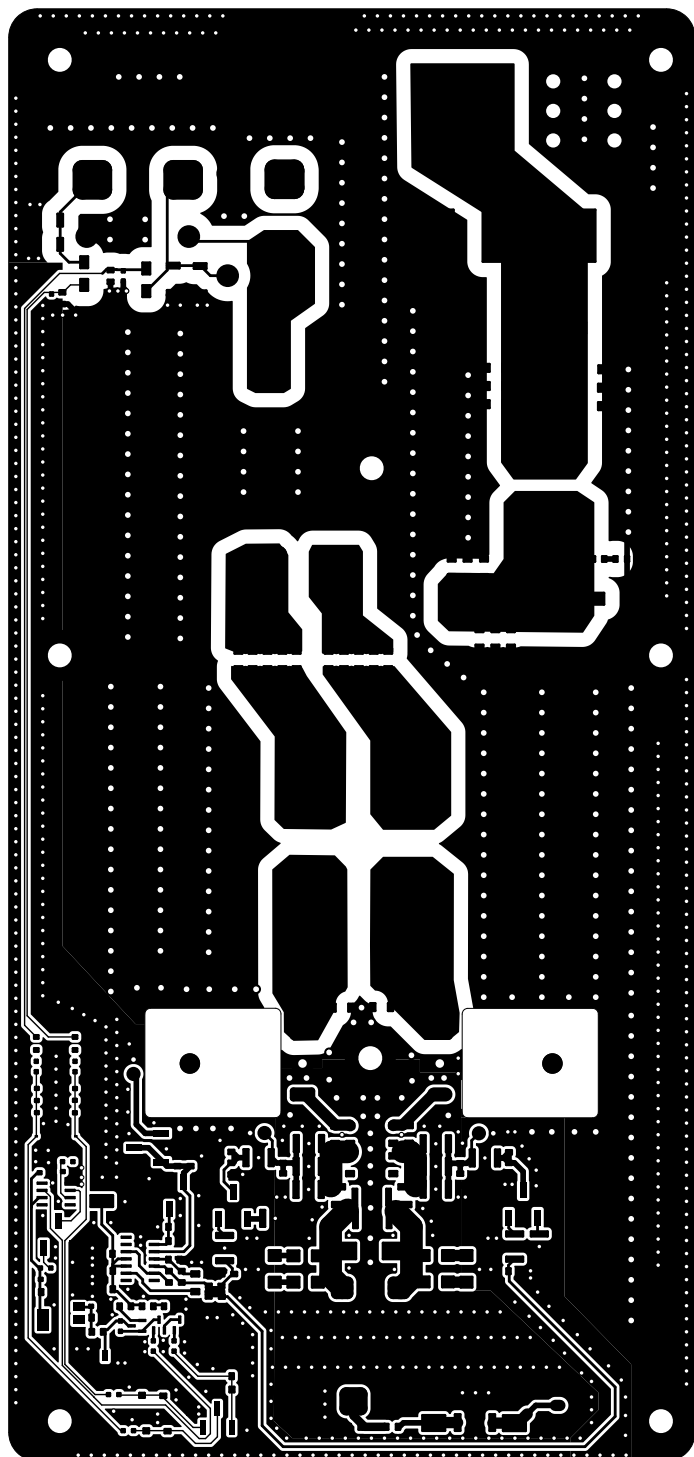
#### 7.12.4 Controller Board Back Silkscreen



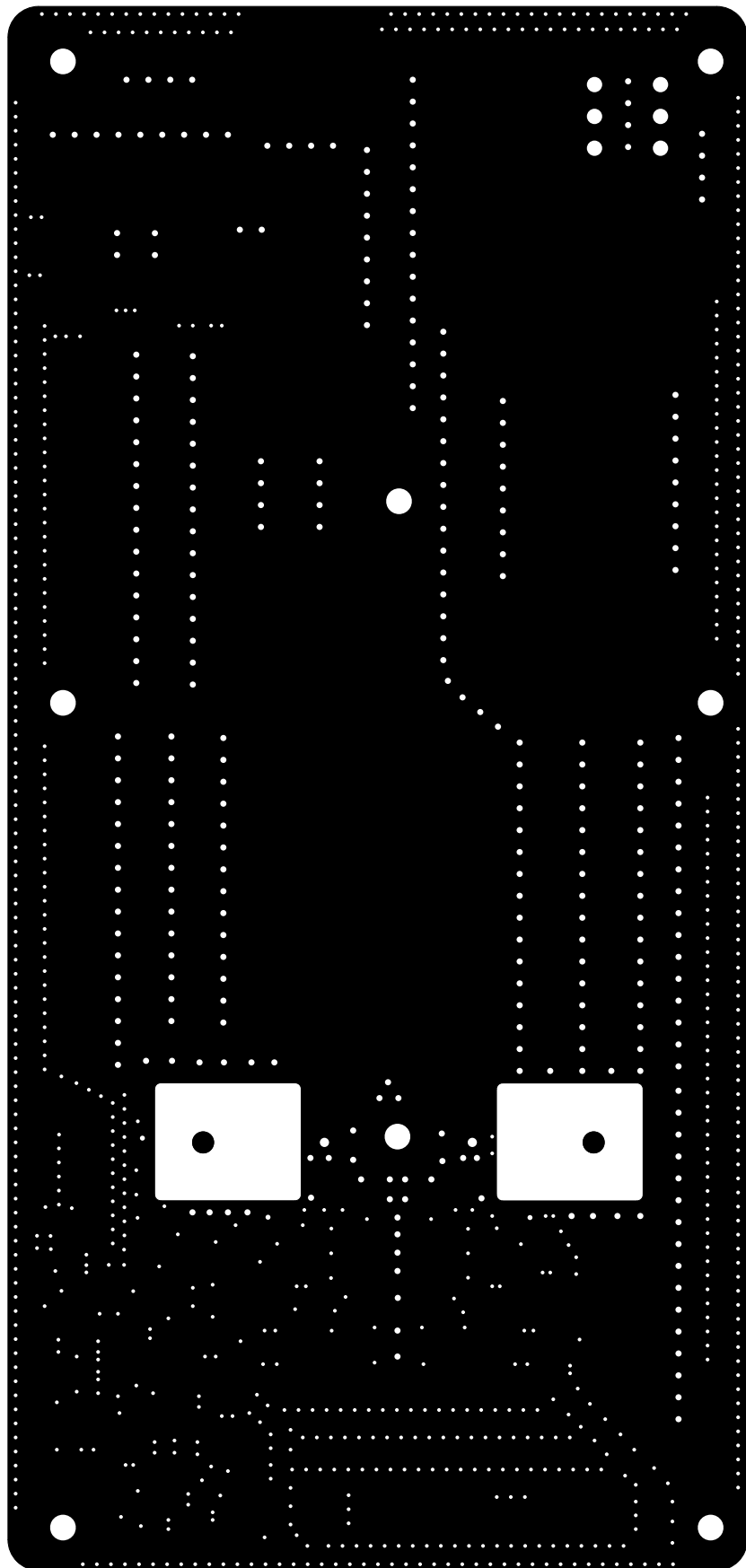
## 7.13 PCB Copper Layers

Presented copper layers are not to scale.

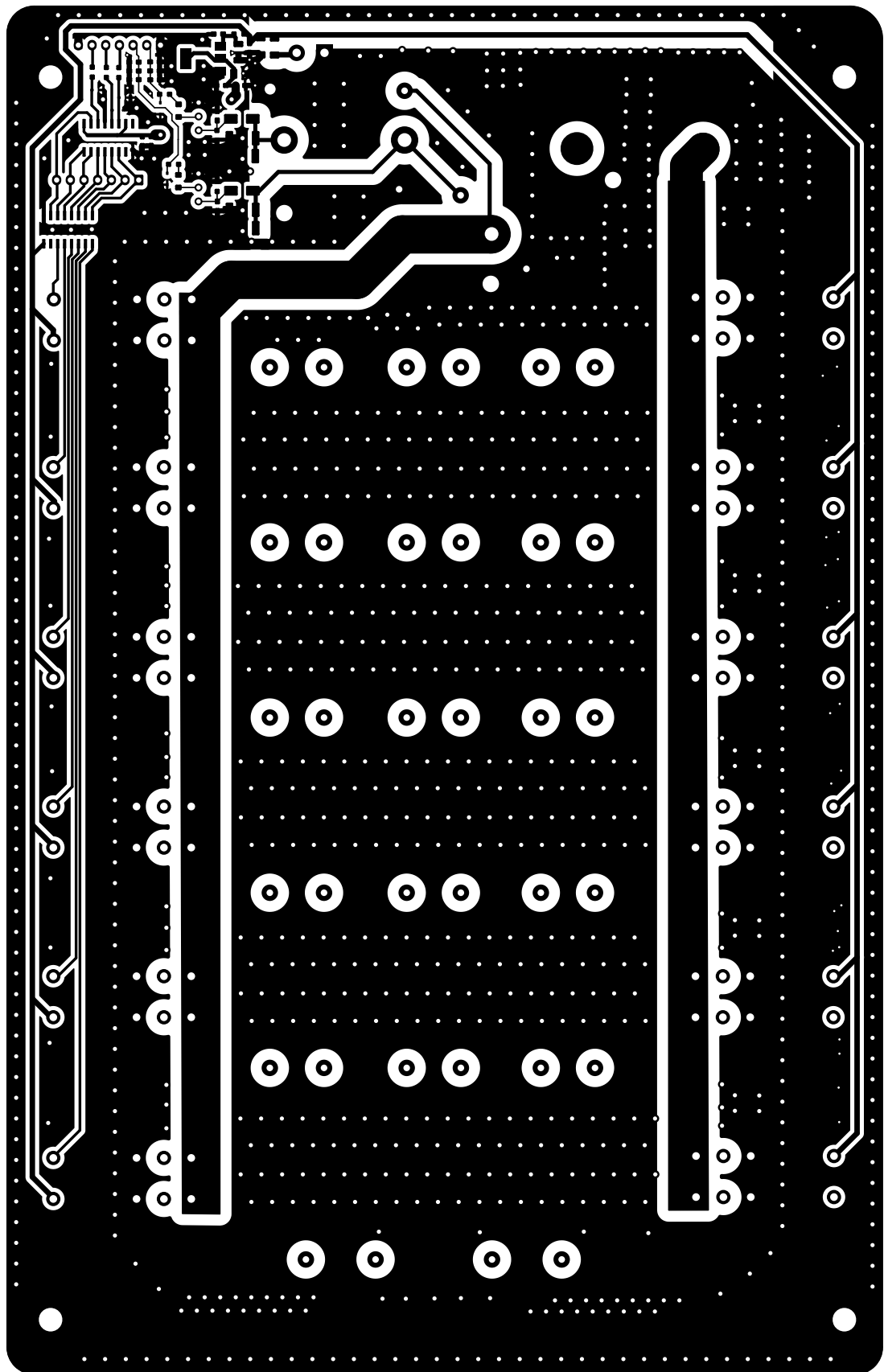
PA Board Front CU



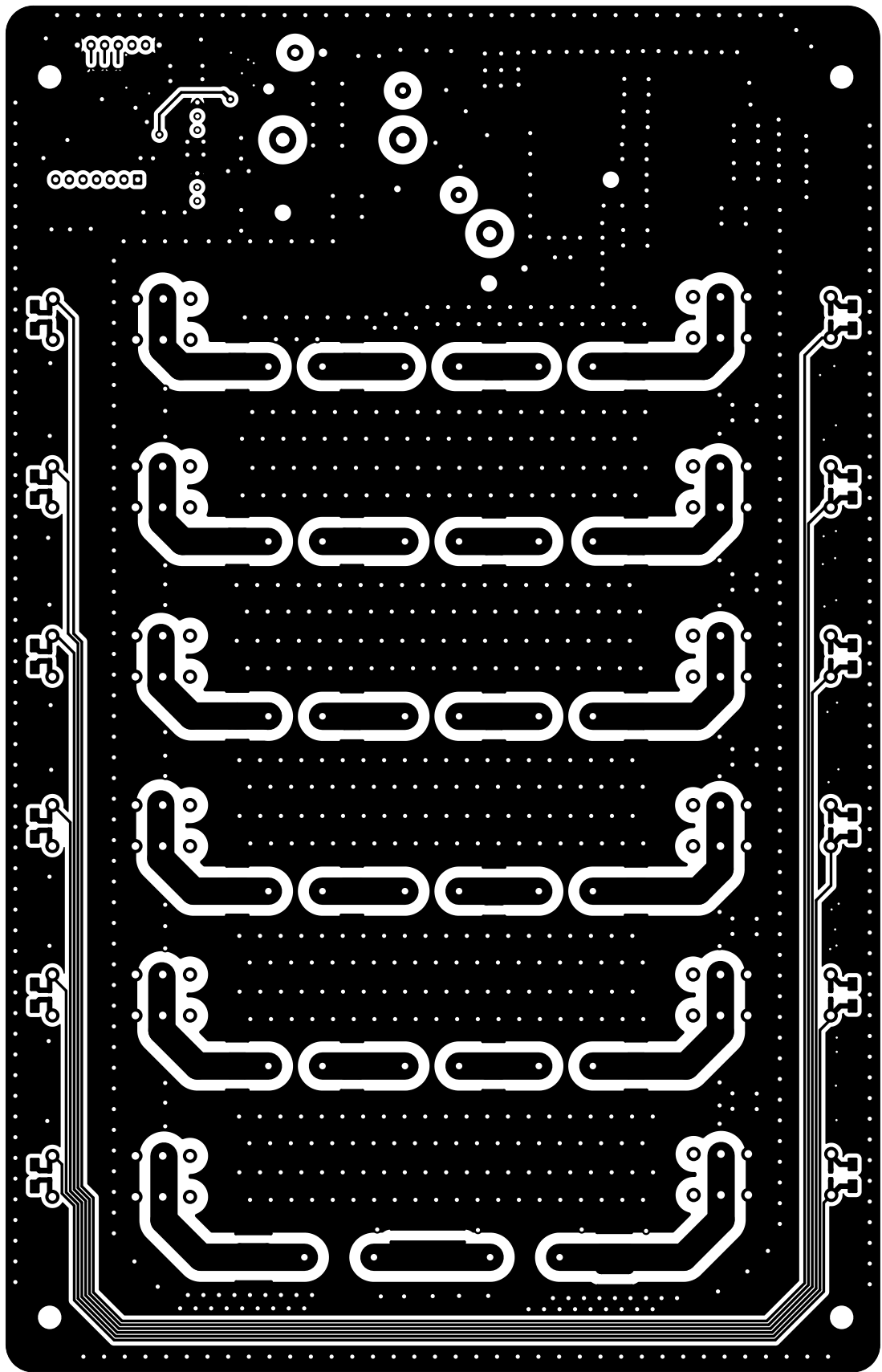
PA Board Back CU



### 7.13.1 LPF Board Front CU

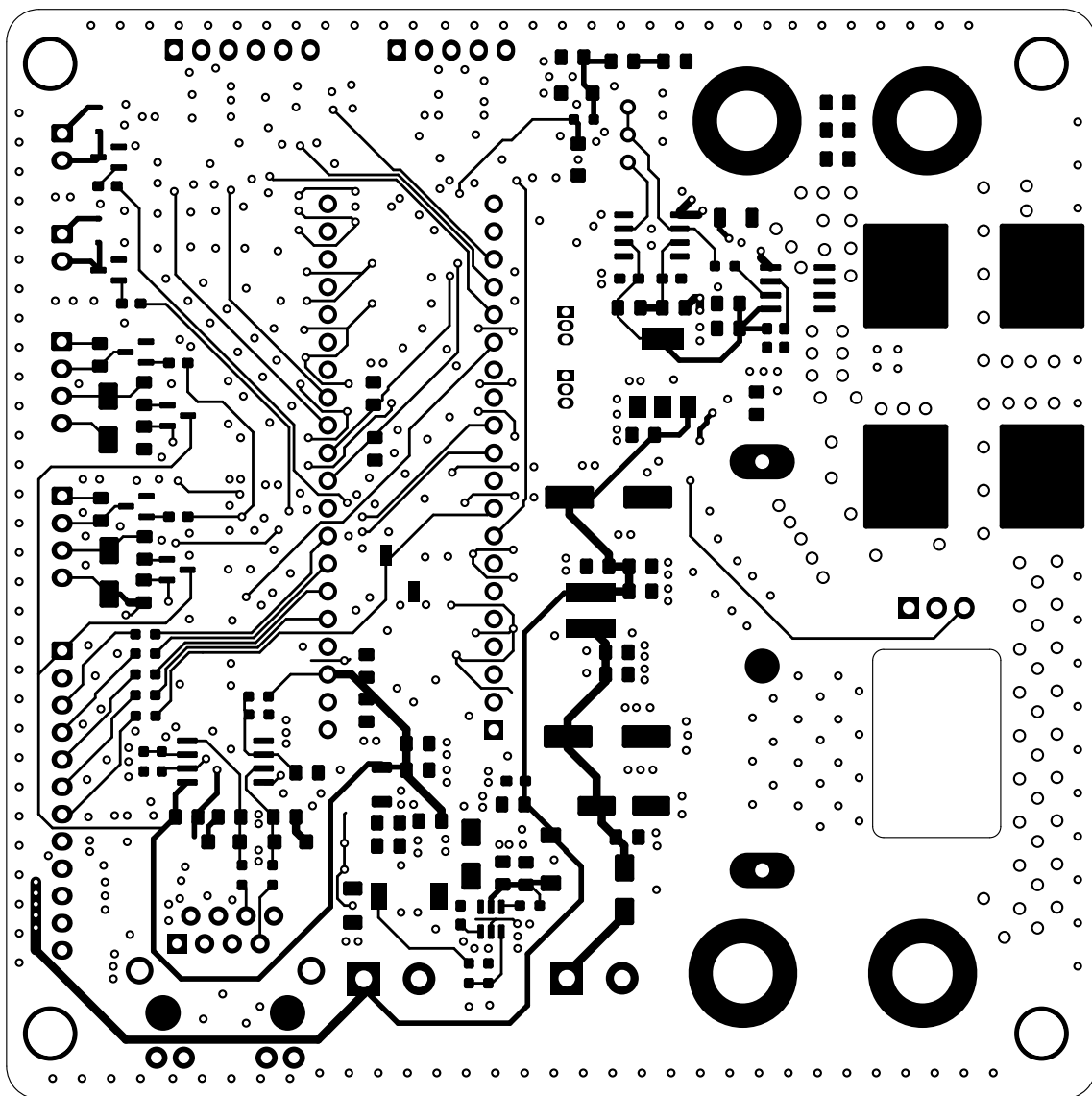


### 7.13.2 LPF Board Back CU

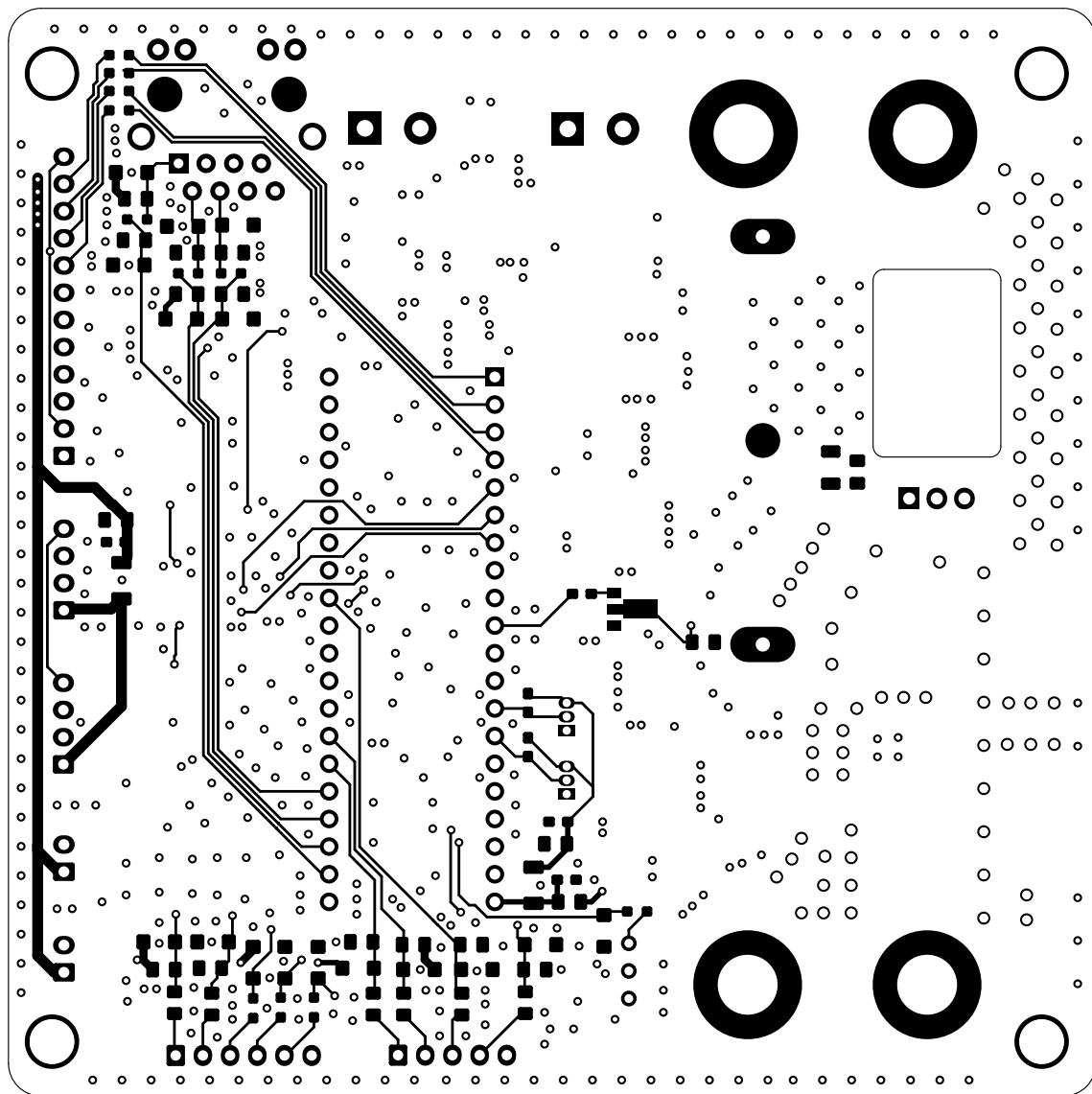


### 7.13.3 Controller Board Front CU

Copper ground pour is not included in order to increase the visibility of the traces.



#### 7.13.4 Controller Board Back CU



## 7.14 BOM

### 7.14.1 PA Deck

References	Value	Footprint	Quantity
C36, C37, C38, C40, C42, C54, C56, C59, C63, C64, C65, C66, C67, C70, C71	100n, 25 V	0805	15
C16, C22, C23, C24, C26, C27, C28, C29, C30, C31, C33, C34	22n, 400 V	1206	12
C10, C11, C12, C13, C20, C21, C25, C32	100n, 400 V	1206	8
C39, C43, C52, C55, C57, C60, C61	10u, 25 V	0805	7
C41, C44, C49, C50, C202, C205	100n, 25 V	0603	6
C53, C62, C68, C69	1u, 25 V	0805	4
C14, C15, C58	100p, 1000 V	1206	3
C3, C4	330u, 63 V	CP_Elec_18x17.5	2
C5, C18	33u, 63 V	CP_Elec_10x10.5	2
C6, C19	10u, 63 V	CP_Elec_10x10.5	2
C7, C8	100n, 400 V	1210	2
C17, C35	10n, 100 n	1206	2
C201, C204	1u, 25 V	0603	2
C203, C206	10n, 25 V	0603	2
C1	33n, 50 V	0805	1
C2	22p, 50 V	0805	1
C9	1u, 63 V	1206	1
C51	47u, 25 V	CP_Elec_10x10.5	1
R37, R38, R39, R40, R43, R44, R45, R46, R47, R48, R49, R50	100, 2W Thin Metal	1812	12
R7, R8, R9, R10	4.7 0.25 W Thin Metal	1206	4
R14, R15, R201, R202	100	0603	4
R17, R18, R20, R21	100	2010	4
R19, R22, R27, R31	10k	0603	4
R16, R33, R34	10	0805	3
R28, R29, R30	1k	0603	3
R1, R3	300 3W Thin Metal	2816	2
R5, R6	33 3W Thin Metal	2512	2
R41, R42	4.7k	0805	2
R2	18 2W Thin Metal	2512	1
R4	47k	1206	1
R13	x	0805	1
R32	470	0805	1
R35	2.2k	0805	1
R36	14k	0805	1
L201, L202	100u	0805	2
L1	4:1	Binocular_trafo_small	1
L3	12 uH 20 A	EMI_inductor	1
L6	2x mat 43. 4T RG174 50 Ohm	Trafo_623-2661102002	1
L7	FT50-61 30T 1T RG-142 coax	FTS2_trafo	1
L8	FTS2-61 30T 1T-RG213 coax	FTS2_trafo	1
D1, D4, D6, D9	1N4148WT	D_SMB	4
D2, D3, D7, D8	4.7	D_SMB	4
D12, D13	Protection TVS 5V	D_SMF	2
D14, D15	1N4148W	D_SMA	2
D201, D202	SD12_SOD323	D_SOD-323	2
D5	D_TVS	D_SMC_Handsoldering	1
D10	3.6	D_SMF	1
D11	48V LED	0805	1
D16	BIAS_LED	0805	1
U1	AMS1117-5.0	SOT-223-3_TabPin2	1
U4	OP07	SOIC-8_3.9x4.9mm_P1.27mm	1
U5	LM723_DIP14	SO-14_3.9x8.65mm_P1.27mm	1
RV3, RV4, RV5	10k	Bourns_3269W_Vertical	3
TH1, TH2, TH3	5k	L6.3mm_D2.5mm_P2.54mm	3
Q3, Q4	BC846	SOT-23	2
RV6, RV7	500	Bourns_3269W_Vertical	2
Q1	MRF300AN	TO-247-3	1
Q2	MRF300BN	TO-247-3	1
Q5	PMOS	SOT-23	1
T1	1:9 TLT	TLT_Trafo	1
J3, J4	Keystone M5	M5_screw_terminal_Keystone	2
J1	SMA	SMA_Vertical	1
J2	5.08mm	1x02 2.54mm	1
J5	Conn_01x05	1x05 2.54 mm	1

### 7.14.2 Controll Board

References	Value	Footprint	Quantity
C2, C5, C6, C8, C11, C12, C14, C15, C16, C21, C24, C27,C28, C35, C36, C44, C45, C46, C47, C48, C49, C50, C51, C52, C54, C55, C56, C58, C59, C60, C61, C62, C63	100n	0805	33
C4, C9, C10, C17, C18, C22, C38, C41, C43, C57, C403	1u	0805	11
C29, C30, C32, C39, C40, C42	100n	0603	6
C7, C19	100u	C_Elec_8x10.2	2
C23, C33	100u	CP_Elec_16x17.5	2
C26, C34	1u	1206	2
C3	1u	0603	1
C13	10n	0603	1
C20	22u	1206	1
C31	1n	0603	1
C37	22n	0805	1
R24, R25, R26, R27, R28, R33, R34, R41, R42, R43, R44, R45, R46, R47, R48, R49, R50, R51, R52	100	0603	19
R14, R15, R16, R20, R21, R22	4.7k	0805	6
R35, R36, R37, R38, R39, R40	100	0805	6
R4, R12, R13, R17, R19	10k	0603	5
R5, R11	1k	0805	2
R6, R7	10k	0805	2
R8, R31	4.7k	0603	2
R9, R10	7.5k	0805	2
R18, R23	4.7k	0603	2
R1	10k	0603	1
R2	51k	0603	1
R3	15k	0603	1
R29	2.3k	0603	1
R30	3.3k	0603	1
R32	5.6k	0603	1
L1	10u	Ferrocore_DLG-0403	1
L2	L_Small	L_6.3x6.3_H3	1
L3	1u	1206	1
D8, D9, D10, D11, D12, D13, D14, D15, D17, D19, D22, D24, D25, D26	D_TVS	D_SMF	14
D16, D18, D20	3.6	D_SMF	3
D4, D6	1SS355VM	D_SOD-323F	2
D5, D7	D_TVS	D_SMA	2
D21, D23	Protection TVS 5V	D_SMF	2
D1	D	D_SMA	1
D2	SS14	D_SMA	1
D3	3.6V	D_SMF	1
U5, U6	MAX31820	TO-92_Inline	2
U1	AMS1117-5.0	SOT-223-3_TabPin2	1
U2	AOZ1280CI	SOT-23-6	1
U3	AC5712xLCTR-30A	SOIC-8_3.9x4.9mm	1
U4	OP07	SO-8_3.9x4.9mm	1
U7	LM358	SO-8_5.3x6.2mm	1
U8	YAAJ_BluePill_Part_Like	YAAJ_BluePill_1	1
F1	1A 12V	D_SMA	1
F2	20A 48V	6.3x32mm	1
Q3, Q4, Q5, Q6, Q7, Q8	BC846	SOT-23	6
FB2, FB3	FerriteBead_Small	1206	2
BZ1	Buzzer	1x02_P2.54mm	1
FB1	FerriteBead_Small	1806	1
Q1	BCX56TA	SOT-89-3	1
Q2	AOB411L	TO-220-3_Vertical	1
RV1	20k	Bourns_3299W_Vertical	1
J1, J2	XT60	TerminalBlock_2_P5.08mm	2
J3, J4	Screw_Terminal_01x02	48Busfootprint	2
J5, J7	Conn_01x02	1x02_P2.50mm_Vertical	2
J6, J8	Conn_01x04	1x04_P2.50mm_Vertical	2
J9	DIN-8	RJ45SS74301-00x	1
J10	Conn_01x06	JST_EH_B6B-EH-A_1x06_P2.50mm_Vertical	1
J11	Conn_01x12	JST_EH_B12B-EH-A_1x12_P2.50mm_Vertical	1
J12	Conn_01x05	JST_EH_B5B-EH-A_1x05_P2.50mm_Vertical	1

### 7.14.3 TX/RX Relay Board

References	Value	Footprint	Quantity
C1, C3, C7, C9, C10, C11, C16, C17, C18, C20, C22, C24	100n	0603	12
C4, C6, C15	22n	0805	3
C5, C8, C14	100n	0805	3
C12, C13, C21	1u	0805	3
C19, C23	10u	0805	2
R1, R4, R7, R13, R20	10k	0603	5
R14, R16, R17, R18, R19	1k	0603	5
R2, R3, R5, R6	100	2010	4
R8, R10	100	0603	2
R11, R12	510	1206	2
R9	50	SMA_Vertical	1
R15	10	2010	1
L4, L6, L7	1m	1812	3
L1, L2	L_Ferrite_Coupled	FT82_traflo	2
L3, L5	L_Small	0603	2
L8	100u	1206	1
D1, D8	1N4007	D_SMA	2
D2, D3	Schottky	D_SMA	2
D4, D5	BAP64	D_SOD-323	2
D6, D7	D_TVS	D_SOD-323	2
U1	OP07	SOIC-8_3.9x4.9mm_P1.27mm	1
U2	AMS1117-5.0	SOT-223-3_TabPin2	1
Q1, Q2, Q5	MMSS8550HE3	SOT-23	3
K1, K2	RT314A05	Relay_SPDT_Schrack-RT1-16A-FormC_RM5mm	2
Q4, Q6	PNP	SOT-23	2
Q3	BC847	SOT-23	1
RV1	10k	Potentiometer_Bourns_3296W_Vertical	1
J1	Screw_Terminal_01x02	TerminalBlock_bornier-2_P5.08mm	1
J2	Conn_01x08	JST_EH_B7B-EH-A_1x08_P2.50mm_Vertical	1
J3	IN	SMA_Amphenol_901-144_Vertical	1
J4	IN RF_Desk	SMA_Amphenol_901-144_Vertical	1
J5	OUT RF_Desk	Coax_solder	1
J6	OUT	Coax_solder	1

### 7.14.4 LPF Board

References	Value	Footprint	Quantity
C1, C2, C3, C4, C5, C6, C8, C9, C10, C11, C12, C13, C14, C16, C18, C20, C39, C44, C45, C47, C50	100n	0603	21
C25, C31, C37, C43	834p	4x1206_2	4
C19, C46, C49	1u	0603	3
C26, C32, C38	C_Small	6x1206	3
C7, C17	10u	1206	2
C21, C39	71p	4x1206_2	2
C22, C40	123p	4x1206_2	2
C23, C41	203p	4x1206_2	2
C24, C42	357p	4x1206_2	2
C27, C33	127p	4x1206_2	2
C28, C34	218p	4x1206_2	2
C29, C35	360p	4x1206_2	2
C30, C36	635p	4x1206_2	2
C48, C51	10n	0603	2
C15	10u	1206	1
R2, R3, R4, R5, R12, R13	100	0603	6
R6, R7, R9, R10	100	2010	4
R8, R11	10k	0603	2
R1	10	0603	1
L1, L2, L3, L4, L5, L7, L8, L9, L10, L11, L13, L14, L15, L16, L17	L	T94-Inductor	15
L6, L12	L	T106-Inductor	2
L20, L21	100u	0805	2
L18	FT50-61_30T_1T_RG-142 coax	T94-SWR_TRAFO	1
L19	FT82-61_30T_1T-RG213 coax	T94-SWR_TRAFO	1
D1, D2, D3, D4, D5, D6, D10, D11, D12, D13, D14, D15	1N4007	D_SMA	12
D7, D8, D9, D16, D17, D18, D21, D22	SD12_SOD323	D_SOD-323	8
D19, D20	Schottky	D_SMA	2
U1	AMS1117-5	SOT-223-3_TabPin2	1
U2	74AHC595	SO-16_3.9x9.9mm_P1.27mm	1
U3	ULN2003	SO-16_3.9x9.9mm_P1.27mm	1
REL1, REL2, REL3, REL4, REL5, REL6, REL7, REL8, REL9, REL10, REL11, REL12	RM85	RM85_Relay	12
RV1, RV2	10k	Potentiometer_Bourns_3266Y_Vertical	2
J1, J4	Conn_01x07	JST_EH_B7B-EH-A_1x07_P2.50mm_Vertical	2
J2	12V INPUT	TerminalBlock_bornier-2_P5.08mm	1
J3	RF input	Coax_Mount	1
J5	RF output	Coax_Mount	1

# Bibliography

- [1] IARU, “Iaru region 1 technical recommendation r.1.” [https://www.qsl.net/ta2mbd/help/sysop/other\\_docs/Technical\\_Recommendation.pdf](https://www.qsl.net/ta2mbd/help/sysop/other_docs/Technical_Recommendation.pdf), 1990. STANDARDISATION OF S-METER READINGS.
- [2] ITU, “Recommendation itu-r sm.329-12, spurious emissions,” 2012. Unwanted emissions in the spurious domain.
- [3] FCC, “Telecommunication – updated september 2014,” 2014. PART 97—AMATEUR RADIO SERVICE, §97.307 Emission standards.
- [4] K. Frank W. Harris, *RCRYSTAL SETS TO SIDEBAND, A Guide to Building an Amateur Radio Station*. 2013.
- [5] L. Zhang, P. Pan, M. Jia, B. Song, K. Ma, and J. Cai, “Demonstration of 0.34 thz traveling wave tube amplifier,” in *2023 24th International Vacuum Electronics Conference (IVEC)*, pp. 1–2, 2023.
- [6] J. C. Whitaker, *Power Vacuum Tubes Handbook*. Springer Science+Business Media New York, 1994.
- [7] “813 tube datasheet,” 1955. RCA.
- [8] M. Albulet, *RF Power Amplifiers*. Noble Publishing, 2001.
- [9] R. York, “Some considerations for optimal efficiency and low noise in large power combiners,” *IEEE Transactions on Microwave Theory and Techniques*, vol. 49, no. 8, pp. 1477–1482, 2001.
- [10] Macom, “Mrf449 rf the rf line npn silicon power transistor datasheet,” v1.
- [11] M. Kossor, “A broadband hf amplifier using low-cost power mosfets (part 2),” *QST*, vol. April, 1999.
- [12] Freescale, “50v rf ldmos,” 2011. NXP.
- [13] T. Erlbacher, *Lateral Power Transistors in Integrated Circuits*. Springer International Publishing Switzerland, 2014.
- [14] V. N. Gromorushkin, “High efficiency 1.5 kw ldmos hf broadband radio transmitter,” in *2021 Systems of Signals Generating and Processing in the Field of on Board Communications*, pp. 1–5, 2021.
- [15] N. Semiconductors, “Nxp mrf300 rf power ldmos transistors | mouser video featured product spotlight,” 2021. Rev. 1.0.

- [16] M. Yamazoe, K. Haeiwa, and S. Hirose, “Development of a high efficiency hf power amplifier,” in *2008 14th Asia-Pacific Conference on Communications*, pp. 1–5, 2008.
- [17] N. Semiconductors, “Mrf300an, high ruggedness n-channel enhancement-mode lateral mosfets.” <https://www.nxp.com/products/radio-frequency/rf-industrial-scientific-and-medical/1-600-mhz-broadcast-and-ism/300-w-cw-over-1-8-250-mhz-50-v-wideband-rf-power-ldmos-transistor:MRF300AN>, 2019. rev. 2.
- [18] Ameritron, “Ameritron al-811h, instruction manual, rev 6.” HF POWER LINEAR AMPLIFIER.
- [19] Ameritron, “Ameritron als-600/s instruction manual.” 600 WATT NO TUNE TMOS-FET AMPLIFIER.
- [20] M. Razvan Fatu, “A 600w broadband hf amplifier using affordable ldmos devices.” QRP Blog.
- [21] D. M. Pozar, *Microwave Engineering*. John Wiley & Sons, Inc., 2012.
- [22] K. JEFFREY C ANDERSON, “Notes on directional couplers for hf.” 2015.
- [23] P. Horowitz and W. Hill, *The Art of Electronics*, pp. 252–253. Cambridge University Press, 1991.
- [24] A. Bjorck, *Numerical Methods for Least Squares Problems*, p. 339. SIAM, Society for Industrial and Applied Mathematics, 1996.
- [25] V. Siliconix, “Sup90p06-09l, p-channel 60 v (d-s),” 2010.
- [26] A. microsystems, “Fully integrated, hall-effect-based linear current sensor ic with 2.1 kvrms isolation and a low-resistance current conductor,” 2023.
- [27] M. integrated, “Ds18b20, programmable resolution 1-wire digital thermometer, datasheet,” 2019.
- [28] STMicroelectronics, “Stm32f103x8, microcontroller data sheet, rev 19,” 2023.
- [29] L. Hitachi, “Hd44780u, dot matrix liquid crystal display controller/driver,” 1998.
- [30] N. Semiconductors, “Remote 8-bit i/o expander for i2c-bus with interrupt, data sheet,” 2013.
- [31] I. Maxim Integrated Products, “Max7219, serially interfaced, 8-digit led display driver,” 2021.
- [32] R. G. Lyons, *understanding Digital Signal Processing, 1st edition*, p. 13. Addison-Wesley, 1997.
- [33] W. Hayward, R. Campbell, and B. Larkin, *Experimental Methods in RF Design*. ARRL, 2019.
- [34] I. MICROMETALS, *Power Conversion& Line Filter Applications*, pp. 3,10–11, 67. 2007.

- [35] I. MICROMETALS, *RF Applications, Iron Powder Cores*, pp. 2, 4, 12. Micrometals, 2005.
- [36] I. Jim Cox, MICROMETALS, *Iron Powder Core Selection for RF Power Applications*, p. 2. Micrometals, 2007.
- [37] Micrometals, “T94-2, micrometals powder core solutions data sheet.” 2019.
- [38] T. instruments, “Uln200x, ulq200x high-voltage, high-current darlington transistor arrays, data sheet,” 2022.
- [39] H. Y. W. Z. R. S. FRED LEFRAK, DAXIONG JI, “How rf transformers work and how they are measured.” 2015.
- [40] M. S. Helge O. Granberg, “A two stage 1 kw solid-state linear amplifier, an758.” 1993.
- [41] W. Lambert, “Second-order distortion in catv push-pull amplifiers,” *Proceedings of the IEEE*, vol. 58, no. 7, pp. 1057–1062, 1970.
- [42] V. Klokov, N. Kargin, A. Garmash, and E. Guznaeva, “Broadband push-pull power amplifier design methodology based on the gan component base for high-performance nonlinear junction detectors,” *ITM Web of Conferences*, vol. 30, p. 01011, 01 2019.
- [43] V. N. Gromorushkin, “High efficientcy 1.5 kw ldmos hf broadband radio transmitter,” in *2021 Systems of Signals Generating and Processing in the Field of on Board Communications*, pp. 1–5, 2021.
- [44] G. Guanella, “New method of impedance matching in radio-frequency circuits,” *The Brown Boveri Review*, pp. 327–329, Sept. 1944.
- [45] W. Jerry Sevick, *Transmission Line Transformers Handbook*, pp. 1–4, 7–9, 33, 35. Amidon Associates, Inc., 1997.
- [46] E. Rotholz, “Transmission-line transformers,” *IEEE Transactions on Microwave Theory and Techniques*, vol. 29, no. 4, pp. 327–331, 1981.
- [47] N. Chris Trask, “Transmission line transformers: Theory, design and applications — part 1,” *High Frequency Electronics*, pp. 46–52, Jan. 2006.
- [48] N. Chris Trask, “Transmission line transformers: Theory, design and applications — part 2,” *High Frequency Electronics*, pp. 26–31, Jan. 2006.
- [49] L. L. Ruthroff, “Some broad-band transformers,” *Proc. IRE*, vol. 47, pp. 1337–1342, Aug. 1959.
- [50] F.-R. P. Corp., “Fair-rite, 2661102002 61 round cable emi supression cores data sheet,” 2011.
- [51] QAxial, “Qaxial hf141-15-pep, handy-form microwave coaxial cable data shett,” 2023.
- [52] N. S. Rock Qiu, “Blf188xr 2-30 mhz 1000 w power amplifier,” 2013.
- [53] I. A. Roșu, “Bias circuits for rf devices,” 2012.
- [54] Ampelon, “Ldmos bias module, r10032,” 2015. Rev. 2.

- [55] D. Jackson, “Build a quality rf sampler,” 2014.
- [56] M. G. Bob Allison, Michael Tracy, *Test Procedures Manual*, pp. 129–136. ARRL., 2010.
- [57] R. Sherwood, “It’s time to clean up our transmitters, qst nov.” 2019.
- [58] STMicroelectronics, “Improving stm32f1 series, stm32f3 series and stm32lx series adc resolution by oversampling, an2668.” 2017.

## Used software and Libraries

- KiCad 7.0.1 - EDA software
- FreeCAD 0.21.2 - Parametric 3D modeling software
- LTspice XVII - spice simulation software
- Spyder 5.5.3 - Python IDE
- Python 3.11, skrf 0.3, matplotlib 3.8.2, Smith chart plots
- Matlab 2023a - Plots and data analysis
- NanoVNA Saver 0.6.2 - Capturing measurements from Lite VNA 64 to S port files
- AWR Designer - LPF plots from S parameters
- LibreOffice 7.5.9.2 - Calc (spreadsheets)
- TeXstudio 4.7.2 - LaTeX editor
- STM32 CubeIDE 1.8.0 - Integrated development environment for STM32 mcu
- STM32 CubeMX - STM32 tool for pin management
- Bluepill footprint by yet-another-average-hoe  
<https://github.com/yet-another-average-joe/Kicad-STM32>
- STM32-LCD-HD44780-I2C by firebull  
<https://github.com/firebull/STM32-LCD-HD44780-I2C>
- DS18B20 STM32 HAL Library by Mateusz Salamon and Michal Dunajski  
[https://github.com/lamik/DS18B20\\_STM32\\_HAL/tree/master](https://github.com/lamik/DS18B20_STM32_HAL/tree/master)
- STM32 74HC595 Driver by GlideLeo  
[https://github.com/GlideLeo/STM32\\_74HC595\\_Driver/tree/master](https://github.com/GlideLeo/STM32_74HC595_Driver/tree/master)
- MAX7219 tutorial and code by EmbeddedExpertIO:  
<https://blog.embeddedexpert.io/?p=2513>

# List of Figures

1.1	Schematic of a simplified tube RF amplifier . . . . .	5
1.2	Flange case of MRF448 . . . . .	5
1.3	LDMOS structure, source metal connects N+ to P+ sinker which connects through P+ substrate to back metal this lowers inductance[12]. Ground shield between gate and drift region lowers transfer capacitance[13] allowing for operation at higher frequencies. . . . .	6
1.4	MRF6V12500HS broadband test fixture by NXP, output power of pulsed 500 W for 960 to 1215 MHz was obtained[12]. It can be seen that microstrip stepped impedance matching is being used. . . . .	6
1.5	Push-pull configuration of MRF300A and MRF300B . . . . .	7
2.1	Block diagram of the amplifier . . . . .	8
2.2	Schematic of a Tandem match . . . . .	9
2.3	Characteristics of coupler . . . . .	10
2.4	Schematic of analog protection . . . . .	10
2.5	Schematic of transmit/receive PCB . . . . .	11
2.6	Assembled TX/RX PCB . . . . .	11
2.7	48 V rail schematic . . . . .	12
2.8	Diagram of ACS712[26]. . . . .	12
2.9	Relay driver schematic . . . . .	13
2.10	Temperature sensors schematic . . . . .	13
2.11	Fan controller schematic . . . . .	14
2.12	PTT schematic . . . . .	14
2.13	Band information input . . . . .	15
2.14	Microcontroller schematic . . . . .	15
2.15	Control board during hardware in the loop testing . . . . .	16
2.16	Back of the panel assembly . . . . .	16
2.17	Front panel during operation . . . . .	16
2.18	Schematic of used LPFs . . . . .	17
2.19	Simulation of designed LPF . . . . .	18
2.20	Simulation of designed LPFs . . . . .	18
2.21	$\mu[\%]$ vs $B_{peak}$ [37] . . . . .	19
2.22	Relay bank connected to a bus . . . . .	20
2.23	Schematic of LPF relay driver . . . . .	20
2.24	Designed LPF PCB, capacitors are mounted on the bottom layer . . . . .	21
2.25	Back side of the LPF PCB . . . . .	21
2.26	Impedance matching diagram . . . . .	22
2.27	DC isolated transformer . . . . .	22
2.28	1:4 input transformer . . . . .	23
2.29	VNA measurement of input . . . . .	23
2.30	PA deck input schematic . . . . .	24
2.31	Bias and input section . . . . .	24

2.32 Schematic of Guanella 1:4 TLT . . . . .	25
2.33 Schematic of Ruthroff 1:4 TLT . . . . .	26
2.34 Schematic of 1:9 TLT . . . . .	26
2.35 Photos of tested TLTs . . . . .	27
2.36 Test setup for TLT . . . . .	28
2.37 Measurement of S11 for various transmission line transformers . . . . .	29
2.38 Diagrams of impedance transformation . . . . .	31
2.39 Output capacitors . . . . .	31
2.40 Test setup for balun common mode attenuation . . . . .	32
2.41 Comparison of two baluns . . . . .	32
2.42 Impact of balun on return loss . . . . .	33
2.43 Ampelon's bias circuit . . . . .	33
2.44 Used bias voltage circuit . . . . .	34
2.45 A gate bias supply network . . . . .	34
2.46 Bias enable circuit . . . . .	34
2.47 Bias circuit test setup . . . . .	34
2.48 Bias circuit test . . . . .	35
2.49 Negative feedback control loop . . . . .	36
2.50 MRF300 connections . . . . .	36
2.51 Schematic of output stage . . . . .	36
2.52 Diagram of the PA deck board . . . . .	37
2.53 Assembled PCB without power transistors . . . . .	37
2.54 PSU under modification . . . . .	38
 3.1 Assembled profiles with mounted radiator (left) and PSU (right) . . . . .	39
3.2 Top of the amplifier during assembly . . . . .	40
3.3 Front of the assembled amplifier . . . . .	40
3.4 Amplifier during assembly without PA board, copper heat spreader and intake fan are visible . . . . .	41
3.5 Right upper corner view of the amplifier, air intake options are visible . . . . .	41
 4.1 Inside of the dummy load . . . . .	42
4.2 Dummy load and sampler. . . . .	42
4.3 Input (left) and output sample port (right) . . . . .	42
4.4 Dummy load return loss . . . . .	43
4.5 S31 measurement of RF sampler . . . . .	43
4.6 Another 50 dB sampler built in a smaller metal box . . . . .	44
4.7 Compact sampler S31 . . . . .	44
4.8 Power meter showing 600 W . . . . .	44
4.9 Xiegu G90 transceiver . . . . .	45
4.10 Test setup diagram . . . . .	45
4.11 Output power measurement . . . . .	46
4.12 SA harmonics measurement . . . . .	46
4.13 Measurement of amplifier at 1.9 MHz CW . . . . .	48
4.14 Measurement of amplifier at 3.6 MHz CW . . . . .	48
4.15 Measurement of amplifier at 10.1 MHz CW . . . . .	48
4.16 Measurement of amplifier at 14.15 MHz CW . . . . .	49
4.17 Measurement of amplifier at 28.5 MHz CW . . . . .	49
4.18 Across bands characteristic of amplifier with tested TLT . . . . .	49
4.19 Measurement of amplifier at 14.15 MHz CW . . . . .	50
4.20 Across bands characteristic of amplifier with tested TLT . . . . .	50
4.21 Measurement of amplifier at 14.15 MHz CW . . . . .	51

4.22 Across bands characteristic of amplifier with tested TLT . . . . .	51
4.23 Comparison of amplifier's PAE for three TLTs across HF spectrum . . . . .	52
4.24 Comparison of amplifier's PAE for three TLTs for increasing input power . . . . .	52
4.25 Output power for 7 W input . . . . .	53
4.26 Increasing output power . . . . .	54
4.27 Plot showing the process of finding the 1 dB point . . . . .	54
4.28 Power level of harmonics for increasing input power . . . . .	55
4.29 Spurious dynamic range between fundamental and harmonic . . . . .	56
4.30 Impact of TLT on SFDR . . . . .	56
4.31 4th and 5th harmonic level . . . . .	57
4.32 Second harmonic cancellation at different frequencies. . . . .	57
4.33 AWR designer schematic . . . . .	58
4.34 For the 160 m (1.8-2.0 MHz) LPF, the octave of the lowest allowed frequency is 3.6 MHz but the -40 dB marker is at 4.285 MHz, still this filter should be sufficient to attenuate the second harmonic below 50 dBc. Next harmonics will be attenuated even more, however, at some point, capacitive coupling causes the filter to decrease in performance. . . . .	58
4.35 80 m (3.5-3.8 MHz) LPF, an octave apart from 3.5 MHz is 7 MHz. It can be seen that -40 dB was achieved for that frequency. Insertion loss is very small, and excellent return loss of more than -20 dB was achieved. . . . .	59
4.36 40 m (7.0-7.20 MHz) and 30 m (10.1-10.15 MHz) LPF, the octave frequency of the lowest operating point is 14 MHz, and the -40 dB marker is on 15.9 MHz, quite close. Insertion loss is smaller than 0.4 dB, and the return loss for the worst case is -14.12 dB, presenting a good match. . . . .	59
4.37 20 m (14.0-14.35 MHz) and 17 m (18.068-18.168 MHz) LPF, this filter has the lowest frequency octave at 28 MHz, and the -40 dB marker is at 28.8 MHz. This filter represents good return loss, of about -20 dB for 20 m band and better than -10 dB for 17 m. Higher insertion loss might be due to the T80-10 cores used instead of T80-6, which would have a higher Q and lower losses at this frequency range. . . . .	60
4.38 15 m (21.0-21.45 MHz), 12 m (24.89-24.99 MHz), and 10 m (28.0-29.7 MHz) LPF, this filter fulfills the -40 dB octave requirement for 10 and 12 m but not for 15 m. However, the mentioned requirement had a significant margin of error, so the filter still might be good enough. Return loss is again excellent for all three bands.	60
4.39 6 m (50-54 MHz) LPF, high ripple is visible in the filter however, the frequencies of the 6 m band are within one of the peaks, providing an insertion loss of -0.75 dB. The marker of -40 dB is 3 MHz before the octave of the lowest frequency of operation, ensuring sufficient suppression. Return loss is very good, around -16 dB, providing a VSWR better than 1.4. . . . .	61
4.40 Output with LPF, 160m band . . . . .	61
4.41 Output with LPF, 80m band . . . . .	62
4.42 Output with LPF, 40m band . . . . .	62
4.43 Output with LPF, 30m band . . . . .	62
4.44 Output with LPF, 20 m band . . . . .	62
4.45 Output with LPF, 17 m band . . . . .	63
4.46 Output with LPF, 15 m band . . . . .	63
4.47 Output with LPF, 12 m band . . . . .	63
4.48 Output with LPF, 10 m band . . . . .	63
4.49 Example of IMD produced by the amplifier, it can be seen that each peak is lower than in case of CW because total power is spread over more peaks. . . . .	64
4.50 The dual-tone test of the signal source shows a far from ideal input to the amplifier.	64
4.51 Comparison of 8 KHz spectrum for three levels of input power at 3.8 MHz. . . . .	65

4.52	Comparison of 8 KHz spectrum for three levels of input power at 14.15 MHz. . . . .	65
4.53	Comparison of 8 KHz spectrum for three levels of input power at 28.5 MHz. . . . .	66
4.54	IP3 for 1:9 TLT made with $17 \Omega$ coaxial cable on 61 type ferrite . . . . .	66
5.1	CubeMX diagram of pinout . . . . .	67
5.2	GPIO switching by the ADC task shows frequent execution of this code with low downtime, hinting at high priority. Observed low periods show the time where other tasks are executed. . . . .	68
7.1	1 - 16x2 Liquid Crystal Display (LCD), 2 - Output power bar graph, 3 - Status LEDs (from left to right: AC power (PWR), transmit mode (TX), fault detected (WARN)), 4 - Total drain current bar graph, 5 - Standby (STDBY) button, 6 - Standing Wave Ratio (SWR) bar graph, 7 - Band switching mode button (MODE), 8 - Manual band selection buttons, 9 - AC power switch . . . . .	72
7.2	1 - Digital band data, 2 - Analog band data, 3 - PTT, 4 - ALC (option), 5 - RF output, 6 - RF input, 7 - AC input, 8 - Fuse (slow 5 A), 9 - Ground . . . . .	72

## List of Tables

2.1	Truth table for band decoding . . . . .	15
2.2	The voltage ranges for analog band switching. The discontinuity between the second and third range arises from the fact that on the 60 m band, the legal power limit is very small. The amplifier will refuse to operate for any undefined band. . . . .	15
2.3	Built comparison of four tested TLTs. '*' denotes the theoretical impedance of parallel coaxes. Comma denotes variations on the same TLT. . . . .	27
2.4	Example settings of RV5 for given ratio of gate voltage change to $1 ^\circ C$ . . . . .	35
4.1	Initial test of the power amplifier and sampler. CW at 14.15 MHz . . . . .	46
4.2	Wide harmonic measurement using spectrum analyzer and sampler . . . . .	47
4.3	P1dB for three tested TLTs at 14.15 MHz . . . . .	55
4.4	P1dB for 1:9 TLT at different bands . . . . .	55